A STUDY OF BISTATIC RADAR AND THE DEVELOPMENT OF AN INDEPENDENT BISTATIC RADAR RECEIVER

M DEL MISTRO

FEBRUARY 1992

Submitted to the University of
Cape Town in partial fulfilment
for the degree of Master of
Science in Engineering

Declaration

I, Mario Del Mistro, submit this thesis in partial fulfilment of the requirements for the degree of Master of Science in Engineering. I claim that this is my work and that it has not been submitted in this, or any similar form, for a degree at any University.

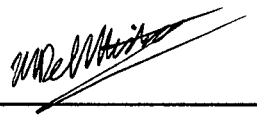

Signature of candidate

Acknowledgements

It is with great pleasure that I take this opportunity to thank the staff in the Department of Electrical and Electronic Engineering at the University of Cape Town who assisted me with this thesis project. In particular, I owe much to my supervisor Professor Inggs who was always ready to assist and advise me.

Terms of Reference

This thesis report was commissioned by Professor M.R. Inggs of the Electrical Engineering Department at the University of Cape Town. The project was to develop an experimental bistatic radar receiver at UCT. The bistatic system would use the already operational L-Band transmitter at D.F. Malan airport. Research for this project commenced in February 1991.

The bistatic receiver was built around the following guidelines:

1. Establish the detection range possible with a non-moving receiver antenna.

2. Large target echoes, clutter and the direct illumination of the transmitter main beam must not saturate the receiver.

3. The receiver must maintain PRF and azimuth synchronization with the transmitter at all times.

4. The receiver must display the received echoes and correct for bistatic distortion on a PPI display.

Synopsis

This report contains a literature review of bistatic radar and also describes an experimental L-Band bistatic radar receiver which was built at the University of Cape Town.

In a bistatic radar the transmitter and receiver are separated by an amount which is comparable to the distance to the targets which are being displayed. The separation of the transmitter and receiver cause various parameters to change when comparing the bistatic radar to a monostatic radar. Some of these parameters are listed below.

1. The radar range equation is now a function of $R_T^2 R_R^2$ and no longer R_M^4. The gain of the transmitter and receiver antenna must be taken into account as two different antennas are being used.

2. In a monostatic radar the constant range contours form circles around the collocated transmitter and receiver whereas in a bistatic radar they form ellipses and the transmitter and receiver are the foci of the ellipses.

3. The constant power contours of a monostatic radar are also circles. In a bistatic radar they are ovals surrounding the transmitter and receiver. As the ovals get closer to the line separating the transmitter and receiver (baseline) the ovals collapse and start forming separate circles around the transmitter and receiver.

4. The coverage of a bistatic radar is the area which is illuminated, simultaneously by both the transmitter and the receiver. The coverage area can never exceed that of a monostatic radar.

5. The range and cell area resolution degrades as the target approaches the baseline. In order to compete with a monostatic radar very narrow transmit and receive antenna beams are required.

6. Due to the separation of the transmitter and the receiver, a PPI display will be distorted. This distortion is commonly called bistatic distortion.

7. The bistatic radar target cross section (RCS) varies according to target position relative to the transmitter and the receiver. When the target crosses the baseline, its forward RCS is observed. The forward RCS is sometimes 15dB larger than the monostatic reverse RCS. As the target moves further away from the baseline the bistatic RCS starts approximating the monostatic RCS.

8. As the cell area (area of ground illuminated by the transmitter and receiver antenna) of a bistatic radar is larger than that of the monostatic radar near the baseline, the bistatic radar is inherently more susceptible to clutter.

The receiver must maintain synchronization in transmitter azimuth and PRF, at all times, in order to correct for bistatic distortion on a PPI display. This distortion is corrected by converting the transmitter-to-target azimuth to the receiver-to-target azimuth and determining the target-to-receiver range which is a function of the delay time. The delay time is the time difference between the direct pulse and the reflected pulse. This will cause the trace on the display to move in a complex pattern, hence correcting this distortion.

A bistatic radar receiver was built for the Electrical Engineering Department at UCT. The purpose of the radar is to monitor aircraft approaching and departing from D.F. Malan airport. The motivation for this project is to utilize one of the many advantages of the bistatic radar. This advantage is [5]:

> "For military and civilian air surveillance radar application in an area where there are several airfields. Each airfield will have its own bistatic radar receiver. The targets will be illuminated by one high power, expensive transmitter located in the required coverage area. The advantage is that mutual interference between several transmitters will be eliminated and the utilization of the spectrum improved."

The receiver is designed to "hitchhike" off the L-Band transmitter at D.F. Malan airport which is 15km away. The peak power of the transmitter is 2.5MW and the transmitted pulse width is 2.5μsec. The design of the receiver at UCT, which is shown in Figure 1, can be broken down into five sections, namely:

1. The antenna which floodlights the coverage area. This is a simple dipole antenna with one reflector.

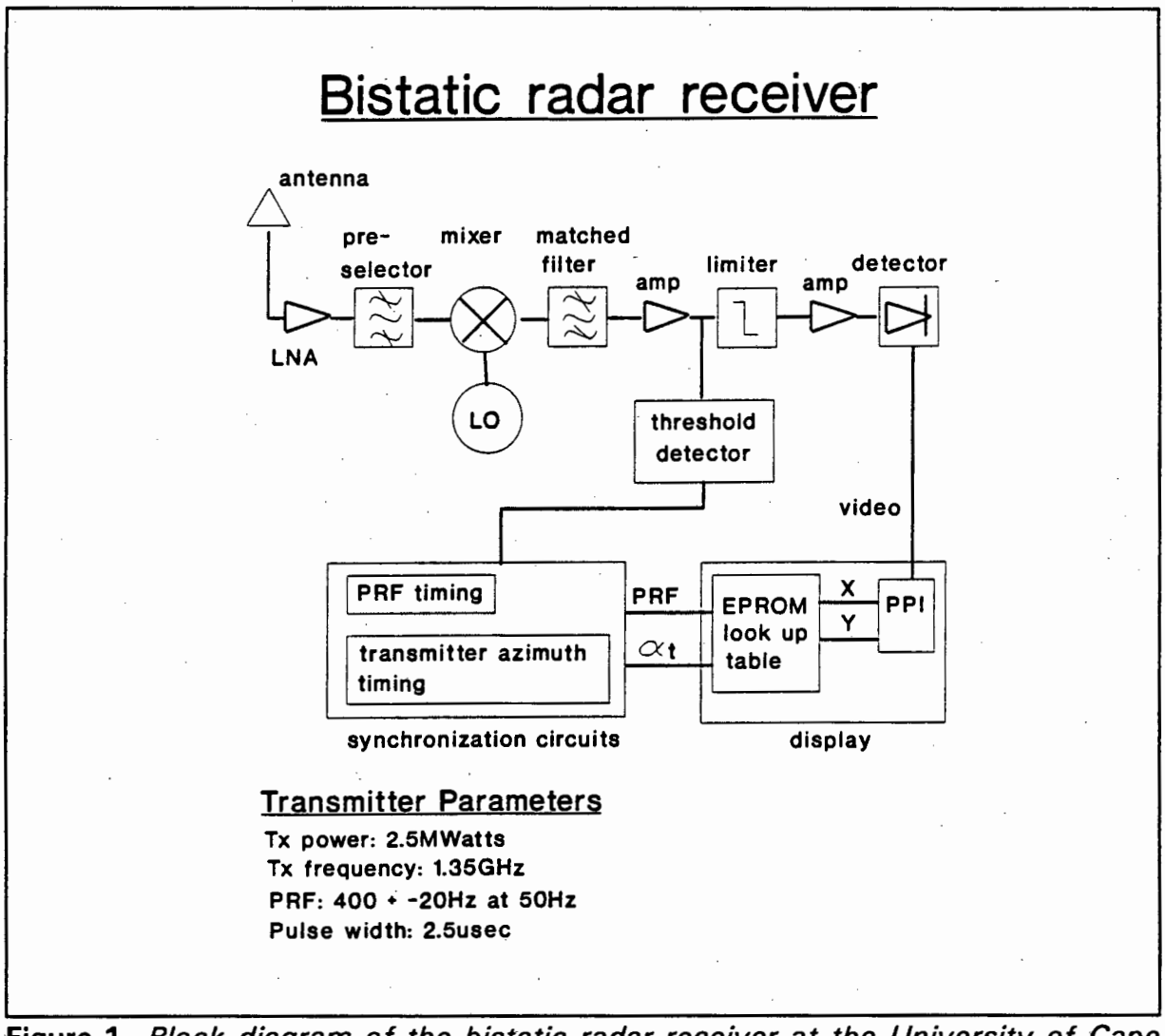

Figure 1 *Block diagram of the bistatic radar receiver at the University of Cape Town.*

2. The receiver front end. This is a superheterodyne type, providing a down conversion from 1.35GHz to 70Mz. There are three amplifiers and an STC circuit producing a variable gain from 24dB to 76dB. The amplifier after the antenna is a low noise

amplifier. The total receiver losses are 24dB and it has a noise figure from 14dB to 47dB depending on the gain of the STC circuit. To maximize SNR, matched filtering is used after the detector stage. The receiver has variable sensitivity of -103dBm to -24dBm with a SNR of 12dB at the display. The maximum range of the receiver is 127km for a target with an RCS of $50m^2$.

A local oscillator generates 1.42GHz at a level of 7dBm to feed the mixer. At present manual tuning is used to cater for the 7MHz drift of the transmitter.

The output of the IF amplifier passes through the detector and the video signal is then applied to the PPI display. Preceding the STC circuit is a power splitter. Here part of the signal is level detected. This is required for the synchronization circuits.

3. The azimuth synchronization system. This synchronization is performed when the receiver is illuminated by the transmitter (dwell period). The centre of the dwell period is determined and a counter is reset. The counter then counts 1024 discrete azimuth positions corresponding to the transmitter antenna azimuth.

   To avoid errors caused by variations in the antenna's rotation rate, the output of the azimuth counter is checked before resetting and if required, is corrected by the operator. The azimuth synchronization circuit has a resolution of 2.1°.

4. Range synchronization system. During the dwell period the PRF is also synchronized at the receiver. The PRF is 400Hz wobulated at 50Hz by the local mains supply. This requires synchronization to 400Hz and 50Hz. A square wave 400Hz VCO is used to regenerate the PRF independently at the receiver. The VCO is then frequency modulated at 50Hz which is derived from the mains. The 50Hz is adjusted in phase and amplitude and the VCO will be reset during the dwell period in order to remain in alignment with the transmitter.

5. The display system. This system must correct for bistatic distortion. For every discrete transmitter azimuth position the display must determine the receiver azimuth and target

to receiver range for a set number of delay times. This is achieved with the use of an EPROM look-up table. The EPROMs store the azimuth and range information in cartesian coordinates in order to drive the display. A counter is used to address the memory and synchronization is maintained by the PRF and transmitter azimuth information derived by the synchronization systems. The display has an angular resolution of 1.3° and a range resolution of 782m.

It was shown that relatively simple PRF and azimuth scanning synchronization is achievable, allowing for a conventional PPI display of target information.

Table of Contents

Declaration i

Acknowledgements ii

Terms of Reference iii

Synopsis iv

Table of Contents ix

List of Illustrations xiv

1. INTRODUCTION 1

2. AN OVERVIEW OF BISTATIC RADAR 4
   2.1 DEFINITIONS AND REQUIREMENTS 4
   2.2 THE HISTORY OF BISTATIC RADAR 6
   2.3 APPLICATIONS OF BISTATIC RADAR 9
   2.4 AN ANALYSIS OF BISTATIC RADAR 11
      2.4.1 THE GEOMETRY 11
      2.4.2 THE RADAR RANGE EQUATION 13
      2.4.3 CONSTANT RANGE CONTOURS 13
      2.4.4 CONSTANT BISTATIC ANGLE AND RANGE RATIO CONTOURS 15
      2.4.5 CONSTANT POWER CONTOURS 18
      2.4.6 TARGET LOCATION AND COVERAGE 21
      2.4.7 RANGE AND CELL AREA RESOLUTION 25
      2.4.8 BISTATIC DISTORTION AND DISPLAY CORRECTION 30
      2.4.9 BISTATIC DOPPLER CHARACTERISTICS 34
      2.4.10 RADAR TARGET CROSS SECTION 36

2.4.11 CLUTTER 40
2.5 OTHER ASPECTS ON BISTATIC RADAR 42
2.5.1 PULSE CHASING 42
2.5.2 BEAM SCAN ON SCAN 44
2.6 CONCLUSION 46

3. AN INDEPENDENT BISTATIC RADAR RECEIVER 49
3.1 GEOGRAPHICAL LAYOUT OF THE RADAR 50
3.2 TRANSMITTER PARAMETERS 52
3.3 RECEIVER SYSTEM ANALYSIS 56
3.3.1 RECEIVER REQUIREMENTS 57
3.3.2 BANDWIDTH REQUIREMENTS 59
3.3.3 THE COMPONENTS OF THE RECEIVER 61
3.3.3.1 ANTENNA 61
3.3.3.2 LOW NOISE AMPLIFIER AND ANTENNA FEED 64
3.3.3.3 PRESELECTOR FILTER 67
3.3.3.4 MIXER 68
3.3.3.5 MATCHED FILTER 71
3.3.3.6 PREAMP AND POWER SPLITTER 73
3.3.3.7 SENSITIVITY TIME CONTROL 75
3.3.3.8 IF AMPLIFIER 81
3.3.3.9 ENVELOPE DETECTION AND INTEGRATION 83
3.3.3.10 THRESHOLD DETECTOR 87
3.3.4 SPECIFICATIONS OF THE RECEIVER 88
3.3.4.1 POWER OF DETECTED DWELL PERIOD PULSES . . . 88
3.3.4.2 MAXIMUM DETECTED POWER LEVEL OF A TARGET 89
3.3.4.3 SYSTEM NOISE FIGURE AND SENSITIVITY 90
3.3.4.4 RADAR RANGE AND COVERAGE 97
3.3.4.5 RESOLUTION 98
3.3.5 AZIMUTH SYNCHRONIZATION 101
3.3.6 PULSE REPETITION FREQUENCY SYNCHRONIZATION 104
3.3.7 THE PLAN POSITION INDICATOR DISPLAY 108

3.4 CLUTTER PREDICTIONS 109
3.5 CONCLUSION 116

4. CONCLUSION 117

5. RECOMMENDATIONS 118

BIBLIOGRAPHY AND REFERENCES 120

APPENDIX 1 122

APPENDIX 2 124

APPENDIX 3 126

APPENDIX 4 129

APPENDIX 5 130

APPENDIX 6 136

APPENDIX 7 140

APPENDIX 8 143

APPENDIX 9 146

APPENDIX 10 151

APPENDIX 11 154

List of Illustrations

Figure	Illustration	Page
1	Block diagram of the receiver	vi
2.1	Bistatic radar coordinate system	12
2.2	Constant range contours	15
2.3	Constant bistatic angle contours	18
2.4	Ovals of Cassini	20
2.5	Ratio of bistatic to monostatic coverage area	24
2.6	Geometry showing the cell area	29
2.7	Bistatic distortion on a PPI display	31
2.8	Receiver range vs delay time	32
2.9	Receiver azimuth vs delay time	33
2.10	PPI scan pattern for a bistatic display	34
2.11	Curves of constant doppler reduction	36
2.12	Coordinate system for clutter measurements	40
2.13	Receiving arc due to Tx beamwidth	43
3.0	Geographical coverage area of the radar	51
3.1	PRF sampled during the dwell period	52
3.2	Transmitter elevation radiation pattern	54
3.3	Transmitter azimuth radiation pattern	55
3.4	Block diagram of the receiver	57
3.5	Sin(x)/x transfer function	59
3.6	Receivers frequency map	60
3.7	Receiver antenna and balun construction	62
3.8	Receiver antenna gain pattern	62
3.9	Receiver antenna S11 parameters	63
3.10	Coaxial attenuation characteristics	65
3.11	LNA circuit diagram	66

3.12 LNA gain characteristics 66
3.13 Preselector filter S21 parameters 68
3.14 Mixer I/P power vs O/P power 70
3.15 Mixer conversion loss vs LO power 71
3.16 Chebyshev filter circuit diagram 72
3.17 Chebyshev filter S21 parameters 73
3.18 Preamp and power splitter circuit diagram 74
3.19 Preamp gain characteristic 75
3.20 Gain control circuit diagram 76
3.21 STC gain variation vs control voltage 78
3.22 STC return loss vs control voltage 79
3.23 STC control voltage vs time 80
3.24 STC control voltage generating circuit 81
3.25 IF main amplifier gain characteristics 82
3.26 IF amplifier NF and gain vs frequency 83
3.27 Envelope detector circuit diagram 84
3.28 Detector gain characteristics 85
3.29 Threshold detector circuit diagram 87
3.30 Noise measurements (LNA at antenna) 93
3.31 Noise measurements (LNA at mixer) 94
3.32 Noise measurements (Gain = maximum) 94
3.33 Noise measurements (Gain = 0) 95
3.34 Noise measurements (Loss = maximum) 95
3.35 Range resolution at constant range of 17km 99
3.36 Range resolution at constant range of 59km 99
3.37 Area resolution at constant range of 17km 100
3.38 Area resolution at constant range of 59km 100
3.39 Azimuth synchronization circuit block diagram 102
3.40 Centre of dwell period determination pulse 103
3.41 PRF synchronization circuit block diagram 104
3.42 PLL error voltage (circuit detuned) 107
3.43 PLL error voltage (circuit tuned) 107

3.44 SCR (receiver azimuth = 80 degrees) 111
3.45 SCR (receiver azimuth = 45 degrees) 111
3.46 SCR (receiver azimuth = 12 degrees) 112
3.47 SCR (receiver azimuth = 30 degrees) 112
3.48 Larson's clutter coefficient data 113
3.49 SCR (constant range contour = 19km) 114
3.50 SCR (constant range contour = 27km) 115

CHAPTER 1

INTRODUCTION

In a bistatic radar the transmitter and receiver are separated by an amount which is comparable to the distance to the targets which are being displayed. The separation between the transmitter and receiver introduces certain factors which have to be taken into account.

- the receiver must have some way of synchronizing to the PRF as well as the transmitter azimuth angle at any particular point in time.

- the receiver must correct for bistatic distortion on the Plan Position Indicator (PPI) display.

Why use bistatic radar which requires this additional synchronization and display conversion? Some advantages of the bistatic radar over the monostatic radar are listed below.

1. A monostatic radar with co-located transmitter and receiver are susceptible to external interference sources, such as jamming. The transmitter, being an active input, clearly advertises its position. In a bistatic system the receiver is a passive element, hence difficult to detect.

2. For air surveillance applications in an area where there are several airfields, each airfield will have its own receiver. The targets will be illuminated by one high power, expensive transmitter. In this case mutual interference between several transmitters will be eliminated.

3. The bistatic forward radar target cross section is several times larger than the monostatic radar target cross section.

An experimental L-Band bistatic radar receiver and display system is in development at the University of Cape Town (UCT). The receiver will hitchhike off the transmitter at D.F Malan airport. The objective of the receiver is for air surveillance purposes and to detect these aircraft as they approach and depart from D.F. Malan airport.

The objectives of this report are:

1. To briefly give the history of bistatic radar and several examples of previous systems and their applications.

2. To determine the advantages and disadvantages of a bistatic radar and to give several applications where the advantages outweigh the disadvantages when compared to a monostatic radar.

3. To give the reader a basic understanding of the bistatic radar geometry and theory.

4. To explain the detailed design of the bistatic receiver, which was developed to achieve certain requirements.

5. To provide a detailed outline of the performance of the receiver.

6. To draw conclusions and make recommendations.

The information on which this report is based was gathered from text books and several papers.

The first chapter is a literature review of bistatic radar. The chapter begins by defining bistatic radar and explaining its various configurations. The history and several applications are then covered. The bistatic radar is then analyzed with respect to; geometry, radar range

equation, constant range contours, constant power contours, coverage, resolution, doppler characteristics, bistatic distortion, clutter and radar target cross section.

The second chapter discusses the specific bistatic radar, where the receiver is at the University of Cape Town. Firstly the geometry is described and then the expected requirements of the receiver are given. Secondly the receiver is broken down into its several component systems (receiver front end, synchronization circuits and display) and described. The parameters of each component are also given. Finally the specifications of each component are listed and the performance of the receiver determined. The system design parameters are then compared to the actual performance.

CHAPTER 2

AN OVERVIEW OF BISTATIC RADAR

A Bistatic radar is a system where the transmit and receive antennas are located on separate sites. Target detection is achieved by the illumination of the target by the transmitter and the scattered signal from the target (target echoes) is then detected by the receiver.

This chapter is written in order to give the reader background information on bistatic radar. This information will be both historical and technical. The information was gathered from several publications. At several points in this chapter the bistatic characteristics for a particular application will be mentioned.

This particular application is a bistatic system used for air surveillance purposes. The transmitter has a rotating fan beam antenna and the receiver has a floodlight antenna.

2.1 DEFINITIONS AND REQUIREMENTS

Skolnik [10] defines a bistatic radar as:

> "...a bistatic radar is assumed to be one in which the separation between transmitter and receiver is comparable to the target distance."

If separate transmit and receive antennas are on the same site then the system is considered to be monostatic, according to the above definition. These systems are also

known as "quasi-bistatic" [9]. When two or more receive sites with common spatial coverage are employed and target data from each is combined at a central location, the system is called a multistatic radar. Multiple transmitters can be used with any of these configurations. They can be located at separate sites or collocated with the receive sites. Bistatic radars can operate in either of three different modes [1], namely:

1. **Dedicated** - This is defined as being under both design and operational control of the bistatic radar system.

2. **Cooperative** - This system is designed for other functions but found suitable to support bistatic operations and the transmitter can be controlled to do so.

3. **Non-cooperative** - This system is designed for other functions and is suitable to support bistatic operation, however the transmitter cannot be controlled.

To determine target location the receiver must know the transmit azimuth and elevation and the timing of the transmitted signal. For matched filter operation, the transmitted waveform must be available and for coherent receiver operation the phase of the transmitted waveform must be available to the receiver. Hence in a bistatic or multistatic system synchronization between the transmitter and receiver must be maintained [1][9]. This can be achieved in either of three ways:

1. **Direct synchronization** is when a signal is sent from the transmitter to the receiver. This signal is used to synchronize a clock. This can be accomplished by either a land line, communication link, or directly at the transmitters RF if an adequate line of sight exists between transmitter and receiver.

2. **Indirect synchronization** is achieved by using identical stable clocks at the transmitting and receiving sites. The clocks however must be periodically synchronized.

3. **Direct breakthrough synchronization** is achieved when the transmitting beam scans past the receiving site, given an adequate line of sight. The receiver then synchronizes on the pulses received during the main beam illumination period (dwell period).

For this application the system is non-cooperative and direct breakthrough synchronization is used. In other words the receiver is hitchhiking off the transmitter.

2.2 THE HISTORY OF BISTATIC RADAR

In 1904 the first radar was developed by a German engineer, Christian Hulsmeyer [1] to detect ships. This was bistatic in nature. Several countries, during the 1920s and 1930s, were conducting radar experiments simultaneously and independently. These were the United States, the United Kingdom, France, Italy, Russia, Japan and Germany. Later in the late 1930s the first array of radars started to make their appearance. These radars were predominantly bistatic. With the advent of the duplexer at the US Naval Research Laboratory in 1936, research into the bistatic radar became virtually dormant. The duplexer allowed transmitting and receiving to be done with the same antenna. This was the advent of the monostatic (single site) radar. It was not until the 1950s that interest in bistatic radars was revived. The research work was primarily focused on theory and measurements, forward scatter fences, semiactive homing missiles and multistatic radars. In the 1970s and 1980s a second bistatic resurgence [1] took place. This was initiated by the ability of the enemy to home in on the transmitter radiation. To make the transmitter less vulnerable it could be moved out of the battle field and into a sanctuary. A second threat which began to emerge was the retrodirective jammer, in which a high gain jamming antenna is directed toward the monostatic radar. By selecting the correct bistatic geometry (bistatic angle) the

effectiveness of the retrojammer could be reduced. Research into clutter tuning also began.

The first bistatic radars used CW transmitters and detected a beat frequency produced between the direct-path signal from the transmitter and the doppler frequency shifted signal scattered by a moving target. The target would be detected when crossing the base line. This effect was called CW interference [3]. At the Naval Research Laboratory, A. Taylor and L.C. Young detected a wooden ship using a CW wave interference radar with a wavelength of 5m. In 1932 they accidentally detected an aircraft 3.2 km away while working at 33 MHz. Later that same year they detected an aircraft 80 km away [6].

In 1935, Sir Robert Watson-Watt of the UK used radios to detect aircraft. This developed into the Chain Home network of radars along the British coast. They operated at HF. This system played an important role in the Battle of Britain in 1940. The French, in 1941, also developed a bistatic CW radar in a two-fence configuration which had a wavelength of 4 m.

In 1934 the Soviet Union developed bistatic radars which operated at 75 MHz. These were known as RUS-1. They were later replaced by RUS-2 and RUS-2C. In 1941, 45 RUS-1 systems were built in the Far East and Caucaus. At the same time the Japanese deployed 100 bistatic CW fence radars (Type A). They were able to detect aircraft up to 800 km away, operated between 40 and 80 MHz and had a transmitter power of 400 W. They remained in service till the end of the second world war.

During World War 2 the Germans built the Klein Heidelberg. This was the first noncooperative bistatic configuration. It used the British Chain Home radar transmitters. The receivers were then able to detect Allied bombing raids while still over the English Channel, without endangering the German ground sites.

During the first resurgence of bistatic radar in the early 1950s, RCS theory and measurements for the reverse and forward scatter areas were developed and taken respectively. This led to clutter measurements. Bistatic radar theory was also codified by Skolnik. In 1954 the Canadian Air Force detected scale model aircraft flying across the beam in the forward scatter region. During the 1960s the AN/FPS-23 Fluttar radar was developed. This is a CW fixed beam bistatic fence radar. It was used to detect penetration of the Distant Early Warning (DEW) line, in the Arctic by low flying bomber aircraft [6].

A great deal of research and development work was done on the semiactive homing missile detector. At the same time Navspur was developed [6]. This was used to detect orbiting objects and ballistic missiles as they passed through the electronic fence over the continental United States. Also developed was the AZUSA, the Udop and the Mistram which were multistatic radars. They were used for precision measurements of trajectories at missile and test ranges.

During the second resurgence of bistatic radar, Sanctuary, an experimental bistatic radar system, was developed by Technology Service Corporation. The system used a ground based coherent radar receiver site operating with a cooperative airborne transmitter to perform surface-to-air surveillance and target tracking [6]. The Sanctuary provided protection from antiradiation missiles (ARM) and retrodirective jamming.

The Environmental Research Institute of Michigan developed an experimental synthetic aperture radar (SAR). The system uses X-Band transmitters and receivers mounted in a Convair CV-50 aircraft. This system was used to produce two dimensional images of mapped areas. Another SAR system, the BTT/TBIRD was developed. This was to demonstrate clutter tuning, forward-looking SAR operation and side-looking moving target indication operation.

A bistatic pulse doppler intruder detection radar was also developed to protect military aircraft on the ground from intruders, known as an aircraft security sensor (ASR). Five

portable transmitter-receiver units, separated by 65m, were located around the aircraft, with one transmitter servicing the adjacent receiver. It was configured for near forward scatter operation [3].

The TRADEX L-Band and ALTAIR UHF monostatic radars are also used in multistatic configurations [6]. This configuration was developed to track ballistic missile skin echoes. The system which was developed in 1980 is projected to measure three dimensional position and velocity with accuracies better than 4m and 0.1m/s respectively.

Some other non-military developments of bistatic radar have been high-resolution imaging at short ranges for use by robotics in an industrial environment; airport ground vehicle and aircraft collision warning and avoidance using a baseband bistatic radar; planetary surface and environment measurements using a satellite-based transmitter and an earth-based receiver; ocean wave spectral measurements using a Loran-A system and detection of tropospheric layers and ionospheric layers using ground-based sites.

2.3 APPLICATIONS OF BISTATIC RADAR

Several applications for bistatic radar will be mentioned below. The applications have been divided into two categories, namely military and non-military applications.

Military Applications

1. Bistatic techniques were used in semiactive homing missiles. Here the large, heavy and costly transmitter could be off-loaded from the small expendable missile onto the launch platform.

2. When the target crosses the line joining the transmitter and the receiver (baseline), the radar system operates in the forward-scatter mode (forward-scatter fence). In this mode the bistatic radar target cross section (RCS) increases when compared to the monostatic RCS. The improvement is a result of the forward scatter phenomenon [14]. The magnitude of the forward scatter return is not dependent on the targets material composition. Hence detection of an object with a monostatic RCS reduced through shaping or by treatment of radar absorbing materials, as the stealth bomber, is possible.

3. The transmitter can be placed in a sanctuary where it is protected from antiradiation missiles and retro-directive jamming. The receiver can then be operated relatively safely in the field.

4. A bistatic receiver can be placed on an aircraft which then uses transmitters of opportunity (hitchhiking) to detect targets near the aircraft or transmitting site. This setup can warn the pilot of an intruding aircraft or missile while the pilot's primary sensor is off. This concept is known as passive situation awareness (PSA) [1].

Non-military applications

1. For civilian (as well as military) air surveillance radar applications in an area where there are several airfields. Each airfield will have its own receiver. The targets will be illuminated by one high power, expensive transmitter located in the required coverage area. This will eliminate mutual interference between several transmitters and receivers and the utilization of the spectrum is improved. An additional advantage is that the receivers will operate passively [7][11].

2. Synthetic aperture radar (SAR) images can be produced by placing the transmitter and receiver on different airborne platforms. In this configuration the separate

velocity vectors can be changed to control or "tune" the ground clutters doppler shift and doppler spread. This concept is known as clutter tuning.

3. A short-range bistatic radar can be used in precollision warning/avoidance and ground-air traffic control. Subnanosecond video pulses drive a wideband transmitting antenna. The radiated pulse reflects off a target and returns to a similar receiving antenna and display network [6].

4. It can be used for planetary surface and environmental measurements using a satellite-based transmitter and an earth-based receiver or a planet-based transmitter and a satellite-based receiver.

2.4 AN ANALYSIS OF BISTATIC RADAR

This section describes the basic principles of a bistatic radar. The principles covered, amongst others are the geometry or the layout of the bistatic radar. This geometry then gives the bistatic radar its unique qualities, such as isorange contours, constant bistatic angle contours, ovals of Cassini, spatial coverage, forward scatter RCS, bistatic clutter and bistatic distortion. These topics will all be covered briefly, below.

2.4.1 THE GEOMETRY

The coordinate system used to describe the bistatic geometry will be the two dimensional, North-referenced coordinate system. This is shown in Figure 2.1. The bistatic plane is the plane in which the transmitter (T_x), receiver (R_x) and target (Tgt) lie. This is also known as the bistatic triangle. The distance between

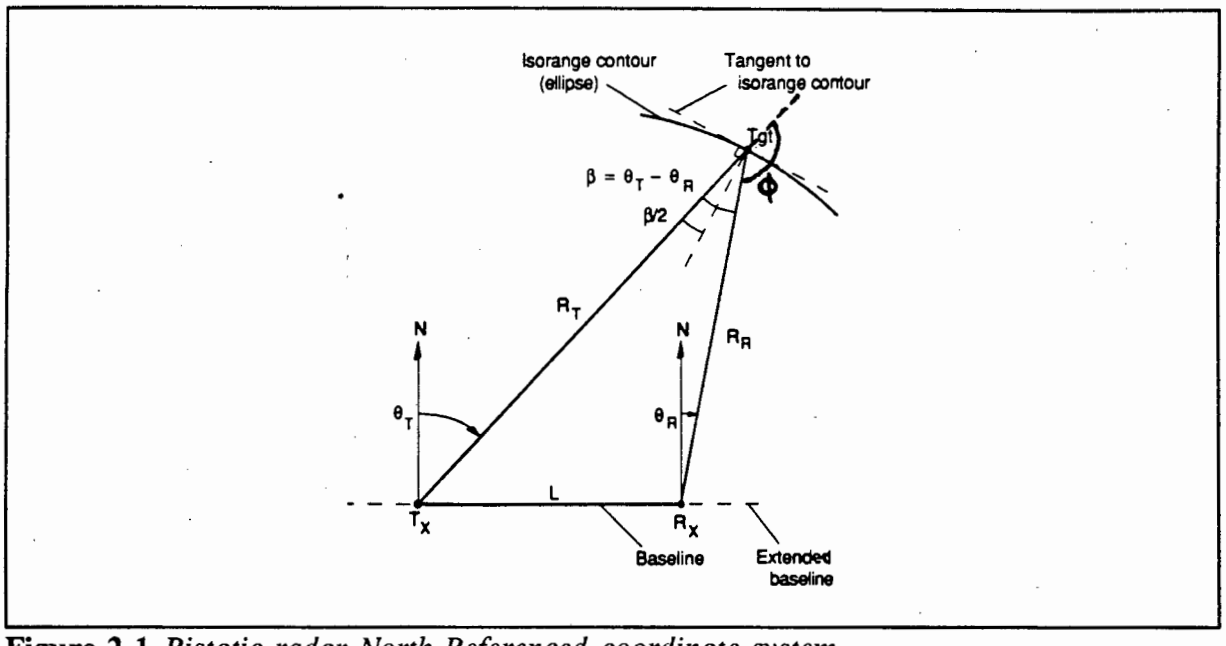

Figure 2.1 *Bistatic radar North-Referenced coordinate system.*

the transmitter and the receiver is called the baseline (L). The extended baseline is defined as continuing the baseline beyond the transmitter or receiver. The distance from the transmitter to the target is defined as R_T and from receiver to target as R_R.

The bistatic angle β is the angle between the transmitter and receiver with the vertex at the target. The receiver look angle is θ_R and the transmitter look angle is θ_T. Note that;

$\theta_T + \theta_R = \beta$ for $0° < \theta_T < 180°$ and $180° < \theta_R < 360°$.

The look angles are taken as positive in the clockwise direction. They are also known as the angles of arrival (AOA) [1].

In general, the performance and operation of the bistatic radar is the same irrespective of whether the target lies above or below the baseline. This is due to the symmetrical nature of the geometry.

2.4.2 THE RADAR RANGE EQUATION

The bistatic radar range equation is derived in exactly the same way as in the monostatic case. A derivation can be found in reference [2]. There are several differences however, which will be described later. The bistatic range equation [1][11] is shown below.

$$(R_T R_R)_{max} = \sqrt{\frac{P_T G_T G_R \lambda^2 . \sigma_B . F_T^2 F_R^2}{(4.\pi)^3 . k . T . B . (S/N)_{min} . L_T L_R}}$$

$$(R_T R_R)_{max} = \kappa$$

where

R_T = transmitter to target range

R_R = receiver to target range

P_T = power of the transmitter

G_T = gain of the transmitter's antenna

G_R = gain of the receiver's antenna

λ = wavelength

σ_B = bistatic radar target cross section

F_T = transmitter pattern propagation factor

F_R = receiver pattern propagation factor

k = Boltzmans constant

T = receiver noise temperature

B = receiver noise bandwidth

$(S/N)_{min}$ = signal to noise ratio needed for detection

L_T = losses in the transmitter

L_R = losses in the receiver

κ = bistatic maximum range product

For the bistatic range equation to be reduced to the monostatic range equation the following changes are made:

1. $\sigma_M = \sigma_B$
2. $L_T.L_R = L_M$
3. $R_T^2.R_R^2 = R_M^4$

Also note that $(R_M)_{max} = \sqrt{\kappa}$. Hence when the target range in the bistatic radar is extended to infinity, the bistatic radar reduces to the monostatic case.

The pattern propagation factors take into account the gains of the transmit and receive antennas as a function of pointing angle. They also take into account the loss that the signal experiences (atmospheric absorption, diffraction, refraction) while propagating through the atmosphere.

2.4.3 CONSTANT RANGE CONTOURS

The total distance travelled by the signal from the transmitter to the target to the receiver is:

$$T = R_T + R_R$$

When the total range (T) is kept constant, constant range sum ellipses (isoranges) are formed. The transmitter and receiver then form the foci of the ellipse. This is shown in Figure 2.2.

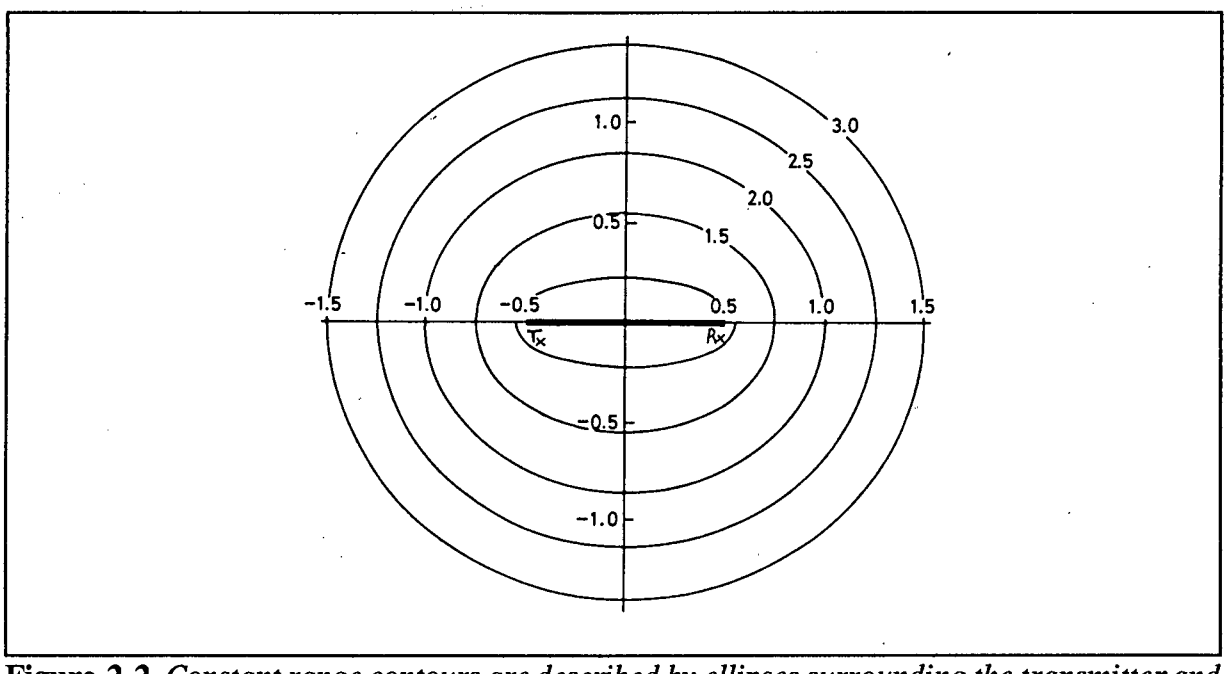

Figure 2.2 *Constant range contours are described by ellipses surrounding the transmitter and the receiver.*

The constant range contours are also known as constant delay time contours. Note that the bisector of the bistatic angle is orthogonal to the tangent of the isorange contour at any point on the contour [1]. The following equations express the isorange contours in cartesian coordinates.

$$\frac{x^2}{a^2}+\frac{y^2}{b^2} = 1$$

$$\frac{L^2}{4} = c^2 = a^2-b^2$$

The origin of the cartesian coordinates will be at the midpoint of the base line. The transmitter and receiver are placed at $\pm c$ *(the foci)*. The semimajor axis is represented by a and the semiminor axis by b. Also note that $(R_T + R_R) = 2a$.

Knowing the eccentricity of the isorange contour simplifies expressions involving these contours. The eccentricity (e) of an ellipse is:

$$e = L / (R_T + R_R)$$
$$= L / 2.a$$
$$= \sqrt{(a^2 - b^2)} / a$$

The value of e lies in the range of $0 < e < 1$. When $e = 0$, then $L = 0$ and the ellipse is a circle, ie representing a monostatic radar.

2.4.4 CONSTANT BISTATIC ANGLE AND RANGE RATIO CONTOURS

For certain bistatic configurations, operation of the radar is constrained by a maximum or minimum bistatic angle. An example of this is if the system operates in the forward scatter mode. In this case one does not want the bistatic angle to deviate much from 180°. In this section the maximum bistatic angle in the ellipse is determined and constant bistatic angle contours are plotted.

Contours of constant range ratio are also shown. The importance of this will be discussed later in the section on pulse chasing.

When the bisector of the bistatic angle is perpendicular to the baseline, it will cut the baseline at the midpoint or origin. At this point the bistatic angle is a maximum (β_{max}). The bisector is also the semiminor axis of that constant range ellipse. When the bistatic angle is a maximum then;

$$R_T = R_R$$
$$\theta_T = \theta_R$$

From the above the following equations can be derived [1]:

$$\beta_{max} = 2.\sin^{-1}(L / 2.R_T)$$
$$\beta_{max} = 2.\sin^{-1}(L / 2.R_R)$$
$$\beta_{max} = 2.\sin^{-1}(e)$$

Note also that at this point θ_T and $\theta_R = \sin^{-1}(e)$.

Points that have a constant bistatic angle are known to lie on circles passing through the transmitter and receiver [8]. These contours are centred on the midline or perpendicular bisector of the baseline at;

$$d_\beta = L / (2.\tan\beta)$$

The radius of the circles are;

$$r_\beta = L / (2.\sin\beta)$$

These contours are also known as iso-β contours. Iso-β contours are shown in Figure 2.3. For $\beta = 0°$ the contour lies on the extended baseline and for $\beta = 180°$ the contour lies on the baseline.

Note that as $\beta_{max} \rightarrow 180°$, $e \rightarrow 1$. In general when $\beta_{max} > 140°$ many approximations used in estimating bistatic radar performance break down [1].

From Figure 2.3 one notes that the transmitter (circles not shown) and receiver are surrounded by circles. These circles are constant range ratio contours ($K = R_T/R_R$) [8]. The centres lie on the extended baseline.

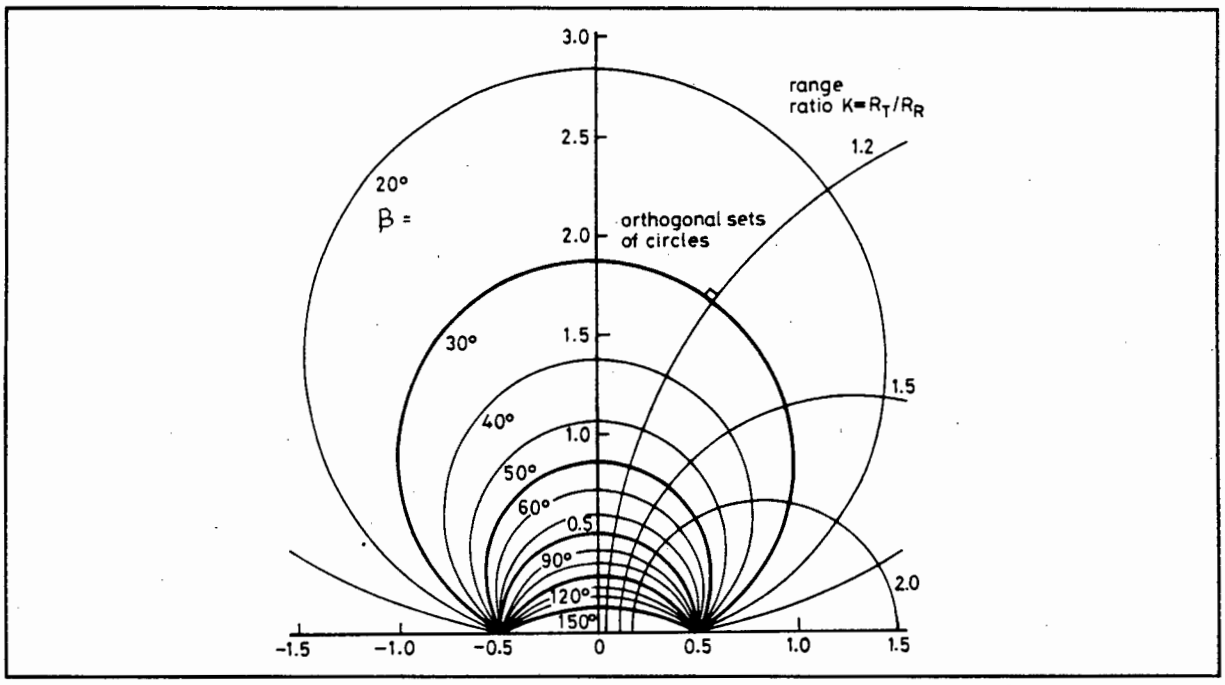

Figure 2.3 *Constant iso-β contours and constant range ratio contours (R_T/R_R).*

The equations for the centre (c) and radius (r) are given below.

$$r = \frac{K}{K^2-1}$$

$$c = \left(\frac{K^2+1}{K^2-1}\right) / 2$$

The intersection of the tangents of iso-β and range ratio contours are perpendicular. The K value changes from a negative value to a positive value as the centre of the baseline is crossed from the transmitter to receiver. It is close to unity at long ranges from the transmitter or receiver.

When the transmitter's look angle lies between 180° and 360°, the range ratio starts from zero and increases towards unity at a decreasing rate as R_T is increased. For other look angles the sightline crosses the midline into the receivers area and the ratio rises to a maximum exceeding unity and then falls back again towards unity.

2.4.5 CONSTANT POWER CONTOURS

Bistatic geometry affects the received echo power differently from the monostatic case. This is because the path loss factor for the bistatic case is $1 / R_T^2.R_R^2$ where as for the monostatic case it is $1 / R_M^4$. Now the effective range is the geometric mean $\sqrt{(R_T.R_R)}$. This section will illustrate how this affects the received power or signal to noise ratio on the bistatic plane [1][8].

Signal to noise ratio contours, where $R_T.R_R$ are kept constant for each contour are called ovals of Cassini. To obtain these curves one would solve the radar range equation described in section 2.4.2 for the SNR. This is shown below.

$$S/N = \frac{k}{R_T^2.R_R^2}$$

where

$$k = \frac{P_T G_T G_R \lambda^2 \sigma_B F_T^2 F_R^2}{(4\pi)^3 K.T.B.L_T L_R}$$

The term k is called the bistatic radar constant. The minimum SNR contour can be determined from:

$$(S/N)_{min} = k / \kappa^2$$

The ovals of Cassini are shown in Figure 2.4. These contours apply to any bistatic plane.

One notes from Figure 2.4 that the ovals shrink and finally collapse around the transmitter and receiver as the SNR increases. This same effect occurs if the baseline (L) length is increased. The point on the baseline where the ovals break into two parts is called the cusp. Here the oval is called a lemniscate (two parts).

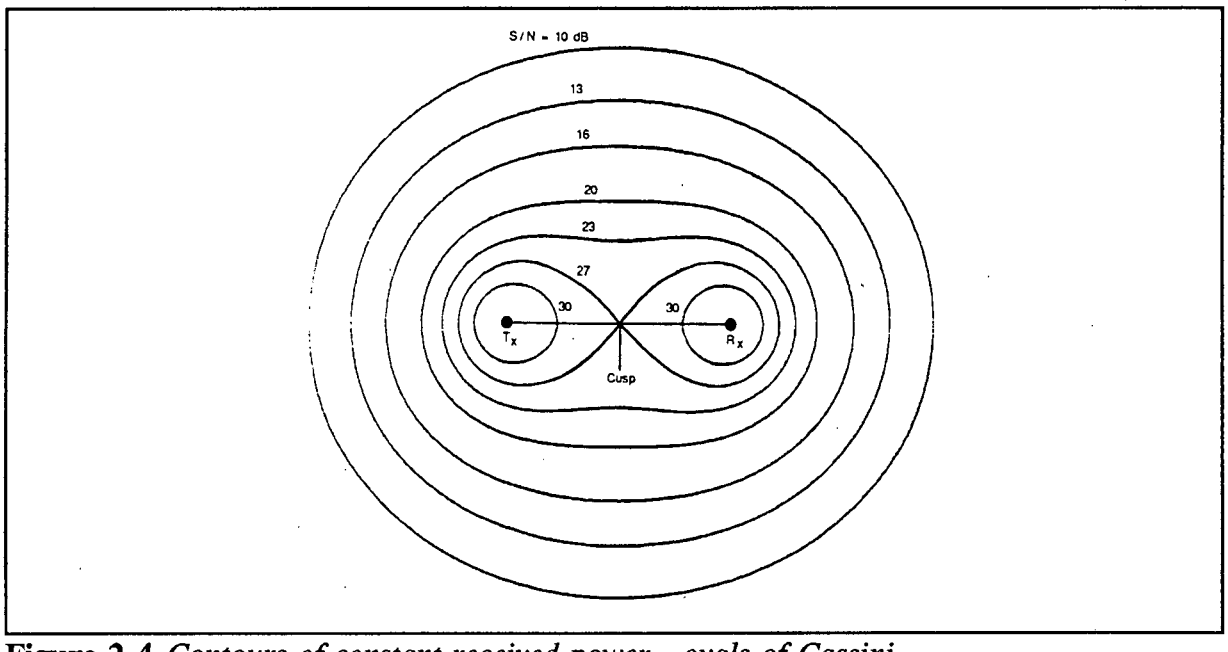

Figure 2.4 *Contours of constant received power - ovals of Cassini.*

At this point the target would be at the centre of the baseline and one arrives at the following equation [1]:

$$(S/N) = (16.k) / L^4$$
$$(S/N) = 2.\sqrt{\kappa}$$

From these equations three operating regions can be defined, namely:

1. **The receiver centred region.** This occurs when $L > 2\sqrt{\kappa}$ and $R_T >> R_R$. Here the ovals break into two parts.

2. **The transmitter centred region.** This occurs when $L > 2\sqrt{\kappa}$ and $R_R >> R_T$. Here the ovals break into two parts.

3. **The cosite region.** This occurs when $L < 2\sqrt{\kappa}$. Here the ovals remain single.

When L = 0 the ovals become circles which is the monostatic case. Some bistatic radar applications for the different regions are given in Appendix 1.

Another method of characterizing constant SNR contours is to plot the SNR contours as a function of bistatic ranges, each normalized to the baselength. This, however, is not shown here. See reference [1].

2.4.6 TARGET LOCATION AND COVERAGE

In a bistatic radar configuration one usually wants to know the target range and azimuth relative to the receiver, ie R_R and θ_R need to be calculated. This section will provide several equations which are used to determine these coordinates and the measurements required to solve them, such as the delay time. Other techniques are also briefly mentioned. This section concludes with a discussion of the coverage area of a bistatic radar.

In order to solve the target location (R_R, θ_R) from the receiver site certain parameters need to be known. These parameters are the baseline length (L), transmitter azimuth (θ_R) and the range sum. The baseline length is either set or it can be measured with a transmitter location system. The receivers look angle can either be measured directly or θ_T can be converted to θ_R.

Two methods are used to determine the range sum, namely:

1. **The direct method** [3]. With this method the receiver measures the time interval ΔT between the reception of the transmitted pulse and the target echo. The range sum is then calculated from:

$$(R_T + R_R) = c.\Delta T + L$$

2. **The indirect method** [3]. With this method synchronized stable clocks are used by the receiver and transmitter. The receiver measures the time interval ΔT between transmission of the pulse and reception of the target echo. The range sum is then calculated from:

$$(R_T + R_R) = c.\Delta T$$

Where c is the approximate speed of light (3×10^8 m/s) in a vacuum.

The equations that follow are used to solve for R_R and θ_R. These equations are obtained by solving the bistatic triangle described in section 2.4.1.

$$R_R = \frac{(R_T+R_R)^2-L^2}{2(R_T+R_R+L\sin\theta_R)}$$

$$R_R = \sqrt{(R_T^2+L^2-2.R_T L.\sin\theta_T)}$$

$$\theta_R = \theta_T - 2.\arctan\left(\frac{\cos\theta_T}{(c.\Delta T/L)+1-\sin\theta_T}\right)$$

Several other techniques can be used to solve the target location. The techniques used depend on the geometry of the system. Sometimes more than one receiver is required, such as in a netted multistatic system. Some examples are given below.

A theta-theta location technique uses the angles θ_T and θ_R and the baseline length. Normally θ_T is provided by a monostatic radar which acts as a cooperative bistatic transmitter [3][1].

Two or more receiving sites (multistatic system) can be used to detect targets. Target location is by means of combined angle measurements from each site. This technique is known as triangulation [18][19].

Another technique which only uses range information (trilateration) can also be used. Here the receiver measures the difference in propagation times from three separate transmitters. The locus of the target will lie on two hyperbolas. The point of intersection of these hyperbolas will indicate the targets position. This is also known as the hyperbolic measurement system [3].

By using only doppler measurements, it is also possible to determine the trajectory of the target [10]. Here a continuous record of the variation of the doppler frequency caused by the target must be measured as a function of time. This curve must then be matched with curves previously calculated for various trajectories.

The next important point in locating the target is to be able to define the coverage area of the bistatic radar. The bistatic coverage of a bistatic radar is defined as the region or area on the bistatic plane where the target is visible, i.e. detectable by the receiver and within line of sight of both transmitter and receiver [1]. Bistatic coverage is established in either of two ways, namely:

1. Detection-constrained coverage. Here the coverage is established by the maximum range oval of Cassini ($(R_T R_R)_{max}$). When the oval of Cassini surrounds both the transmitter and receiver (the cosite region), the coverage area will be approximated by the following expression:

$$A_{B1} \approx \Pi.\kappa\{1 - (1/64)(L^4/\kappa^2) - (3/16384)(L^8/\kappa^4)\}$$

When the oval of Cassini surrounds the transmitter and receiver with two separate circles (receiver-transmitter-centered region), the coverage area will be approximated by the following expression:

$$A_{B2} \approx (2\Pi\kappa^2/L^2)(1 + 2\kappa^2/L^4 + 12\kappa^4/L^8 + 100\kappa^6/L^{12})$$

The coverage area for a monostatic radar is (L = 0):

$$A_M = \Pi.\kappa$$

Figure 2.5 shows how the coverage area varies as a function of baseline length when compared to the monostatic coverage area [1]. It is assumed that a suitable LOS exists.

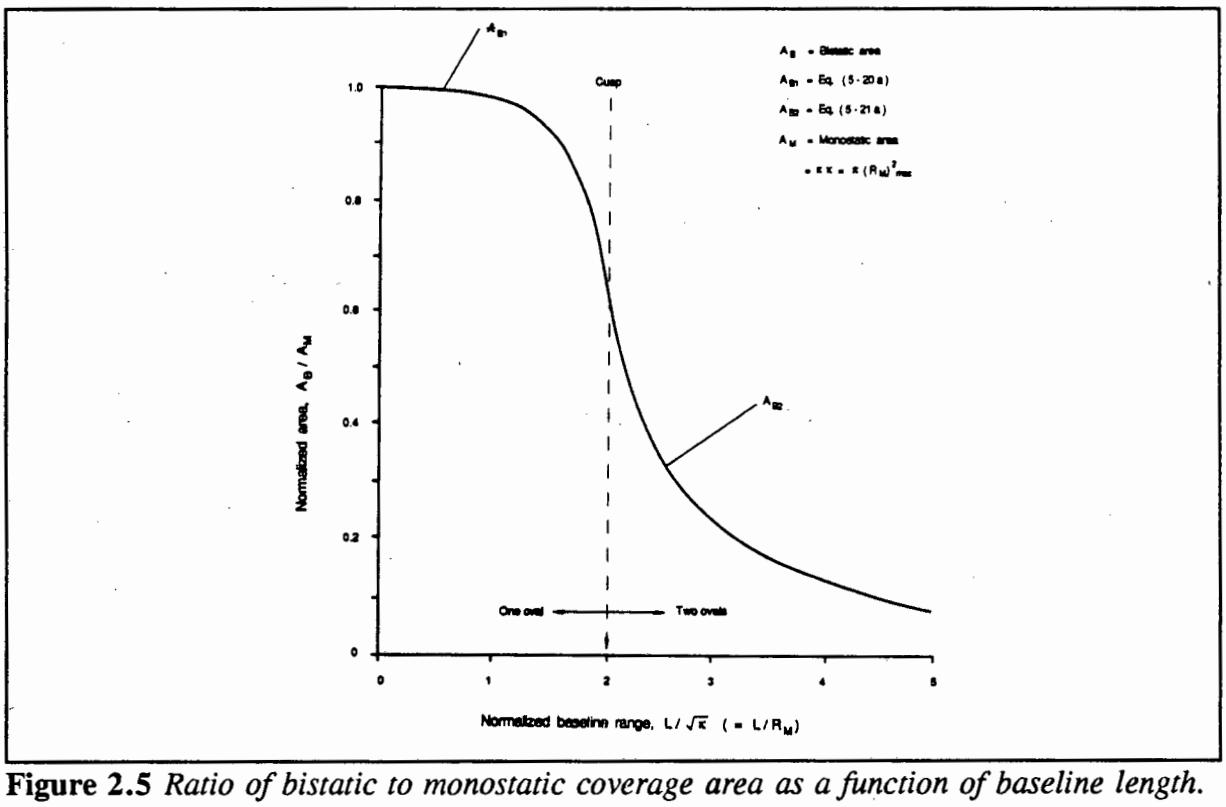

Figure 2.5 *Ratio of bistatic to monostatic coverage area as a function of baseline length.*

2. Line-of-sight-constrained coverage. Here the target must be simultaneously illuminated by the transmitter and receiver. For a smooth earth these requirements are established by coverage circles centered at each site. The bistatic coverage area is the area common to both circles [1]. Under realistic conditions

this form of coverage is affected by multipath, refraction, diffraction, shadowing and the earth curvature. For a 4/3 earth model, ignoring multipath, the radii of these coverage circles (in km) are approximated by [1][8]:

$$r_R = 130(\sqrt{h_t} + \sqrt{h_R})$$

$$r_T = 130(\sqrt{h_t} + \sqrt{h_T})$$

where

r_R = coverage area of the receiver

r_T = coverage area of the transmitter

h_t = target altitude

h_R = receiver antenna altitude

h_T = transmitter antenna altitude

The common coverage area is then the intersection of the two circles. This is:

$$A_c = 0.5[r_R^2(\phi_R - \sin\phi_R) + r_T^2(\phi_T - \sin\phi_T)]$$

where

$$\phi_R = 2\arccos\left(\frac{r_R^2 - r_T^2 + L^2}{2r_R L}\right)$$

$$\phi_T = 2\arccos\left(\frac{r_T^2 - r_R^2 + L^2}{2r_T L}\right)$$

The above equations are valid for $L+r_R > r_T > L-r_R$ or $L+r_T > r_R > L-r_T$. Whenever the right hand side of the inequality is not satisfied then $A_c = 0$, ie the coverage areas do not intersect. When the left hand side of the first inequality is not satisfied then $A_c = \Pi r_R^2$ and when the second inequality is not satisfied then $A_c = \Pi r_T^2$. This is because the transmitters coverage circle includes the receivers coverage circle or vica-versa.

For this particular bistatic system, the range sum is determined from the direct method and the coverage area is detection-constrained. Also the baseline L is less than $2\sqrt{\kappa}$. Hence the area will be determined by A_{B1}. One must also note that the coverage area is also dependent on the antennas. A_{B1} assumes that both the transmit and receive antennas operate equally in all directions. For this particular case the receive antenna only illuminates in one direction, hence $(R_T R_R)_{max}$ varies according to target azimuth. A_{B1} will therefore not be correct.

2.4.7 RANGE AND CELL AREA RESOLUTION

The range and cell area resolution differ significantly from the monostatic radar. The major differences are noted at the baseline. A relationship illustrating how the range and cell area resolution change as a function of target position will be given in this section.

From Figure 2.2, which shows the constant range ellipses one notices that the range between two ellipses, which are next to each other increases as the bistatic angle moves from the extended baseline to the midpoint line (perpendicular bisector of the baseline). In a monostatic case the distance between two circles is constant however in the bistatic radar, the distance between two range rings is:

$$\Delta R_M = c.\tau / 2$$

where τ is the pulse width. Hence this value determines the range resolution of the monostatic radar [20].

For a bistatic radar given a constant pulse width (τ), the separation between the range rings (ΔR_B) increases as the bistatic angle increases, so that on the extended baseline or at long ranges they become equispaced or start representing the monostatic case. An approximation for ΔR_B, the range resolution, is:

$$\Delta R_B = \frac{\Delta R_M}{\cos(\beta/2)}$$

$$= \frac{c.\tau}{2.\cos(\beta/2)}$$

From the above equation one notes that the bistatic operation is related to the equivalent monostatic operation by the factor $\cos(\beta/2)$. This relation is carried through to other operations. For example, bistatic target doppler is reduced by $\cos(\beta/2)$ compared to the equivalent monostatic doppler. This will be shown in Section 2.4.8. The bistatic RCS of complex targets is equal to the monostatic RCS, but reduced in frequency by $\cos(\beta/2)$ when β is small.

As stated in Section 2.4.4, as the bistatic angle increases, or the eccentricity of the ellipse increases the error in the bistatic approximations increase. The maximum error for ΔR_B (ϵ_{max}) occurs on the perpendicular bisector of the baseline. It is given as [1];

$$\epsilon_{max} = \frac{a(a'-a)}{b(b'-b)} - 1$$

where

a = semimajor axis of inner ellipse
a' = semimajor axis of outer ellipse
b = semiminor axis of inner ellipse
b' = semiminor axis of outer ellipse

ϵ_{max} is always positive hence the expression for ΔR_B yields a separation that is greater than or equal to the exact value. As the bistatic angle tends to 180° this approximation breaks down because the true separation cannot approach infinity.

The actual area illuminated by the bistatic radar is dependent on the transmit and receive antenna beamwidth. This then leads one onto the topic of cell area resolution. Cell area resolution can be divided into two groups, namely beamwidth-limited and range-limited cell area.

Beamwidth-Limited. This cell area is the intersection of the transmit and receive antenna beams. This is shown in Figure 2.6. At small grazing angles, a two dimensional approximation to A_b, which is a parallelogram is [1]:

$$A_b \approx \frac{(R_R.\Delta\theta_R)(R_T.\Delta\theta_T)}{\sin\beta}$$

Where $\Delta\theta_T$ and $\Delta\theta_R$ are the 3-dB beamwidths and $R_R.\Delta\theta_R$ and $R_T.\Delta\theta_T$ are the cross-range dimension for the receiver and transmitter respectively. The cross-range dimension increases as the range increases, hence the cell area increases. The beams are assumed to be parallel as the range sum is much greater than the baseline range. The cell area is at a minimum when $\beta = 90°$.

Range-Limited. This area is shown in Figure 2.6. This is similar to the beamwidth-limited case except that the pulse width needs to be taken into account. The two cross-range dimensions ($R_R.\Delta\theta_R$ and $R_T.\Delta\theta_T$) are multiplied to obtain the overall directivity factor, and in the Gaussian case this is equivalent to the monostatic operation with a 3dB, one way linear beamwidth of [8]:

$$W_E = \frac{\sqrt{2}.R_T.\Delta\theta_T.R_R.\Delta\theta_R}{\sqrt{(R_T.\Delta\theta_T)^2+(R_R.\Delta\theta_R)^2.\cos(\beta/2)}}$$

This corresponds to the transverse dimensions conventionally assigned to the resolution cells of monostatic radars. Note that it is the smaller cross-range dimension which controls the transverse dimension. Now, by combining W_E and the range resolution equation (ΔR_B) we arrive at the bistatic area resolution A_r.

$$A_r \approx \frac{W_E.c.\tau}{2.\cos(\beta/2)}$$

$$\approx \frac{c.\tau.R_T.\Delta\theta_T.R_R.\Delta\theta_R.\sec^2(\beta/2)}{\sqrt{2}.\sqrt{(R_T.\Delta\theta_T)^2+(R_R.\Delta\theta_R)^2}}$$

This equation should not be used when calculating the cell area near the baseline as the range resolution equation breaks down.

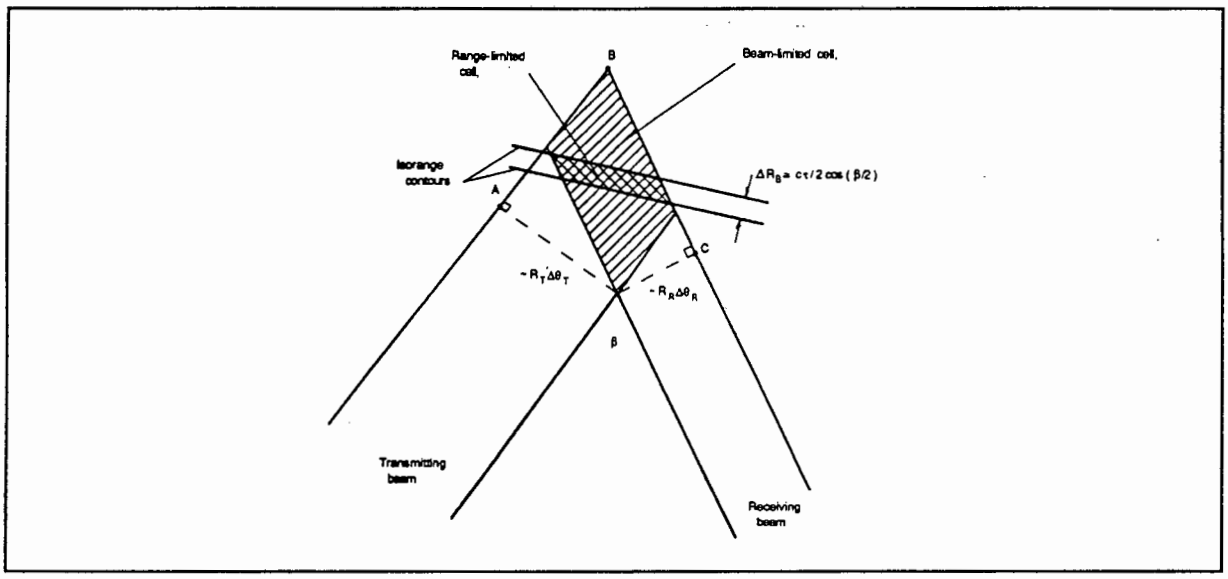

Figure 2.6 *Geometry showing the cell areas.*

2.4.8 BISTATIC DISTORTION AND DISPLAY CORRECTION

If the bistatic radar video signals are fed into a conventional PPI display, the display sweep rate synchronized with the transmitting antenna rotation rate and the target range synchronized to the PRF a radar display will be obtained [7]. This display will, however, be distorted. This section will show how to correct for this bistatic distortion on a PPI display.

The bistatic display will be distorted because it assumes $\Delta T = 2R_T/c$ and therefore the displayed range R is given by [7]:

$$R = (R_T + R_R)/2 - L/2$$

Targets at any point along the baseline are represented as having zero displayed range and cannot be resolved. The display distortion is that given by compressing the geometry so that transmit and receive sites merge to a single point.

Assume an aircraft flies across the centre of the baseline, from North East to South West. The trajectory of the aircraft on a PPI display is shown in Figure 2.7. The PPI display on the left shows the bistatic distortion while the display on the right has been corrected for this distortion.

To correct this distortion, the transmitter azimuth needs to be converted to the receiver azimuth and the receiver-to-target range needs to be determined. This will be for a PPI display centered at the receiver. In Section 2.4.6 equations were given in order to determine R_R and θ_R. These equations are repeated below.

Figure 2.10 shows the shapes the traces must have on a PPI display to correct for bistatic distortion. The PPI display is centred at the receiver.

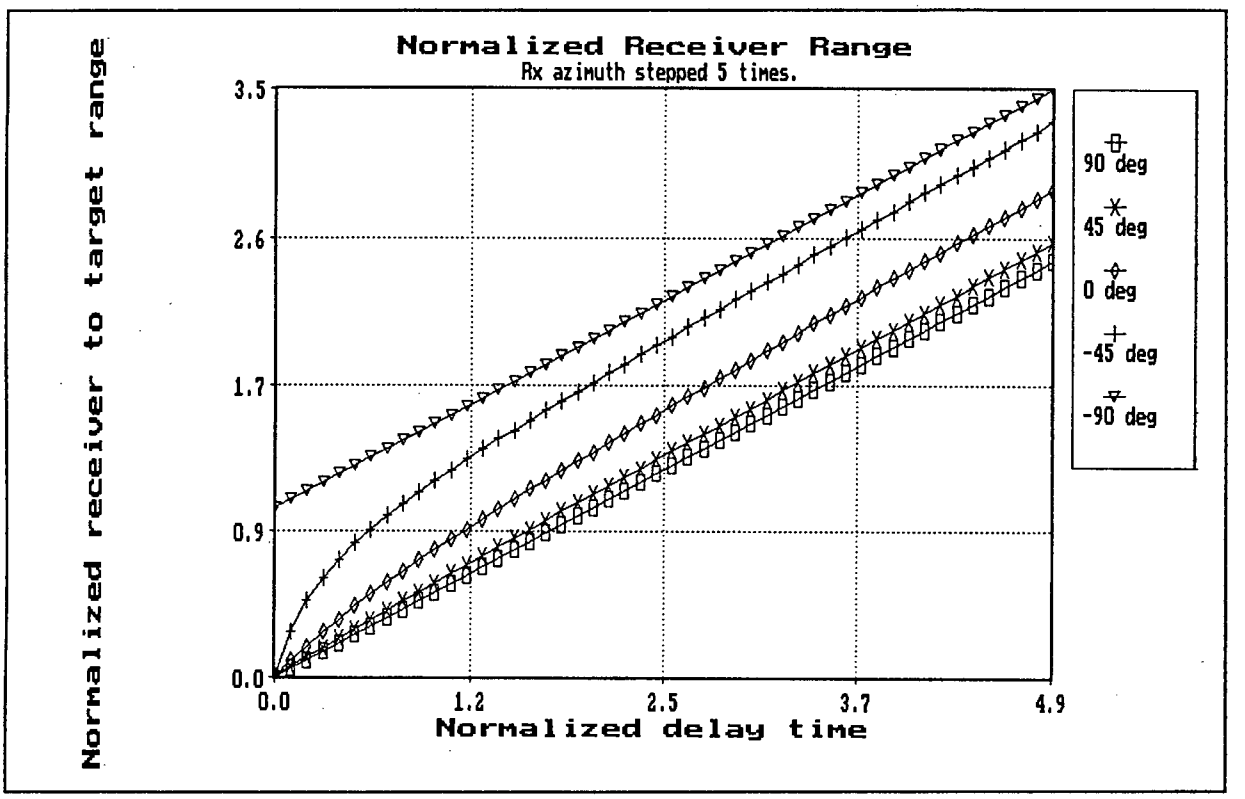

Figure 2.8 *Sweep law for a PPI display with the receiver at the origin.*

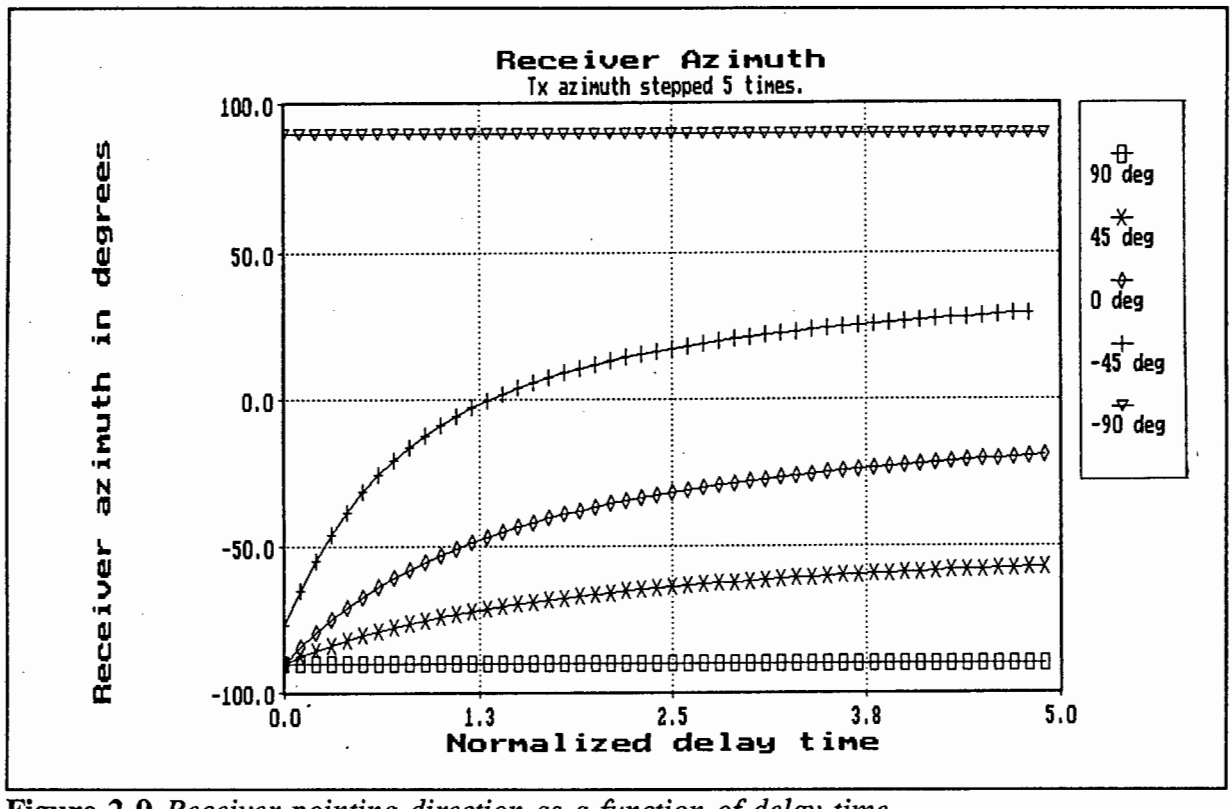

Figure 2.9 *Receiver pointing direction as a function of delay time.*

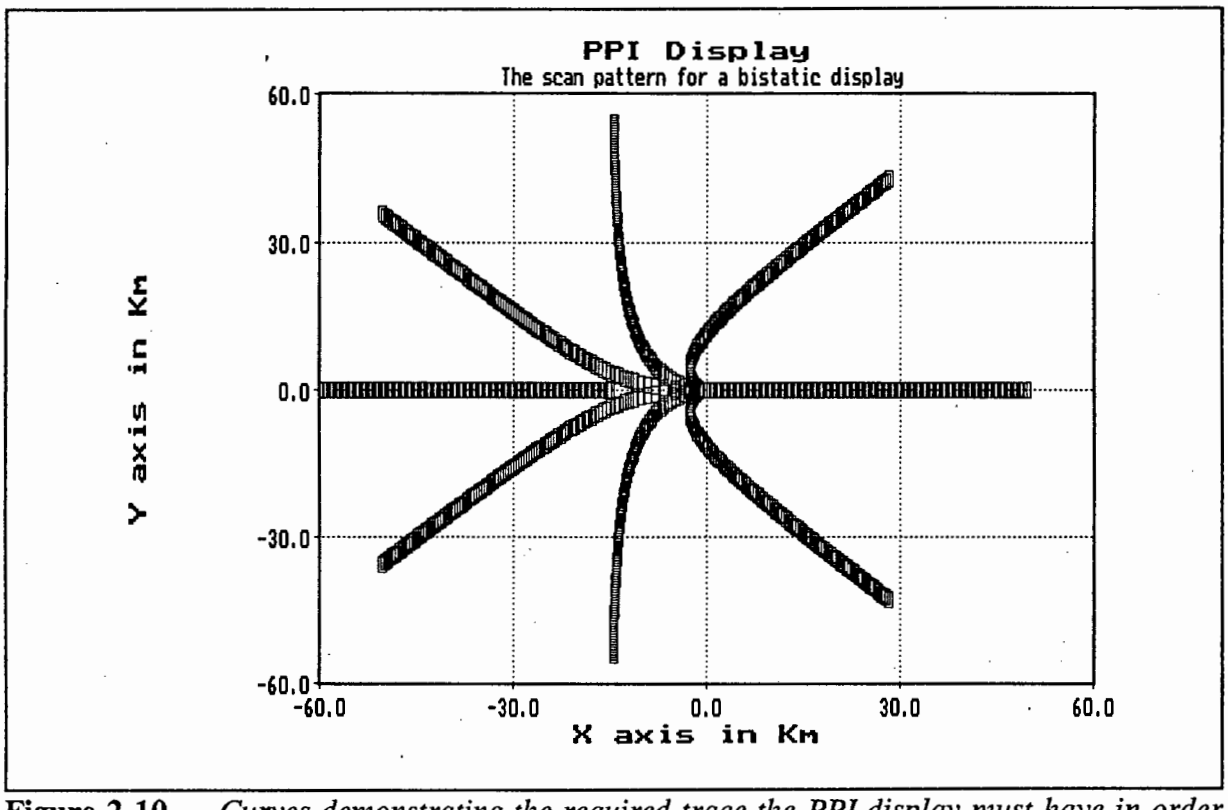

Figure 2.10 *Curves demonstrating the required trace the PPI display must have in order to correct for bistatic distortion.*

2.4.9 BISTATIC DOPPLER CHARACTERISTICS

In a bistatic radar a target flying at a constant velocity does not give a constant doppler shift as a monostatic radar would do. This is due to the geometry of the radar. A brief explanation will be given below, relating doppler shift to the targets position and velocity.

Firstly, an equation will be defined which gives a measure of the shape of the bistatic triangle and position of the target. This is commonly called the triangulation factor (F) [9].

$$F = \sin|(\theta_R - \theta_T) / 2|$$

The doppler frequency in a bistatic system can be split into three parts [9]. The first part gives an expression for the bistatic doppler frequency.

$$f_d = f_o.D.\cos(\delta)$$

Where f_o is the maximum doppler frequency of the target. The second part relates the direction in which the target is moving to an elliptic system by;

$$\delta = \psi - (\theta_R + \theta_T) / 2$$

From the above equation, the paths of zero doppler shift are ellipses and the paths of maximum doppler shift are hyperbolas orthogonal to the ellipses. The third part is the doppler reduction (D) equation caused by the triangulation factor (F).

$$D = \cos((\theta_R - \theta_T) / 2)$$
$$= \sqrt{(1 - F^2)}$$

The curves of constant doppler frequency (D) and the location of the above angles are shown in Figure 2.11.

When a target flies on a hyperbolic trajectory (corresponds to radial trajectory in a monostatic radar), the doppler frequency varies from a monostatic maximum at large ranges to zero when it crosses the baseline. This doppler information is useful in determining the target trajectory but limits the estimation of target velocity [9][10].

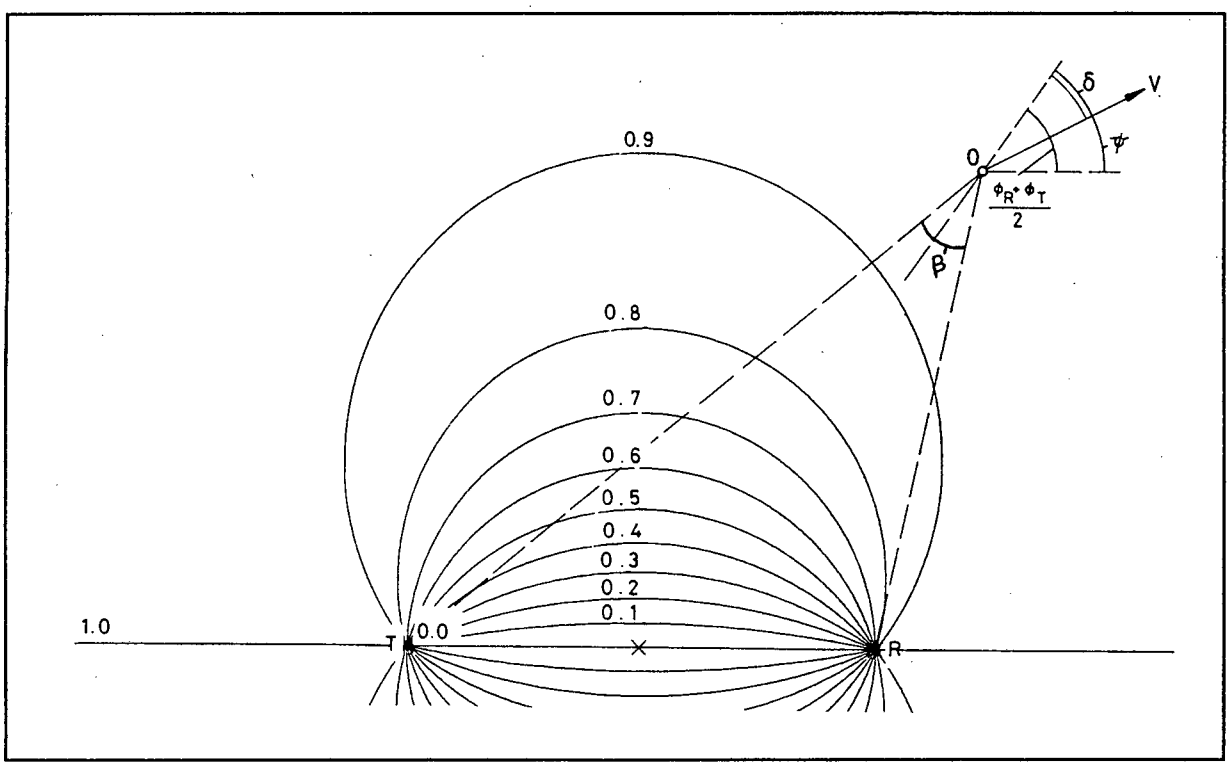

Figure 2.11 *Curves of constant doppler reduction.*

When -90° < δ < 90°, the bistatic target doppler is positive. Hence, a closing target referenced to the bistatic bisector generates a positive or "up" doppler. When $\delta = \pm 90°$ the bistatic doppler is zero, ie when the target flies on an isorange contour (ellipse) it has zero doppler frequency as was mentioned earlier.

2.4.10 RADAR TARGET CROSS SECTION

The radar target cross section (RCS) of a target is defined as an equivalent area producing the same amount of energy returned to the radar as would be produced by the mentioned scatterer [2]. The bistatic RCS is a function of bistatic and aspect angles. Hence it is different to the monostatic RCS. The bistatic RCS will be discussed below.

The bistatic RCS can be divided into three regions, the pseudomonostatic region, the bistatic region and the forward-scatter region [1].

The pseudomonostatic RCS region. The region is defined as the region greater than the bistatic threshold value. The monostatic-bistatic equivalence theorem (by Crispin and Siegel), which is only valid in this region, states:

> "For vanishingly small wavelengths, the bistatic RCS of a sufficiently smooth, perfectly conducting target is equal to the monostatic RCS measured on the bisector of the bistatic angle."

This region varies for different objects. The smaller the object being detected is, compared to the transmitted wavelength, the smaller the threshold value for the bistatic angle. For targets of more complex structures, this region is reduced considerably. Kell [1] developed a variation to the equivalence theorem for more complex targets. It states:

> "For small bistatic angles, typically less than 5°, the bistatic RCS of a complex target is equal to the monostatic RCS measured on the bisector of the bistatic angle at a frequency lower by a factor of $\cos(\beta/2)$."

Kell's complex targets are an assembly of discrete scattering centres. These models approximate various targets (aircraft, ships etc) when the wavelength is small compared to the target size. Whenever the equivalence theorem is valid it is possible to derive bistatic RCS data from the monostatic RCS data.

Another paper [12] determines the effect of coupling on the monostatic-bistatic equivalence theorem. Here an attempt is made to determine the error associated with the equivalence theorem where coupling between scatterers is significant. The paper concludes that very small bistatic angles can significantly affect the

monostatic RCS results obtained from bistatic data, however, this error can be corrected for.

The bistatic RCS region. This region is defined by the bistatic angle. The start of this region is at the bistatic angle for which the equivalence theorem no longer holds. Here the bistatic RCS starts to diverge from the monostatic RCS.

Three reasons have been identified by Kell. These reasons state why the bistatic RCS diverges from the monostatic RCS. They are:

1. Changes in relative phase between discrete scattering centres. This is analogous to fluctuations in monostatic RCS as the target aspect angle changes except in the bistatic radar, the bistatic angle is changing.

2. Changes in radiation from discrete scattering centres. This occurs when energy is reradiated back towards the transmitter. This causes a reduction in energy received by the bistatic receiver. In a monostatic radar the receiver is collocated with the transmitter, i.e. it would detect the reradiated energy, hence the reduction in the bistatic case.

3. Changes in the existence of centres, ie the appearance of new centres or disappearance of present centres. This can be caused by shadowing which occurs in the bistatic case and not in the monostatic case.

In general the bistatic RCS is lower than the monostatic RCS. There are, however, exceptions such as targets that have a low monostatic RCS but a large bistatic specular RCS or shadowing that sometimes occurs in the monostatic geometry and not in the bistatic geometry.

Another advantage of the bistatic RCS is the reduction of glint. In a monostatic radar, phase interference from two or more scatters causes a distortion of the echo

signal. As a result, changes in target aspect angle with respect to the radar cause the apparent phase centre of radar reflections to wander from one point to another. This random wandering of the radar reflecting centres can lead to jittered angle tracking, known as target glint [6].

Forward-scatter RCS region. This region is defined as the region where the bistatic angle is approximately 180°. Within this region the RCS can be more than 15 dB larger than the monostatic RCS. The magnitude of the objects forward scatter return does not depend on its material composition. Hence, a "forward scatter" radar might be able to detect an object with a monostatic RCS specially reduced through shaping or by treatment with radar-absorbing materials.

When a target (can be smooth or complex) is illuminated by the transmitter on the baseline, a shadow is produced if the targets dimensions are larger than the transmitted wavelength [14]. This shadow region occurs on the opposite side of the target from the transmitter. With the use of Babinet's principle it is possible to solve for the forward-scatter RCS [1][14].

Experiments conducted by Glaser [14], which are to determine the forward-scatter RCS, noted that the RCS value is best when the bistatic angle is 180° and deteriorates as the bistatic angle decreases.

2.4.11 CLUTTER

Clutter is defined as radar returns resulting from the interception of the radar beam with the ground, sea etc [2]. The presence of clutter almost always causes degradation of radar performance. The reason for this is that the target returns have to compete with the clutter returns and the radar clutter cross sectional area is usually larger than the target RCS. This section will examine bistatic clutter in terms of its scattering coefficient and give an example relating to this particular bistatic radar.

The equation for bistatic radar cross section of clutter is [3][15]:

$$\sigma_c = \sigma_{Bo}.A_c$$

where

σ_c = bistatic radar cross section of clutter

σ_B° = clutter scattering coefficient (clutter cross section per unit area illuminated surface)

A_c = clutter cell area

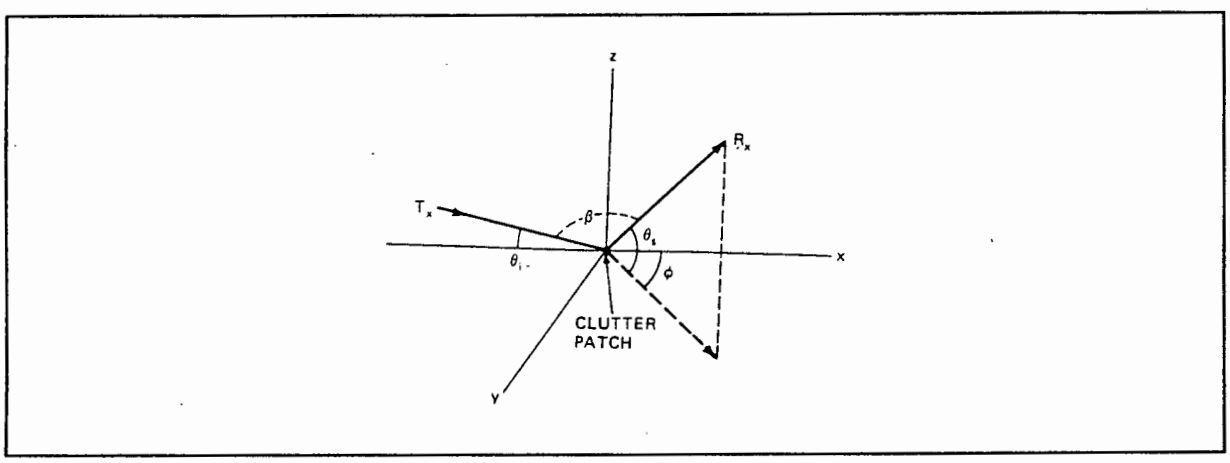

Figure 2.12 *Coordinate system for bistatic clutter measurements.*

The same equations and theory apply to the clutter cell area as was described in Section 2.4.7. Compared to monostatic clutter measurements, very little work has been done on bistatic clutter coefficients.

The clutter scattering coefficient can be split into two sections, namely the in-plane clutter scattering coefficient and the out-of-plane clutter scattering coefficient [3]. See Figure 2.12 which shows the coordinate system for the clutter measurements. The in-plane clutter scattering coefficient is when $\phi = 180°$ and the out-of-plane clutter scattering coefficient is for $\phi < 180°$. The monostatic case is presented when $\beta = 0°$. Also note that;

$$\beta = \arccos(\sin\theta_i \sin\theta_s - \cos\theta_i \cos\theta_s \cos\phi)$$

Clutter measurements are very sensitive and vary as a function of the surface composition, frequency, and the geometry. A summary of several measurement projects performed on bistatic clutter scattering coefficients is taken from [1] and shown in Table 1.2 in Appendix 1.

Clutter will not be discussed in any more detail as these measurements vary significantly from one author to another. For example, the out-of-plane measurements for $\sigma_B°$ done by Cost and Larson show only a limited correlation under identical geometries, polarization, frequency and similar ground compositions (sand, loam and 8cm soyabean foliage by Cost and 120cm weeds and scrub trees for Larson) [1]. The maximum variation is up to 20dB for $\sigma_B°$. It is best to measure the clutter at the radar site and then to design the bistatic radar accordingly. In Chapter 3 the subject of clutter will be readdressed in order to calculate the clutter power returns expected at the receiver for this particular application.

2.5 OTHER ASPECTS ON BISTATIC RADAR

Bistatic radars, unlike monostatic radars suffer from scan on scan coverage losses and when compared to the monostatic radar, are more prone to clutter. The bistatic radar will never exceed the target-receiver range capabilities of a monostatic radar. Methods of improving the performance of a bistatic radar are detailed below.

2.5.1 PULSE CHASING

In order to improve the performance of a bistatic radar, the radar must use all the target-scattered energy which arrives at the receiver and exclude all interfering signals, noise, sidelobe clutter and target echoes from incorrect areas. This means that the receiver has to look at the radar cell from which target echoes caused by the illumination from the transmitted pulse can arrive. In order to do this a high gain steerable receive antenna is required. As a pulse is transmitted the receivers antenna will swing away from the baseline and "chase" the pulse in order to cover the sensitive sector from which echoes might arrive. Hence the term pulse chasing.

In order for the receiver to illuminate the appropriate range cell its beamwidth needs to change as it chases the transmitted pulse. The beamwidth of the receiver is dependent on two criteria, namely the transmitter beamwidth and the pulse duration [8]. See Figure 2.13 for the geometry of the transmit and receiver beams.

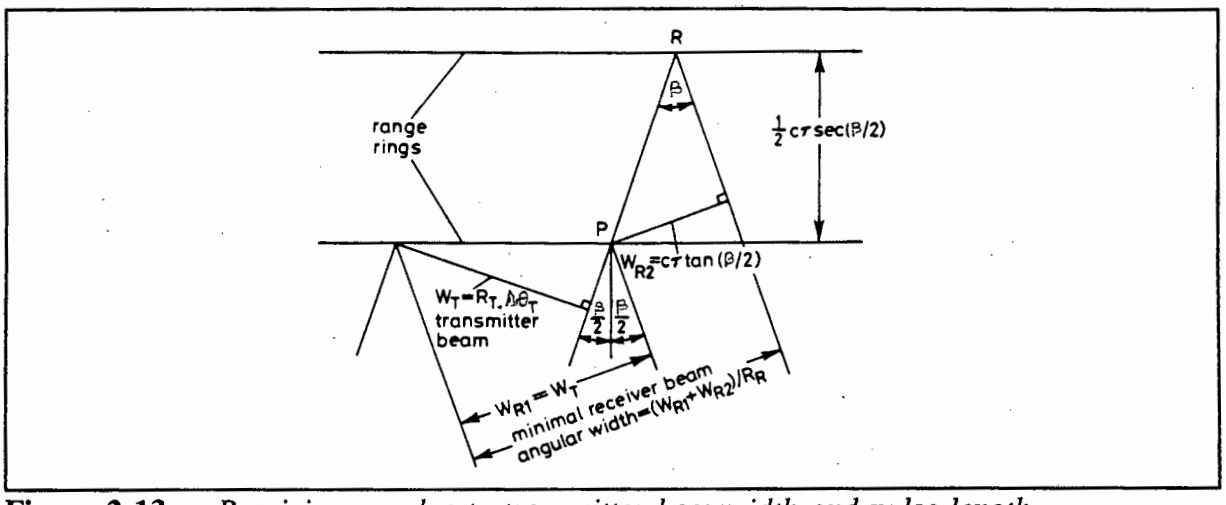

Figure 2.13 *Receiving arc due to transmitter beamwidth and pulse length.*

The beamwidth of the receiver is [8]:

$$\Delta\theta_R = ((\Delta\theta_{R1}.R_R) + (\Delta\theta_{R2}.R_R)) / R_R$$

where

$$\Delta\theta_{R1} = \Delta\theta_T.R_T / R_R$$
$$\Delta\theta_{R2} = (c.\tau.\tan(\beta/2)) / R_R$$

Recall from Section 2.4.4 the contours on constant range ratio (R_T/R_R), the receiver's beamwidth, ($\Delta\theta_{R1}$) will be reasonably narrow except near the receiver but if targets in its immediate vicinity are to be detected then the instantaneous receiving beamwidth must be very wide unless the transmitter's beam is extraordinarily narrow. The receiver's beamwidth ($\Delta\theta_{R2}$) is the reciprocal of the distance from the receiver, as with the transmitter beamwidth effect but now there is an extra strong directional dependence. The receiver's beamwidth requirement is small when the lines-of-sight of the transmitter and the receiver are nearly parallel, as is the case on the extended baseline or at long range. For detection close to the baseline it is large, especially at the receiver end.

The pointing direction of the receiver beam and the rate at which it changes are also important factors. Note that the echo from a target does not come directly from the current transmitted pulse position but from a point behind it where the transmitter beam intersects the appropriate range ring. The distance that the receiver trails behind the transmitted pulse is equal to the receiver range from which a target echo could originate from. From Section 2.4.8 one can see the contour that the receiver azimuth must follow in order to chase the transmitted pulse. The rate at which the receiver's azimuth changes is determined from the following equation [8]:

$$\frac{d\theta_R}{dt} = \frac{c.\tan(\beta/2)}{R_R} \qquad degrees/\mu s$$

In order for the receiver to meet these requirements, it will need either electronic scanning or fast switching over a set of narrow beams as mechanical scanning can not meet these requirements. A phased array antenna would probably be most suited [9].

2.5.2 BEAM SCAN ON SCAN

Beam scan on scan is usually used for surveillance purposes. Inefficient use is made of the radar energy when high gain scanning antennas are used by the transmitter and receiver, since only the volume common to both beams (the bistatic footprint) can be observed at any given time. Targets illuminated by the transmit beam outside the footprint are not detected. There are four remedies to this problem [3], i.e.:

1. **Step scan.** This is when the transmitter beam is fixed giving the receive beam time to scan the surveillance frame. The transmit beam is then stepped

to the next surveillance frame and fixed while the receive beam then scans this area and so on. The disadvantage is that a dedicated transmitter is required. An increase in surveillance time per frame is unsuitable for surveillance purposes.

2. **Multiple simultaneous beams-receivers-signal process.** Here multiple receive beams are used simultaneously to scan the transmit beam and complete the surveillance frame. The disadvantage is that the complexity and cost of the system is increased as separate receivers must be used for each beam.

3. **Pulse chasing.** This is described in section 2.5.1. The disadvantage with this system is that an expensive inertialess antenna (phased array) is required with complex and precise beam scheduling.

4. **Floodlight beams.** Either the transmit or receive beams floodlight the surveillance area and then the receive or transmit beams respectively scan this area. The disadvantage with this system is that there is a reduced S/N ratio as the gain of the system is reduced. It also suffers increased clutter levels and decreased target resolution and angle measurement accuracy.

In this particular system a floodlight receiver beam is used while the transmitter has a fan beam antenna. This causes $(R_T.R_R)_{max}$ to be reduced by a factor of 10 when compared to the base case [1]. The base case is defined as having one transmit and one receive beam with no scan on scan losses.

2.6 CONCLUSION

From this chapter one noted that a bistatic radar is significantly more complex than a monostatic radar. This is due to the bistatic geometry. This separation between the transmitter and receiver give the bistatic radar some distinct advantages. Some of these advantages are listed below.

1. In a military context, a monostatic radar is susceptible to external interference, such as jamming devices. The transmitter being an active input clearly advertises its position due to the emission of RF pulses. In a bistatic system the receiver is a passive element and thus difficult to detect.

2. For air surveillance radar applications in an area containing several airfields. Each airfield will have its own receiver. The targets will be illuminated by one high power, expensive transmitter located in the required coverage area. This will eliminate the mutual interference between several transmitters and receivers and the utilization of the spectrum is improved.

3. If a multistatic environment, as described in 2 above, is netted, the probability of target detection is improved. In addition, the range resolution is improved by triangulation and the cooperation of many units can be a protection against the failure of individual units.

4. When the radar operates in the forward scatter region the targets RCS is improved by up to 15dB. The forward scatter RCS is independent of target shape.

5. Doppler information can be used to determine the trajectory of the target.

6. The transmit and receive antennas can be designed independently to fulfil a specific function such as pulse chasing for air surveillance purposes.

7. An airborne bistatic system has the ability to control clutter (clutter tuning). The ground clutter spectrum can be manipulated by controlling the relative motion of the two aircraft with respect to the target. This is done in forward-looking synthetic aperture radar.

8. Blind speeds are eliminated due to the isorange contours.

Bistatic radars also suffer significant disadvantages when compared to the monostatic radar. Some of these are listed below.

1. Bistatic radars require additional complex circuitry in order to maintain synchronization between the receiver and transmitter. The PPI display also needs to be corrected for bistatic distortion.

2. The resolution (range, isorange, doppler and cell area) is degraded as the target approaches the baseline or the bistatic angle approaches 180°.

3. The receiver is more susceptible to clutter near the baseline due to the degraded cell area resolution. Also if the receiver has a wide beamwidth it is more susceptible to noise interference directed towards it.

4. The coverage area of a bistatic radar can never exceed that of a monostatic radar.

5. Targets on the baseline become indeterminate as the transmitted pulse arrives at the same time as the target echo.

6. The receiver can be saturated when the transmit beam sweeps directly over the receiver. During this period the receiver will have to switch in several dBs of attenuation.

Another point noted is that as the bistatic angle tends towards zero or the target range becomes large, the bistatic theory tends towards that of the monostatic.

It is evident from this chapter that a bistatic radars performance can never exceed that of a monostatic radar. However a bistatic radar has some distinct applications which cannot be implemented by the monostatic radar.

CHAPTER 3
AN INDEPENDENT BISTATIC RADAR RECEIVER

An experimental bistatic radar receiver has been built at the University of Cape Town. This radar has been designed for short range air surveillance purposes. It hitchhikes off the L-Band radar at D.F. Malan airport, where the transmitter is noncooperative. Synchronization between the transmitter and receiver is achieved by direct breakthrough. Target detection is achieved by illuminating the target with the transmitters rotating fan beam antenna and the receiver floodlight antenna. This type of radar has also been called a parasitic radar [1].

Two projects of a similar nature have been noted in the literature. In the first project [7], a totally independent bistatic receiver using the transmissions from a UHF air traffic control radar was built at University College London. In the second project [13] the independent bistatic receiver also hitchhiked off an air traffic control radar. The transmitter transmitted 500kW RF pulses at a frequency of 591MHz. This experimental system was built near the Blackpool airport in St Annes.

The aim of this chapter is to show the reader that it is possible to build a cost-effective, functional bistatic radar receiver which does not involve complex circuitry. The receiver, which is still in the experimental stage, will be broken up into three sections, i.e. the front end, the synchronization section and the display. Each section will be given a technical description. The performance in terms of noise figure, sensitivity etc, will also be discussed. As a bistatic radar is inherently prone to clutter, clutter predictions will also be made. Finally conclusions will be drawn regarding the feasibility of the present system.

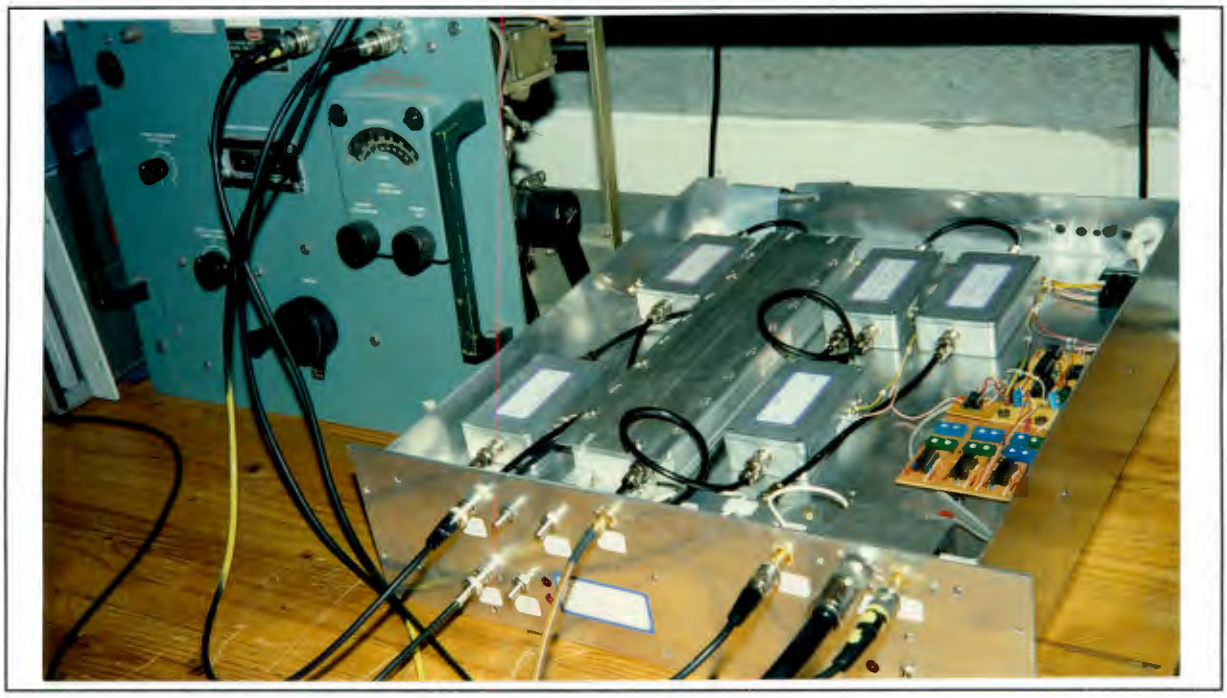

A photograph of the bistatic radar receiver at UCT.

3.1 GEOGRAPHICAL LAYOUT OF THE RADAR

In order for the reader conceptualise the bistatic radar layout and coverage area, a few parameters and a map of the Cape Peninsula will be given in this section.

The transmitter is situated at D.F. malan airport and the receiver at the University of Cape Town. The separation between the transmitter and receiver (baseline range) is 15km. Figure 3.0 shows the geographical layout of the radar system. Note that the baseline runs from West to East with the receiver facing in an Easterly direction. Targets behind the receiver (West of the receiver) will not be detected as they are not illuminated by the receiver. The receiver is also 200m higher than the transmitter. Note the areas where the Cape Flats and mountain ranges are located as these become significant when discussing clutter in Section 3.4. The maximum target range is 127km. How this figure was obtained will be shown in Section 3.3.4.4.

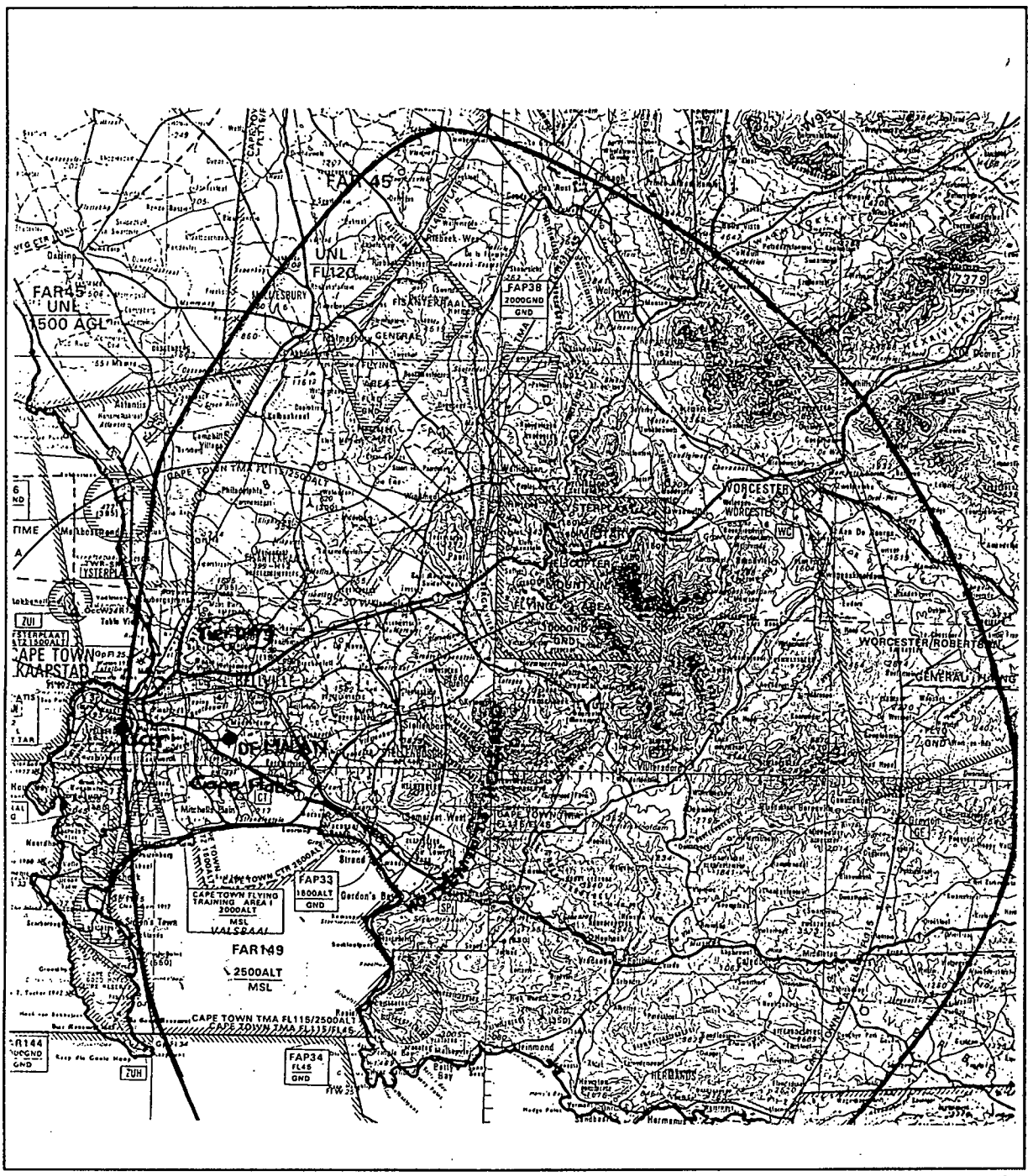

Figure 3.0 *Geographical layout and coverage of the bistatic radar in Cape Town. The maximum on axis range is 127km.*

3.2 TRANSMITTER PARAMETERS

The L-band transmitter of the air traffic control radar at D.F. Malan airport is being used. The transmitter has the following parameters:

1. PRF = 400Hz with a 50Hz wobulation
2. Pulse width = 2.5μsec
3. Transmitted power = 2.5MWatts
4. Antenna rotation rate = 5rpm

The transmitter operates at two frequencies. On odd days it transmits at 1.304GHz $\pm$ 7MHz and on even days at 1.35GHz $\pm$ 7MHz. The PRF is wobulated in order to prevent blind speeds. The 50Hz modulating frequency is derived from the mains in order to generate the wobulated 400Hz frequency. The depth of wobulation is $\pm$20Hz. Two 50Hz cycles in the PRF were measured at UCT. Figure 3.1 shows the variation in frequency during these cycles. The transmitter is also non-coherent from pulse to pulse.

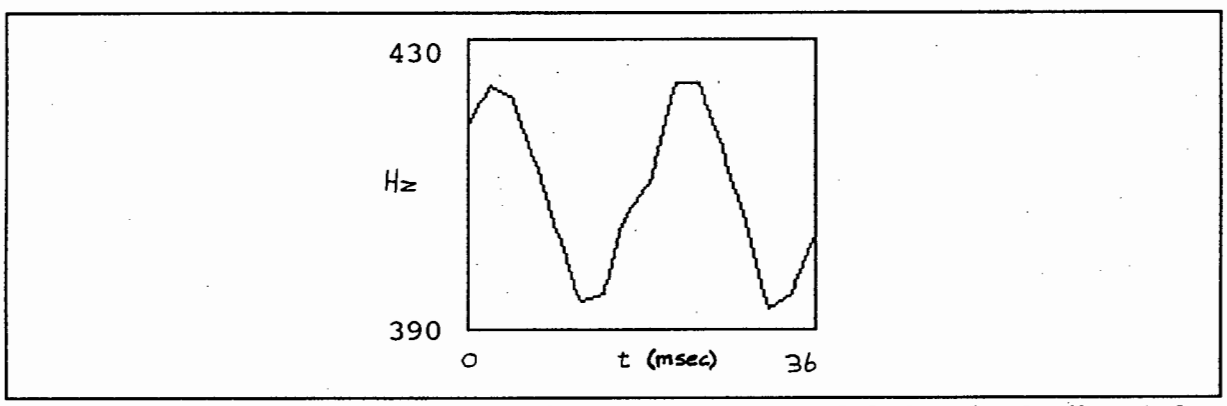

Figure 3.1 *The frequency variation in the PRF was measured during the dwell period at UCT. The graph clearly shows the 50Hz wobulation.*

The radiation patterns of the antenna are shown in Figure 3.2 and 3.3. Figure 3.2 shows the azimuth radiation pattern and Figure 3.3 shows the elevation radiation pattern.

The azimuth radiation pattern has a pencil beam shape. The 3dB beamwidth is 1.35°. The first nulls are at $\pm 2°$ and the first sidelobes are 23dB down from the mainlobe.

The antenna is tilted at 4° from the horizontal in elevation. Above the 4° elevation, the radiation pattern is approximately cosecant-squared and below the radiation pattern is approximated by:

$$G_T = \exp(-a^2 (4 - A_T)^2)$$

where

$a^2 = 2.776/\delta$

$\delta = 4.9°$ (from Figure 3.2)

The antenna polarization is horizontal with a maximum gain of 34dB for clear weather. In wet weather the antenna is circularly polarized with a maximum gain of 31dB.

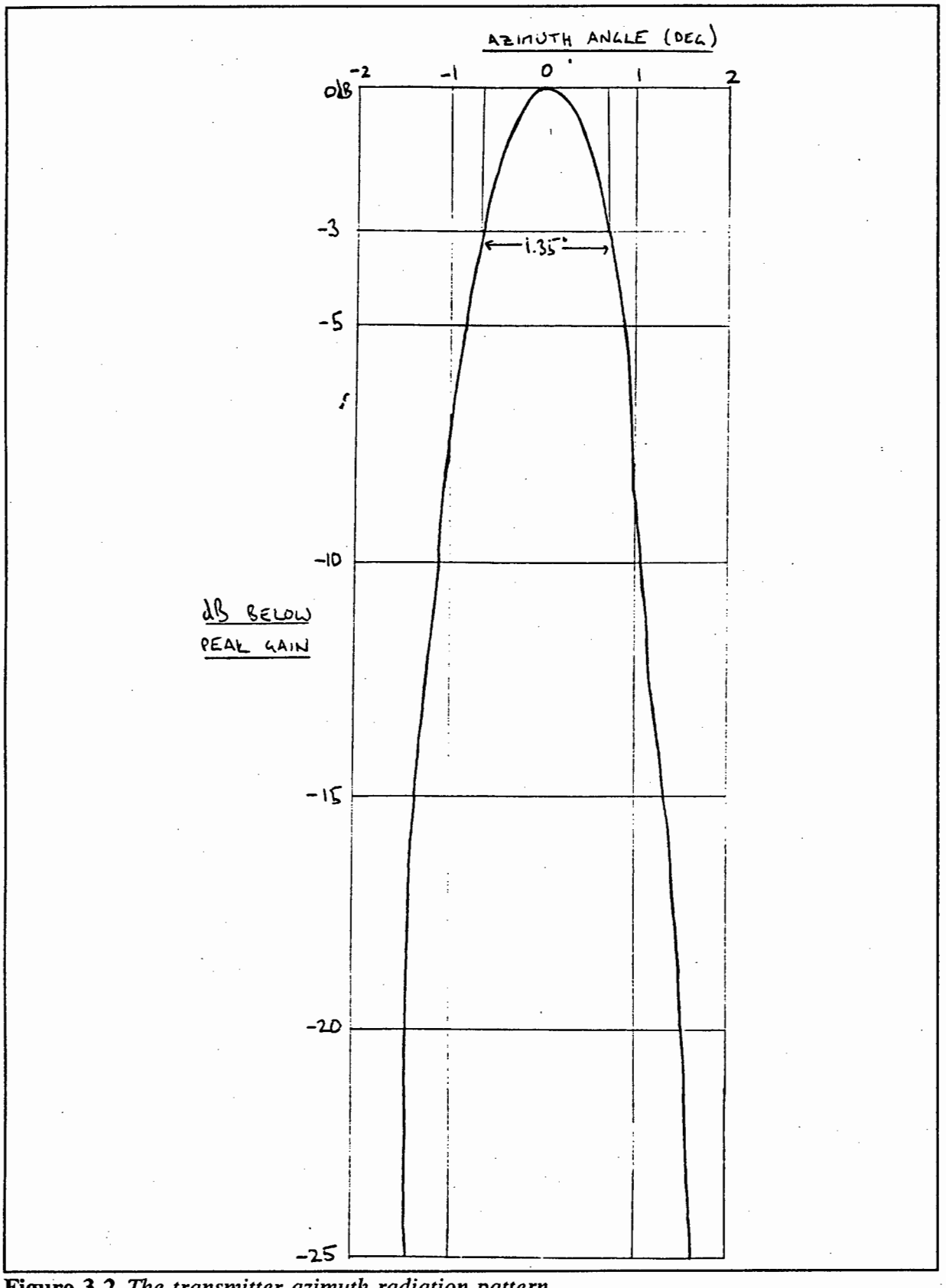

Figure 3.2 *The transmitter azimuth radiation pattern.*

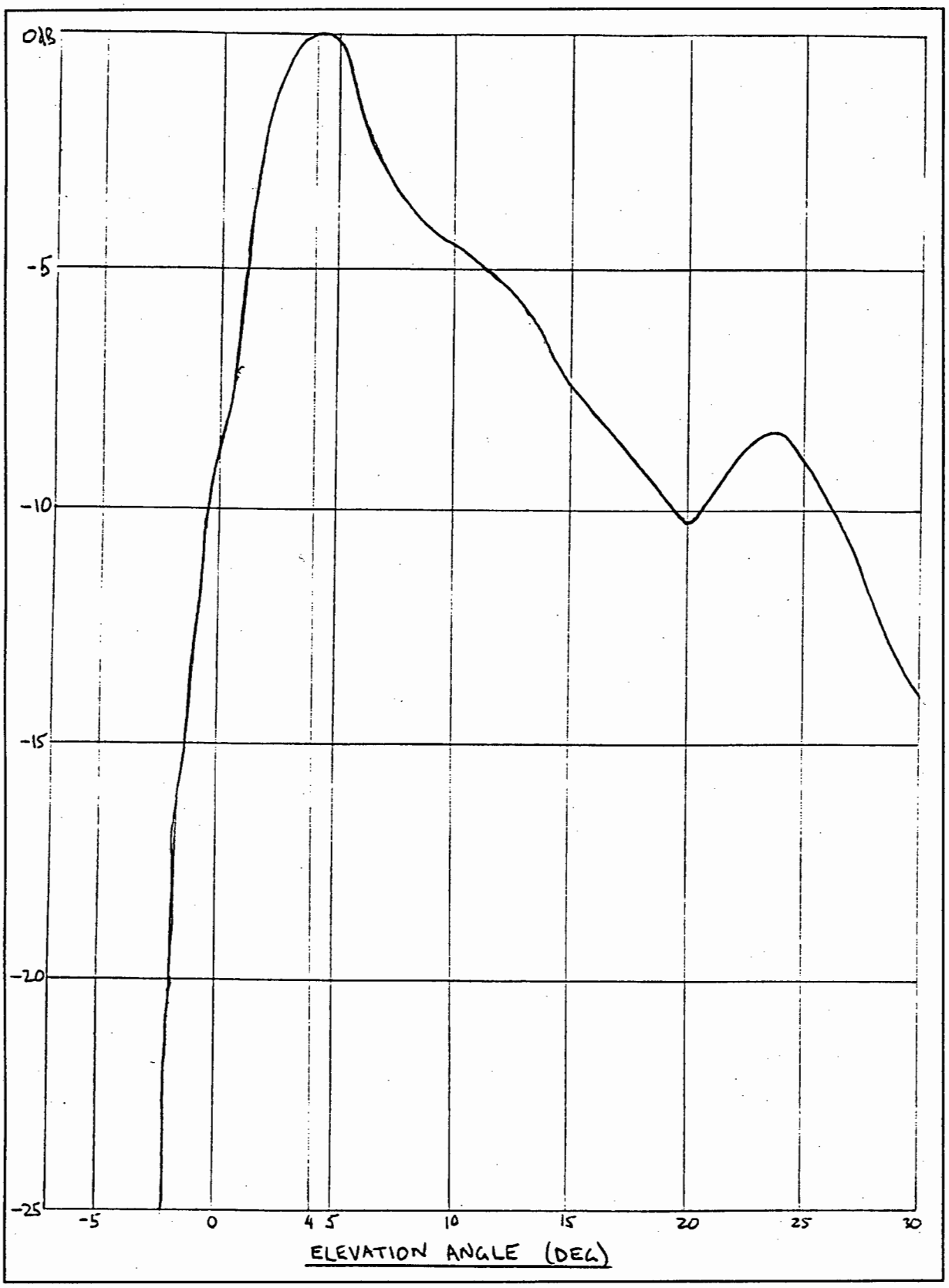

Figure 3.3 *The transmitter elevation radiation pattern.*

3.3 RECEIVER SYSTEM ANALYSIS

This bistatic receiver is comprised of three main components. These are listed below.

1. The superheterodyne receiver used to detect the signal.

2. The synchronization component which regenerates the PRF and transmit antenna azimuth information and synchronizes the display.

3. The display processor which corrects for bistatic distortion on the PPI.

Figure 3.4 shows a block diagram of the bistatic receiver with its individual component systems. The sections which follow will determine the design criteria for the receiver, describe the operation of each component system in the receiver and then give the receiver specifications.

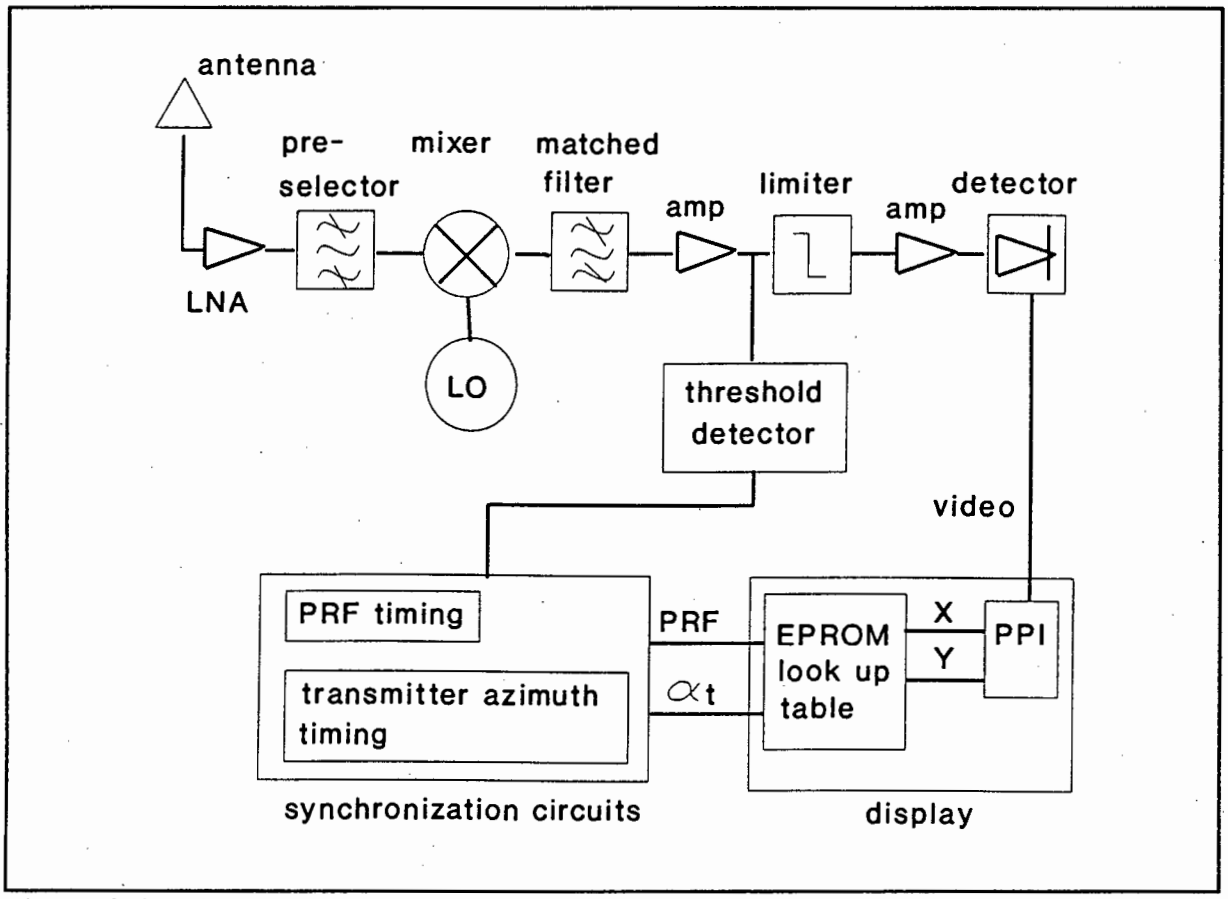

Figure 3.4 *A block diagram showing the main component systems of the bistatic radar receiver at UCT.*

3.3.1 RECEIVER REQUIREMENTS

In order for this bistatic radar to be operational and feasible certain criteria had to be established. The receiver would then be designed to meet them or get as close as possible. These criteria are listed below.

1. It must illuminate a semi-hemisphere with the receiver being at the origin facing D.F. Malan airport.

2. It must have a detection probability of 80% and false alarm probability of 10^{-8}.

3. It must not saturate when detecting a target at the minimum target-receiver range (75m) assuming an RCS of $50m^2$.

4. It must not saturate when being illuminated by the transmitter.

5. It must not saturate when receiving scattered clutter returns.

6. It must regenerate the PRF of the transmitter at the receiver.

7. It must generate transmitter azimuth information.

8. It must correct for bistatic distortion on the PPI display.

For the receiver front end, the aim will be to maximize the sensitivity to obtain the maximum dynamic range. To prevent saturation of the receiver a variable gain amplifier will have to be built. This will prevent saturation by the clutter and the main bang pulses but will still maximize the dynamic range.

No constraints have been put on the accuracy of the regenerated azimuth and PRF information, as this system is still the first prototype and error analysis is not within the scope of this project. Other complications such as the 50Hz wobulated PRF and short dwell period make it difficult to determine a realistic error in the PRF synchronization.

3.3.2 BANDWIDTH REQUIREMENTS

By definition: the instantaneous bandwidth of a component is the frequency band over which the component can simultaneously amplify two or more signals to within a specified gain tolerance. The tuning range is the frequency band over which the component may operate without degrading the specified performance if suitable electrical or mechanical controls are adjusted [21].

The bandwidth of the receiver is an important property as it affects the noise and signal. To maximize the signal to noise ratio matched filtering is required [24]. That is when;

$$BW.\tau = 1$$

Where BW is the bandwidth and τ is the pulse width. Ideally the transfer function of the filter must be the same as that of the pulse. The frequency spectrum of the transmitted 2.5μsec pulse will be a sin(x)/x function. This is shown in Figure 3.5. Hence the ideal bandwidth for the receiver is 400kHz.

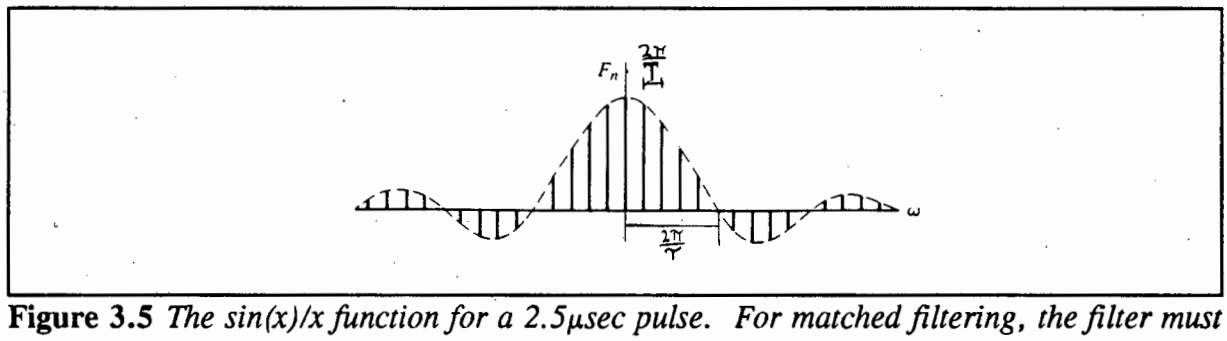

Figure 3.5 *The sin(x)/x function for a 2.5μsec pulse. For matched filtering, the filter must have the same transfer function.*

The front end of the receiver needs to be tunable as two frequencies (1.304GHz and 1.35GHz) are being transmitted. Hence the tuning bandwidth of the receiver must be 60.4MHz. This also takes into account the 7MHz drift in the RF frequency.

The received RF signal is down converted to an IF frequency. The mixing process is described by:

$$IF = RF \pm LO$$

An IF frequency of 70MHz was selected for the receiver for two reasons. Firstly, according to the mixer spurious-effect chart [21], the spurious frequencies in this region originate from extremely high-order terms in the power series model and are consequently sufficiently low in amplitude that they can be ignored. The power series model represents the mixer and is a way of predicting the various spurious effects that are noted in the mixer operation. More will be said about this in Section 3.3.2.4.

Secondly a 70MHz IF main amplifier was already available.

Hence the local oscillator must be tunable at two frequencies, namely 1.374GHz and 1.42GHz. A frequency map of the receiver is shown in Figure 3.6.

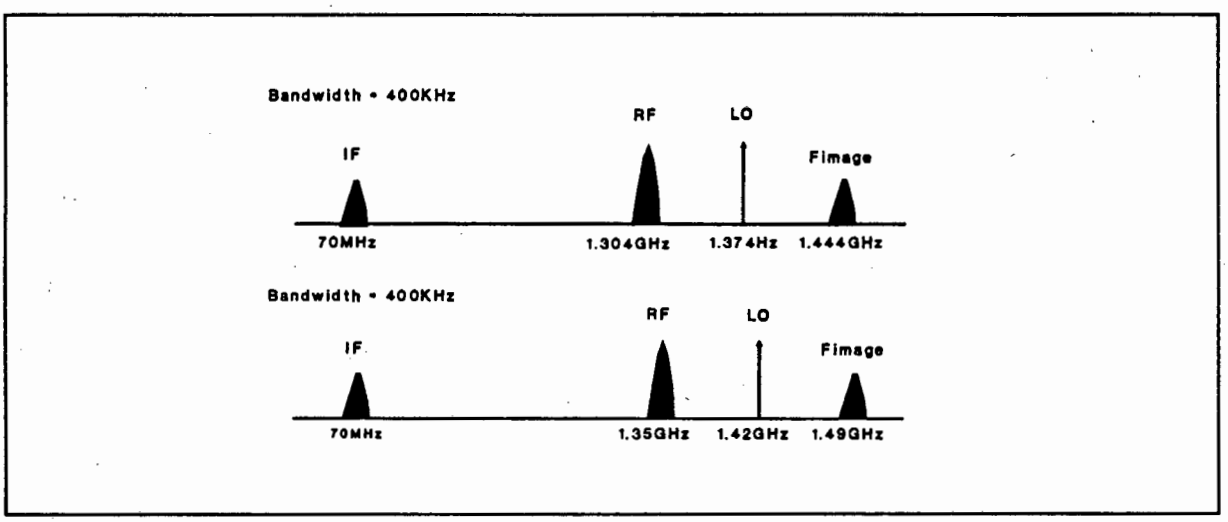

Figure 3.6 *Frequency map of the bistatic radar receiver.*

3.3.3 THE COMPONENTS OF THE RECEIVER

This bistatic radar uses a superheterodyne receiver. The superheterodyne principle is when the received echo pulse (RF) is shifted down to an intermediate frequency (IF) where amplification and filtering can be done more effectively [21]. An advantage of this type of receiver is that the LO frequency can be varied to follow the transmitter frequency without disturbing the filtering at IF. The front end of the receiver can be seen in Figure 3.4 from Section 3.3. Each component in the front end of the receiver will now be described in the following sections.

3.3.3.1 ANTENNA

In this receiver it was decided to floodlight the coverage area. The reason for this is that the antenna design would be much simpler and control over the antenna would not be required. To satisfy this condition and criteria 1 in Section 3.3.1, a dipole array antenna was designed and mounted on the top of the Engineering building.

The dipole array consists of two dipoles lying broadside to each other, the one dipole being parasitic. The parasitic dipole is longer than the driven dipole making it the reflector. This dipole array is also known as a Yagi antenna [20]. Figure 3.7 shows the antenna used by the receiver.

The gain of the antenna is given by [20]:

$$G(\theta) = G_o.\cos((\pi/2)\sin(\theta)) \,/\, \cos(\theta)$$

G_o is the on axis gain and is 1.64. The antenna gain pattern is shown in Figure 3.8. From Figure 8.14 in reference [20] the directivity of the antenna is obtained and is 3.1. The antenna is mounted horizontally, making the polarization horizontal.

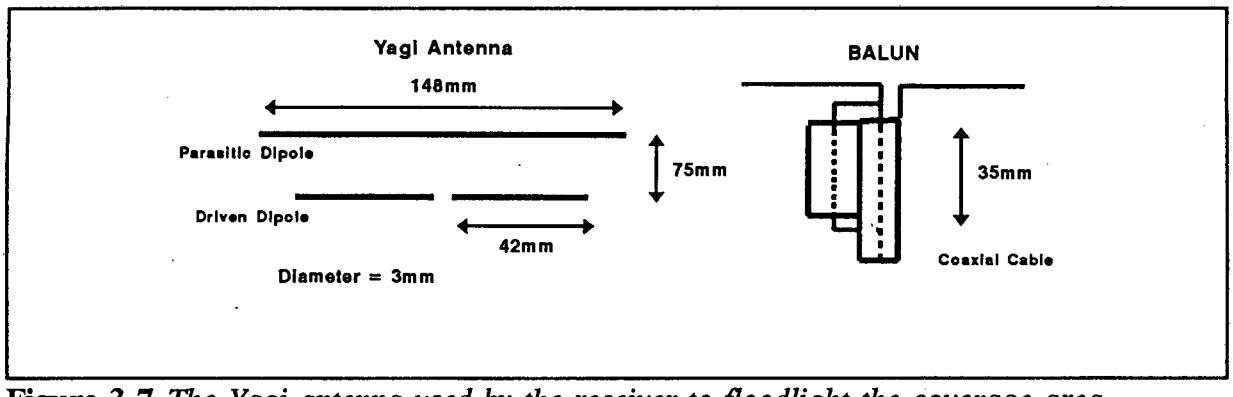

Figure 3.7 *The Yagi antenna used by the receiver to floodlight the coverage area.*

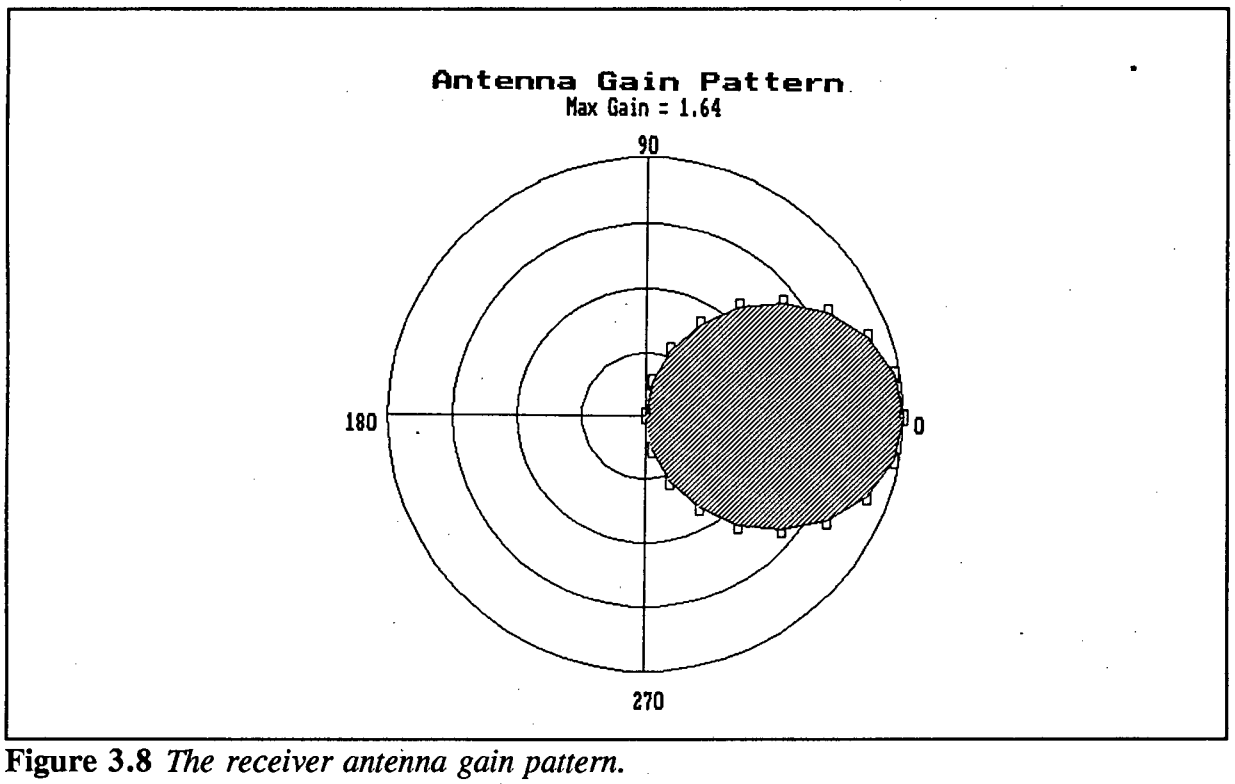

Figure 3.8 *The receiver antenna gain pattern.*

The antenna then feeds into a 50Ω coaxial cable. As this type of antenna is inherently balanced due to its construction, a BALUN is required to match the unbalanced coaxial cable to the antenna [22]. The construction of the BALUN is shown in Figure 3.7.

The return loss (S11 parameter) of the antenna against frequency was measured and is shown in Figure 3.9. From Figure 3.9 the bandwidth and input impedance of the antenna can be determined. The 3dB bandwidth is 10MHz with the centre frequency at 1.337GHz and the return loss at 1.304GHz and 1.35GHz is -23dB. The input impedance is 55Ω, hence the antenna is suitably matched to the coaxial cable.

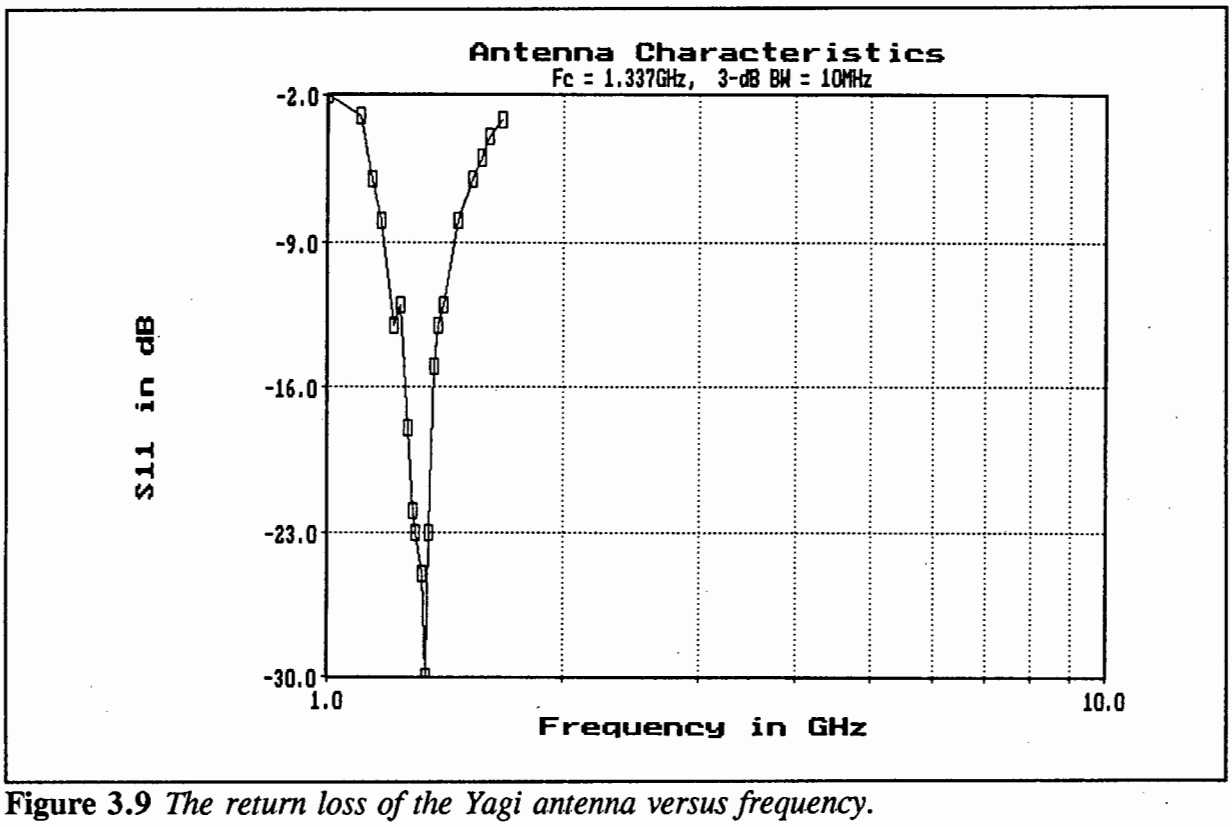

Figure 3.9 *The return loss of the Yagi antenna versus frequency.*

3.3.3.2 LOW NOISE AMPLIFIER AND ANTENNA FEED

A low noise amplifier (LNA) is mounted at the antenna. This was done to compensate for the degradation in the noise figure of the system due to the loss in the coaxial cable feeding the antenna.

An RG 217 coaxial cable was used to connect the LNA to the receiver. The cable is 30m long and a loss of 7.4dB was measured, which agreed with the manufacturers specifications (7.2dB/100ft). The cables S21 parameter can be viewed in Figure 3.10. The delay time of the signal in the cable is 150nsec.

The design for the LNA comes from the Mini-Circuits application notes, reference [22]. The circuit diagram of the amplifier is shown in Figure 3.11. From Figure 3.11, the amplifier is one chip (MAR 6 amplifier) which has been biased to allow 20mA to flow into the collector. A 15V potential is injected into the coaxial cable at the receiver in order to supply power to the LNA at the antenna. The MAR 6 amplifier is soldered onto a microstrip board. The board material is Epoxy-Glass (board thickness = 1.53mm) with a dielectric constant of 4.8 which is suitable at this operating frequency [22]. The microstrip lines have an impedance of 50Ω. The artwork is shown in Appendix 2. As the input and output impedance of the MAR 6 amplifier is 50Ω no matching is required. The measured parameters of the LNA at 1.35GHz are:

1. LNA gain = 12dB
2. Noise figure = 3dB
3. 1dB gain compression point = 0dBm
4. Maximum input power with no distortion = -13dBm
5. Input return loss = 20dB
6. Output return loss = 10dB

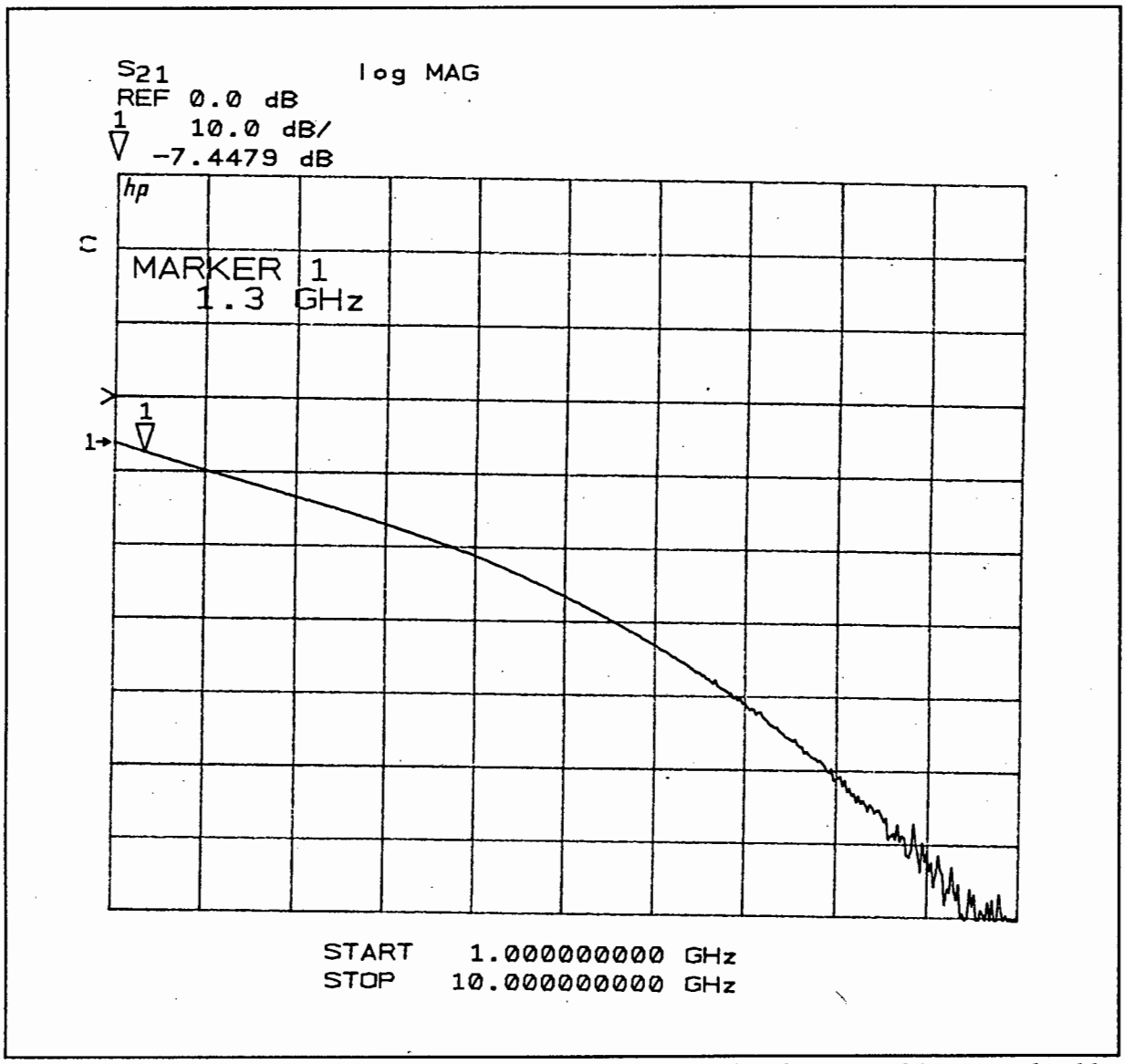

Figure 3.10 *The measured forward transfer parameter (S21) for an RG217 coaxial cable. The cable is 30m long.*

The input power versus output power curve is shown in Figure 3.12. The manufacturers specifications are shown in Appendix 3. The measured gain is slightly less than the manufacturers stated gain (15dB), however, this can be accounted for as there is a 2dB loss in the microstrip board and 15V injection circuitry.

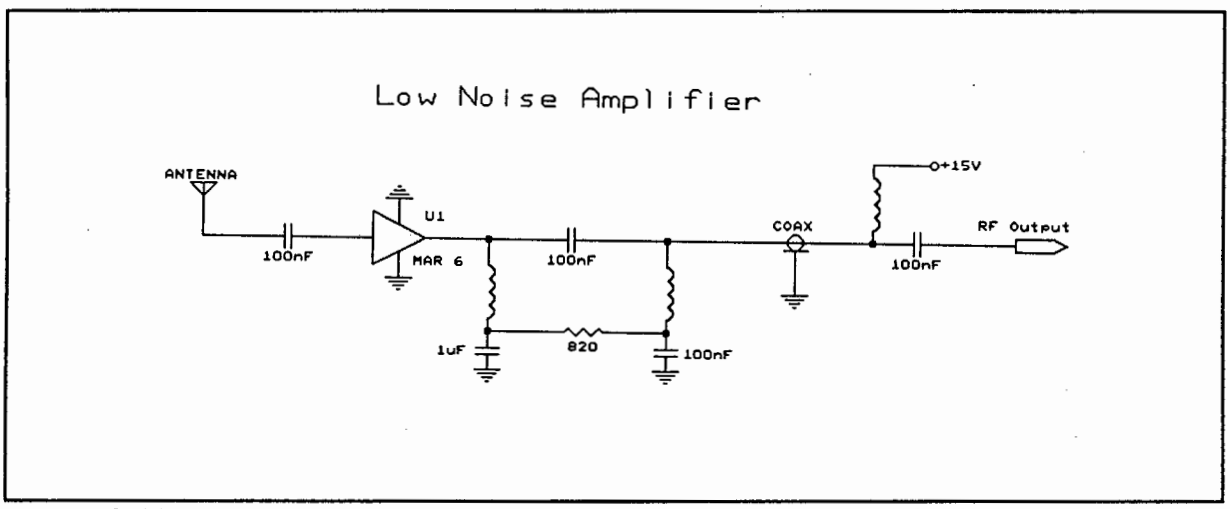

Figure 3.11 *The LNA circuit diagram. The diagram also shows the 15V injection circuit required to supply power to the LNA.*

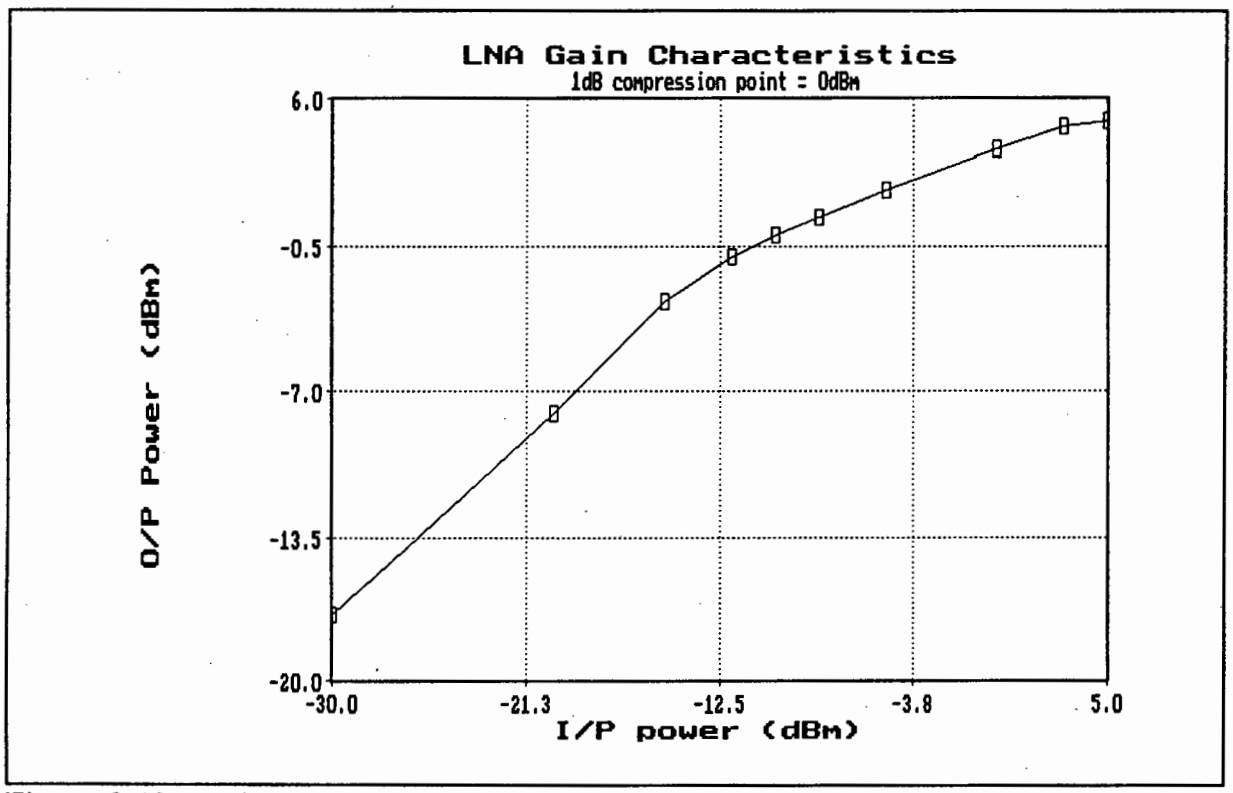

Figure 3.12 *The input power versus the output power of the LNA.*

3.3.3.3 PRESELECTOR FILTER

The preselector filter is placed before the mixer and it must satisfy certain requirements. These requirements are:

1. The IF frequency (70MHz) must be sufficiently attenuated such that it does not exceed the noise level, as the mixer can pass signals from its input port to its output port without conversion due to its imperfect isolation [4].

2. The leakage of the LO frequency must be reduced to the noise level.

3. The image frequency must be attenuated such that it does not exceed the noise level as it will produce an unwanted IF frequency which can not be filtered out [27].

A mechanically tunable waveguide preselector was made available for the receiver. It comes from an old signal analysis system, made by Polarad Electronics. The measured parameters of the preselector are listed below:

1. Tunable frequency range = 100MHz to 2.8GHz.
2. 3dB bandwidth = 14MHz.
3. Insertion loss = -2.8dB

It has a flat frequency response over the tunable range. Figure 3.13 shows the forward transfer characteristics (S21) when it is tuned to either one of the two frequencies, namely 1.304GHz and 1.35GHz.

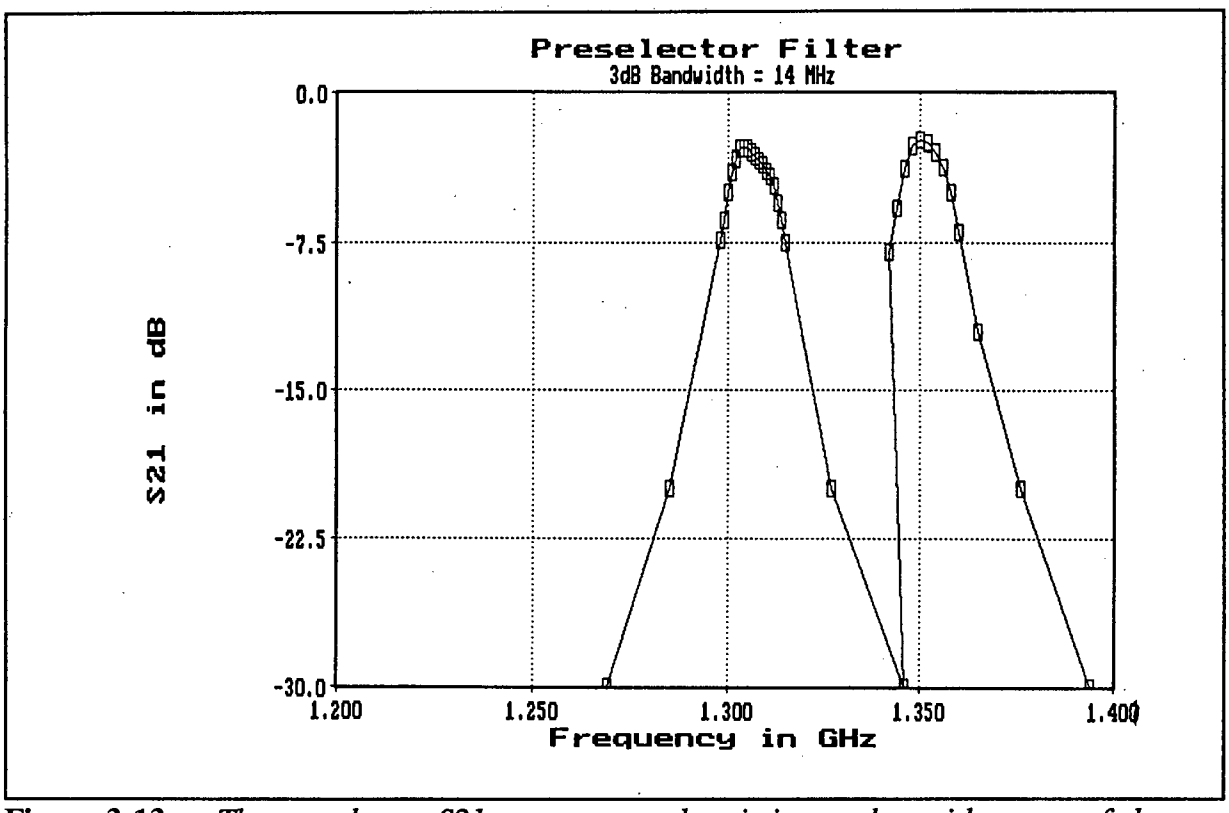

Figure 3.13 *The preselector S21 parameters when it is tuned to either one of the two frequencies, 1.304GHz and 1.35GHz.*

3.3.3.4 MIXER

In a superheterodyne receiver a mixer is required to convert the incoming RF signal down to an intermediate frequency (IF). Any non-linear device can be used as nonlinearity is required for the production of frequencies not in the input [25]. The theory of the mixer is not going to be dealt with here but the reader is referred to references [25] and [27].

For this application the main parameters to look for are the conversion loss and the dynamic range of the mixer. The conversion loss is an indication of the noise

figure and is always lower than the noise figure (±2dB), hence it determines the lower limit of the dynamic range. The upper limit of the dynamic range is determined by the conversion compression point [27].

A double balanced mixer would be ideal for this application as it has the following advantages [25]:

1. High degree of isolation between the three ports.
2. Large dynamic range.
3. Low conversion loss and noise figure.

The frequencies generated by the double balanced mixer are:

$f = n.f_{LO} \pm f_{RF}$ where n is odd.

The unwanted frequencies will be filtered out by the matched filter. A problem with mixers is the spurious response (the production of outputs at the intermediate frequency (IF) due to signals at frequencies other than the desired frequency), ie the image frequency (f_{image} = 2.LO - RF), this inserts an additional 3dB noise power therefore it is important for the preselector to filter these frequencies out as described in Section 3.3.3.3.

The double balanced mixer used in the receiver is an LMX-174 by Mini-Circuits. From Figure 3.14, the measured conversion loss is 8.6dB and the 1dB compression point is 0dBm. The noise figure of the mixer is 11.7dB. This mixer requires an LO level of 7dBm to drive it. The variation in conversion loss as a function of the LO power level is shown in Figure 3.15. The isolation between the ports is:

1. LO-RF isolation = 30dB
2. LO-IF isolation = 20dB

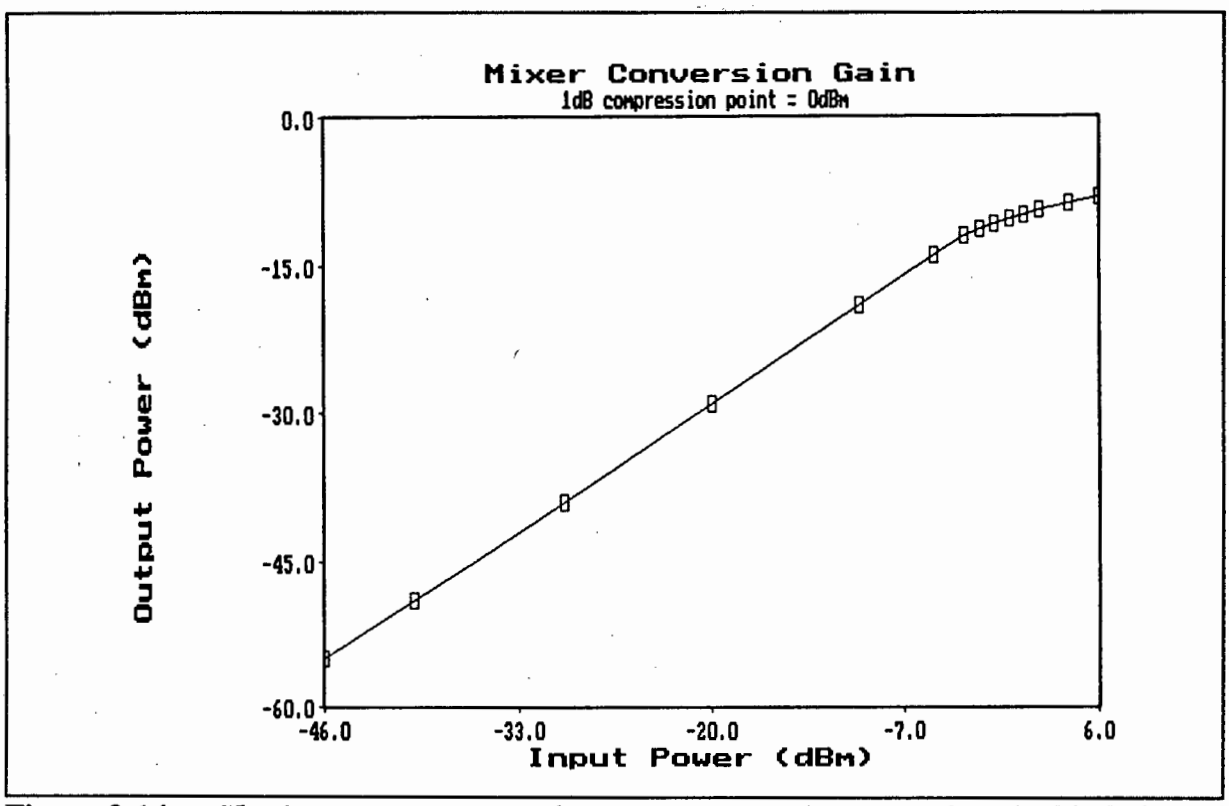

Figure 3.14 *The input power versus the output power of an LMX-174 double balanced mixer.*

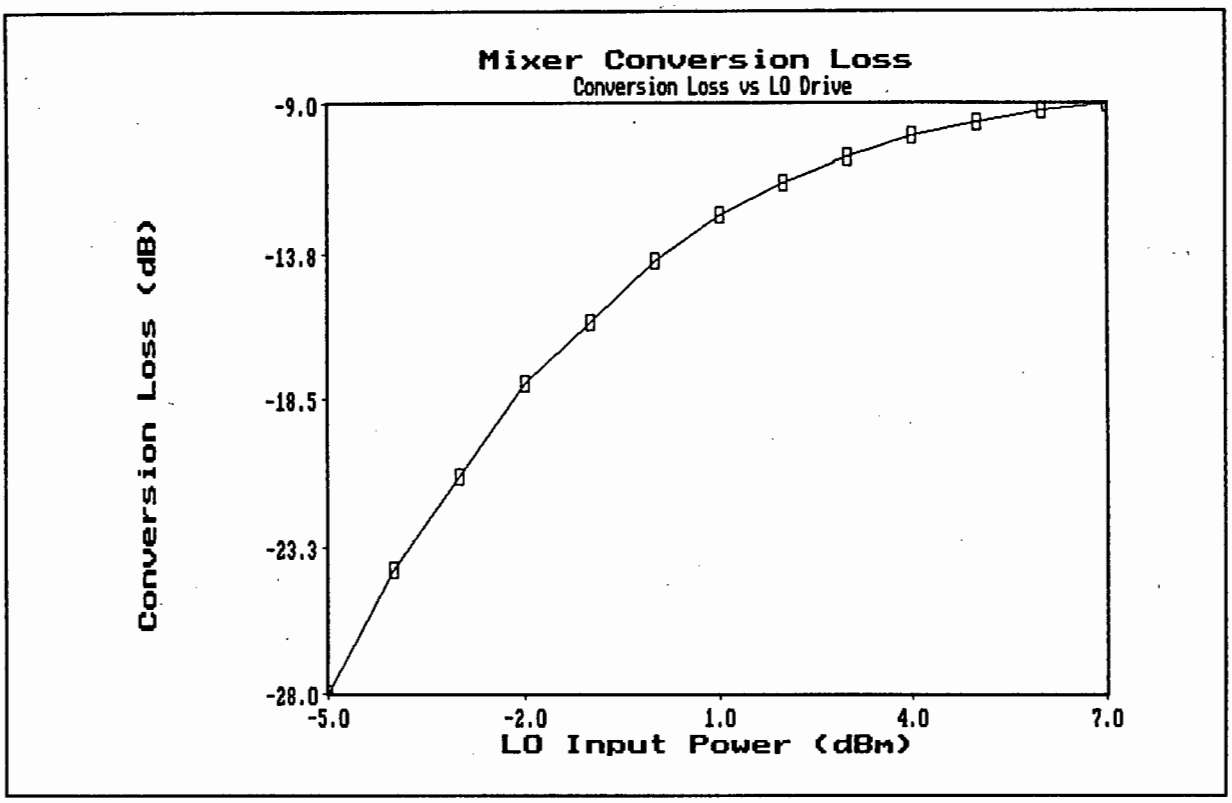

Figure 3.15 *The conversion loss versus the local oscillator power level for the mixer.*

3.3.3.5 MATCHED FILTER

Matched filtering is required to maximize the signal to noise ratio. The theory on matched filtering is given in reference [24]. The filter has been placed after the mixer to suppress the unwanted frequencies produced by the mixer and to cut down on the noise power, thereby reducing the risk of saturating the following amplifier stages.

A Chebyshev bandpass filter has been designed to fulfil this purpose. The filter design was obtained from reference [22]. Figure 3.16 shows the circuit diagram of the filter. It is basically a 6th order high pass and low pass filter which have

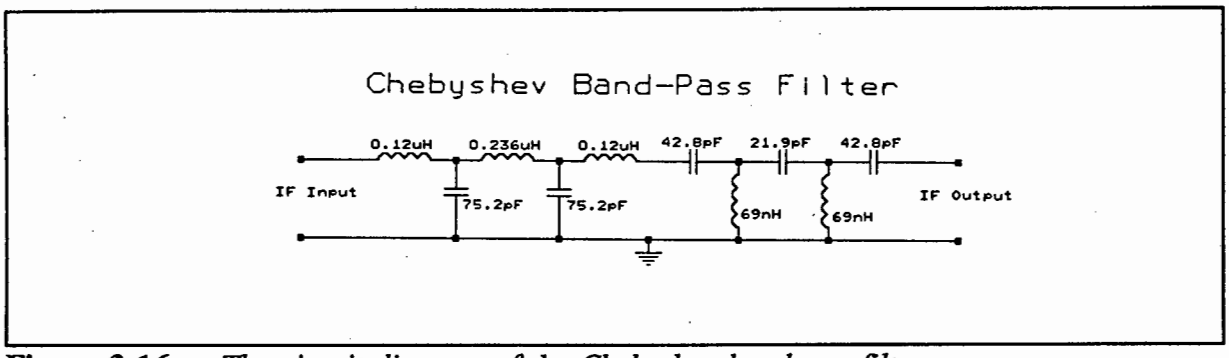

Figure 3.16 *The circuit diagram of the Chebyshev bandpass filter.*

been cascaded together. The coils (inductors) have been made from 1mm thick insulated wire to reduce losses at high frequencies (fringing effect). The coils have been designed according to an inductance formula given in reference [26]. A simulation of the filter was done on PSPICE. The results are shown in Appendix 4. From this simulation the following was determined, the bandwidth of the filter is 4.2MHz and the input and output impedance is 56Ω.

The following measurements (at 70MHz) were taken from the circuit:

1. Input return loss = 10dB.
2. Output return loss = 15dB.
3. Insertion loss = -1.96dB.
4. 3dB bandwidth = 2.2MHz.
5. Noise figure = 1.3dB.

The frequency response versus the S21 transfer parameter is shown in Figure 3.17.

One notes from Figure 3.17 that this filter is not matched, as the bandwidth is 2.2MHz and not 400KHz. Unfortunately it was not possible to build a relatively simple circuit at this frequency with such a narrow bandwidth and still have a low insertion loss. The matched filtering will therefore take place after the detector where the frequency is much lower. Another discrepancy lies in the measured bandwidth (2.2MHz) and the simulated PSPICE model bandwidth (4.2MHz). This

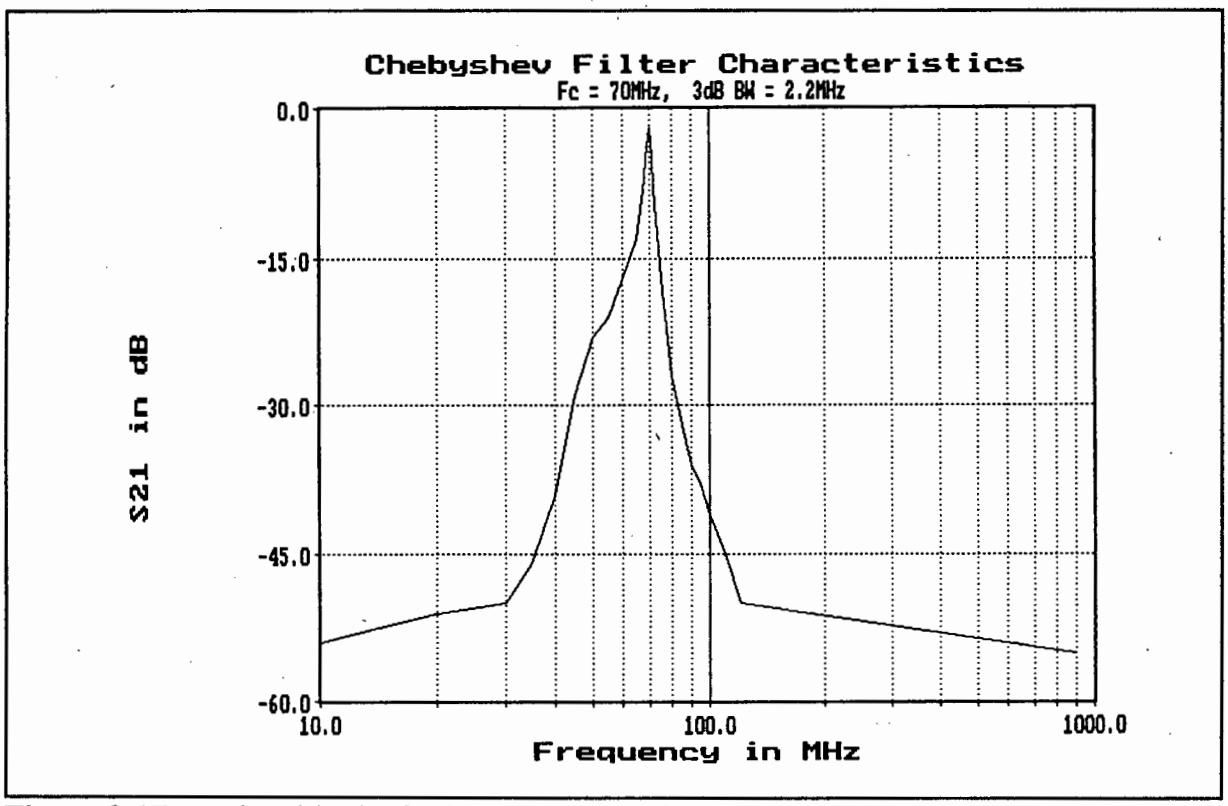

Figure 3.17 *The S21 transfer function against frequency of the Chebyshev bandpass filter.*

can be accounted for by the fact that the PSPICE model does not take into account stray capacitance and inductance.

3.3.3.6 PREAMP AND POWER SPLITTER

To synchronize the receiver with the transmitter, it is necessary to detect the pulses which arrive at the receiver during the dwell period (period during which the transmitter antenna beam illuminates the receiver). A power splitter is used to route half the power of the received signal to a threshold detector. The function and operation of the threshold detector will be described in Section 3.3.3.10. A low noise preamp is inserted before the power splitter to reduce the degradation in noise figure which is caused by the high noise figure of the main IF amplifier.

The preamplifier uses a MAR-6 as in the LNA and Mini-Circuits also supplied a suitable 2 way power splitter (PSC 2-1). Both components are mounted on the same microstrip board. The board is made of Epoxy-Resin (dielectric constant = 4.8) and the width of the microstrip lines are 3mm such that their impedance is 50Ω. The artwork is shown in Appendix 2.

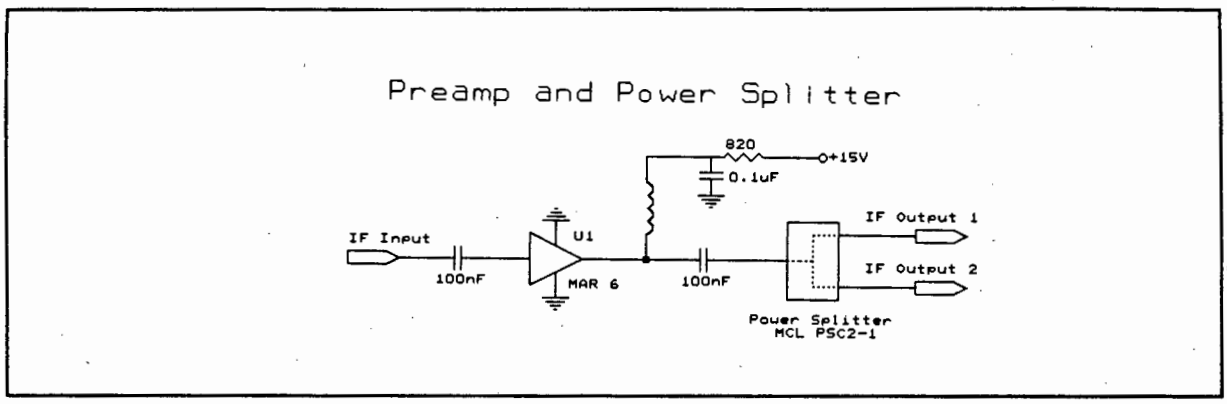

Figure 3.18 *The circuit diagram of the preamplifier and the power splitter.*

The manufacturer's specifications for the power splitter and MAR-6 amplifier are shown in Appendix 3. The circuit diagram of the preamp and power splitter are shown in Figure 3.18. For the correct operation of the preamplifier the open collector must be biased at 20mA. The measured specifications of the circuit are:

1. Gain = 16dB
2. Input return loss = 16dB
3. Output return loss = 26dB
4. Max input power at 1dB compression point = -18dBm
5. Noise figure = 4dB

Figure 3.19 shows the measured response of the input power versus the output power of the preamp and power splitter. Note that the maximum output power during saturation is 6dBm. To prevent destruction of the device the input power must not exceed 15dBm.

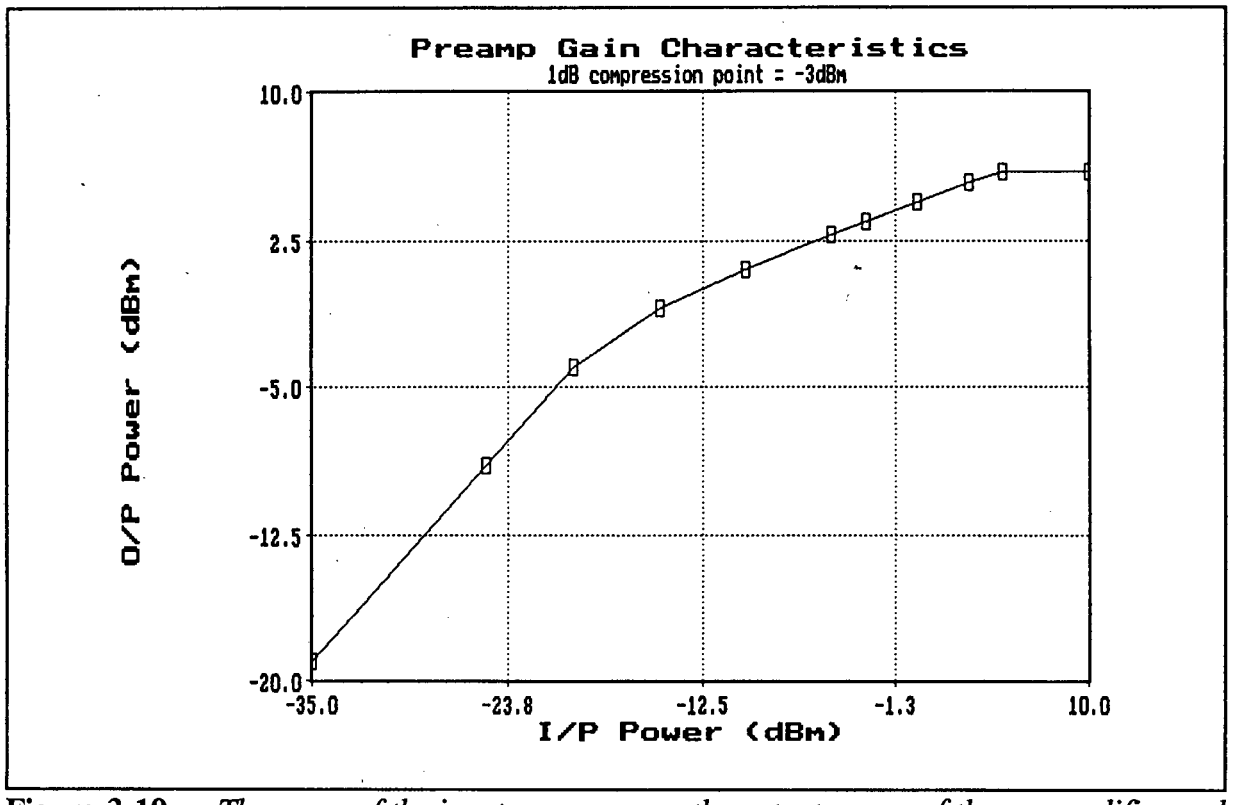

Figure 3.19 *The curve of the input power versus the output power of the preamplifier and the power splitter.*

3.3.3.7 SENSITIVITY TIME CONTROL

Sensitivity time control (STC) is a technique which causes the radar receiver sensitivity to vary with time in such a way that the amplified radar echo strength is independent of range or expressed in another way the receiver gain is programmed as a function of time [3]. Two reasons are given below to necessitate the use of STC.

1. The radar echo power received from a target varies inversely to the fourth power of the range or propagation time.

2. As described in Section 2.4.11, bistatic radar is inherently prone to strong clutter returns especially at close range and near the baseline. These clutter returns can then saturate the receiver.

A PIN diode attenuator circuit is used to perform the STC function. The design came from the Hewlett Packard application note 936 which is shown in Appendix 5. The application note also describes the advantages of using a PIN diode instead of transistors as a voltage controlled attenuator. In order to allow the circuit to have a gain and a loss, a MAR-6 amplifier was added after the PIN diode attenuator section. This is shown in Figure 3.20.

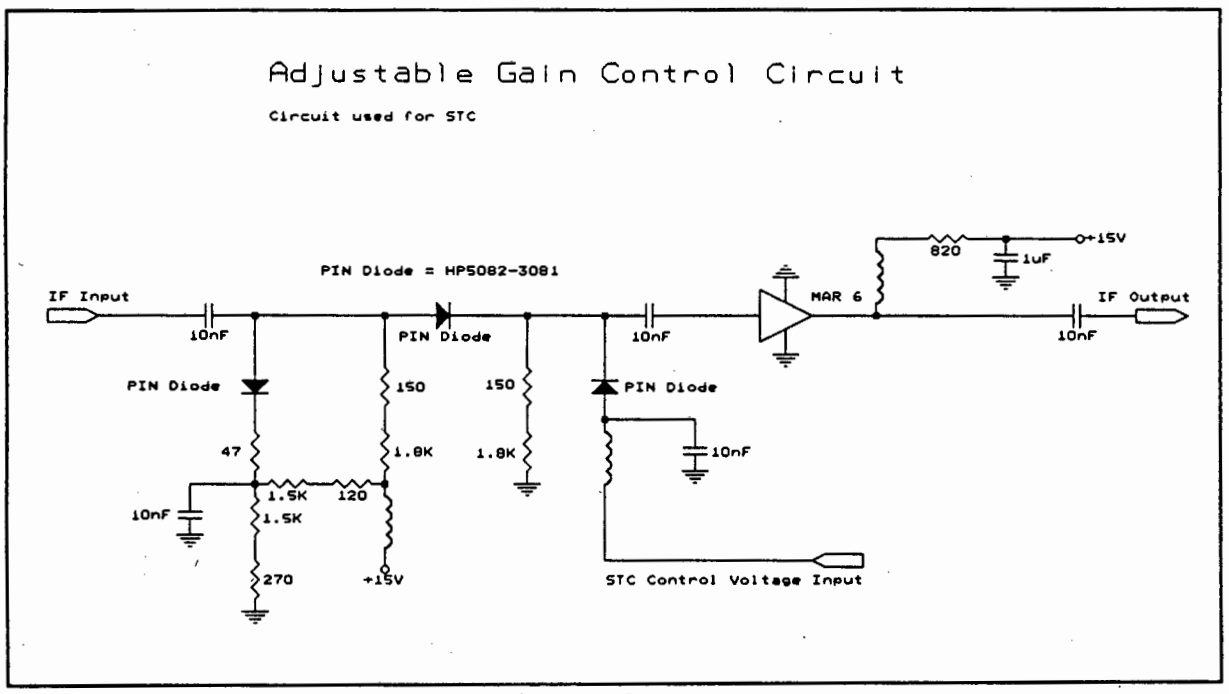

Figure 3.20 *The circuit diagram of the STC circuit.*

An HP 5082-3081 PIN diode is used in the attenuator. The specifications for this diode are shown in Appendix 6. The STC circuit is built on Epoxy-Resin board

with a ground plane on the other side in order to prevent unwanted high frequency anomalies. The artwork can be viewed in Appendix 2. The noise figure and gain of the attenuator and amplifier sections are shown below.

Attenuator:	NF = 2dB	Loss = 1.23dB to 53.5dB
Mar-6:	NF = 3dB	Gain = 17.27dB

According to the noise figure equation [23],

$$NF_{total} = NF_1 + (NF_2 - 1)/G_1$$

The noise figure of the combined system will vary with variation in gain. This is shown for various gains.

1. Gain = 17dB NF = 4.6dB
2. Gain = 0dB NF = 18dB
3. Gain = -35dB NF = 53dB

The gain of the STC circuit is voltage controlled. The curve showing the gain as a function of voltage is shown in Figure 3.21. From this Figure one notes that the maximum gain is 17dB and the maximum attenuation is 35dB. The curve is not linear due to the diodes non-linear characteristics and the maximum change in attenuation (30dB) occurs when the control voltage is between 10 and 11 volts. An advantage of a PIN diode attenuator is that the input impedance does not change much over the entire control voltage range (0V to 13V). This is shown in Figure 3.22 as the input return loss (S11 parameter) and the output return loss (S22 parameter).

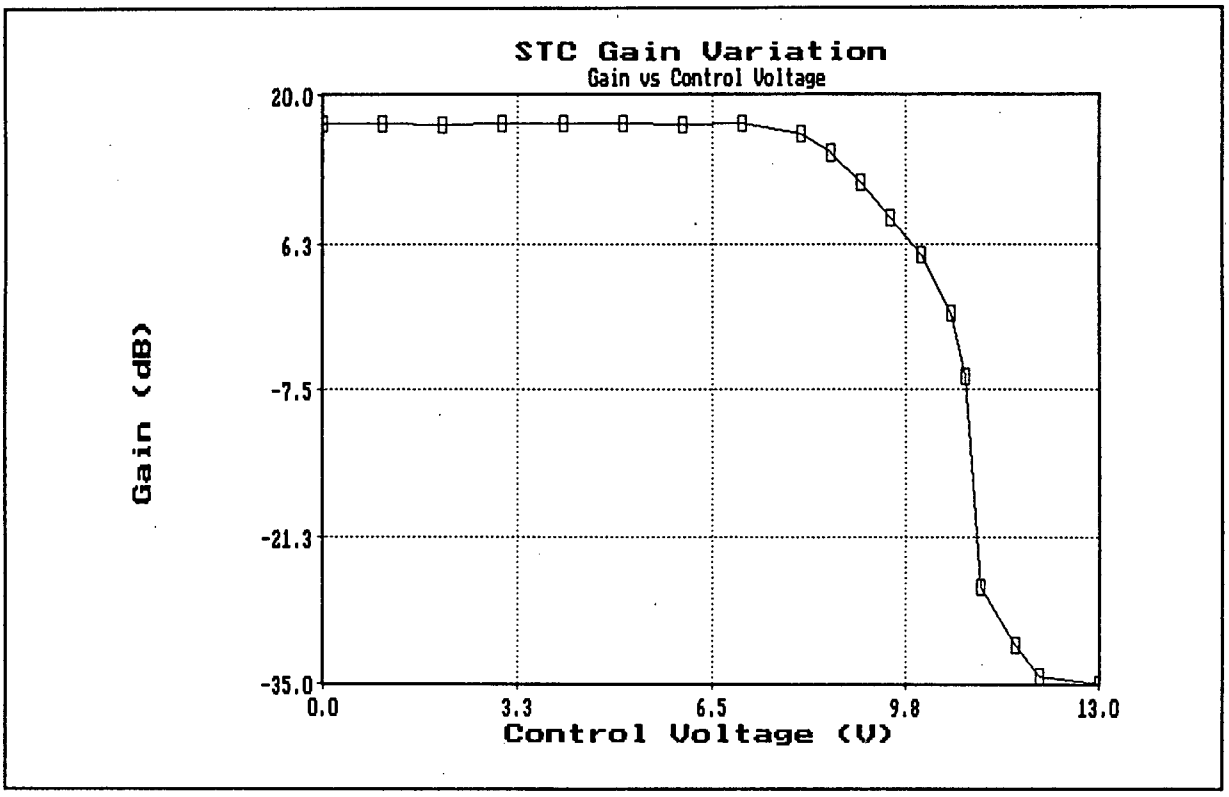

Figure 3.21 *The STC circuit gain variation as a function of control voltage.*

In order to control the gain of the STC circuit as a function of time, a control voltage curve had to be developed. This control voltage curve would then be triggered by the regenerated PRF. The three criteria in developing this curve are:

1. The STC circuit must be set at maximum attenuation during the dwell period.

2. The bistatic clutter returns must not saturate the main IF amplifier.

3. The sensitivity of the receiver must increase as a function of time.

As no measurements have been done to determine the magnitude of the clutter returns as a function of time and azimuth, the control voltage curve will be based on the predicted clutter values which will be determined in Section 3.4. When reading Section 3.4 one will note that the bistatic clutter returns are a function of

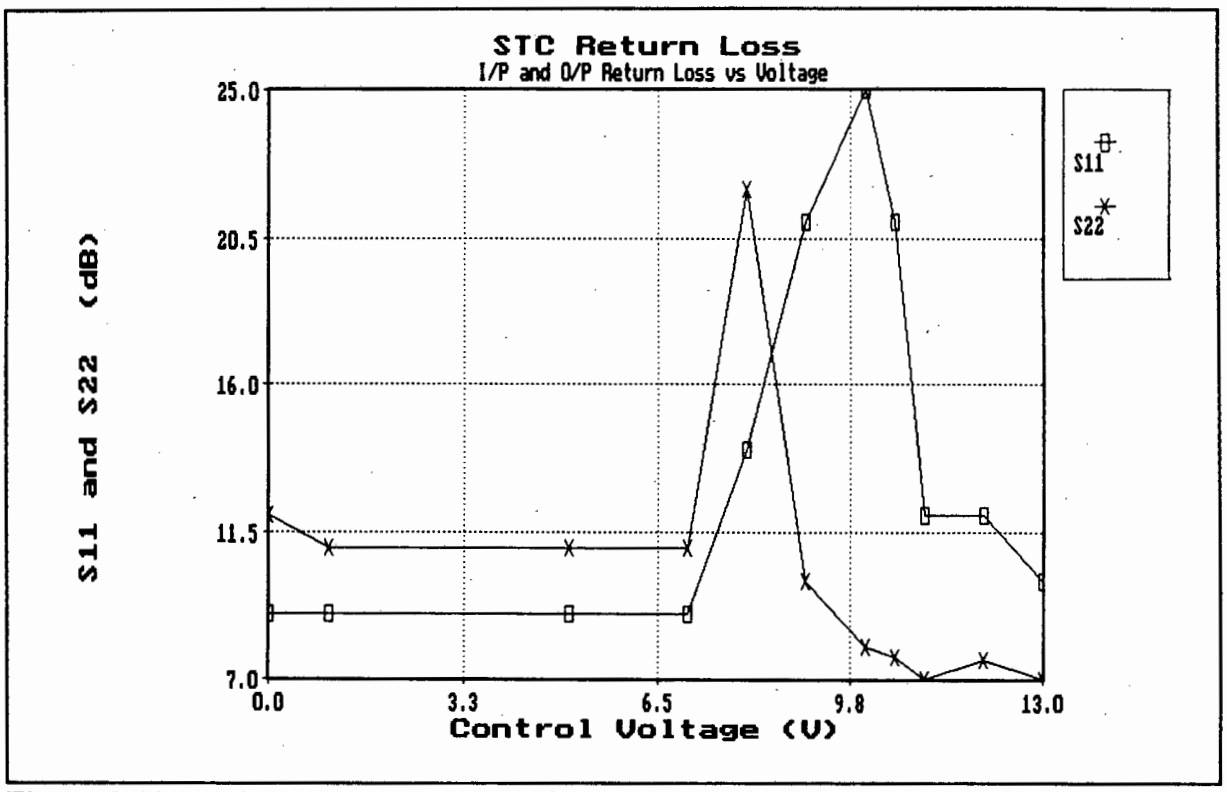

Figure 3.22 *The STC circuit input and output return loss as a function of control voltage.*

time as well as azimuth. As this STC circuit cannot generate a new curve for each azimuth position, an average value has been taken over all azimuth positions as a function of time or range. By using the STC attenuation curve (Figure 3.21) and the clutter information (Section 3.4), the required control voltage curve was calculated in order to obtain the correct attenuation. This curve is shown in Figure 3.23. One notes from this curve that there is a notch at t = 150μsec, this is to prevent echo returns from the Hottentots Holland mountain range from saturating the receiver. Large returns were noted from this area. The gain is set to be variable over a range of a 100km from the receiver. During the rest of the period (including the period when the direct pulses from the transmitter are received) the attenuation is set to a maximum.

The circuit generates this curve by switching two sections in, one after the other. Timing pulses for the switching are derived from the regenerated PRF. The first section switches in the variable curve. This is obtained by switching in six

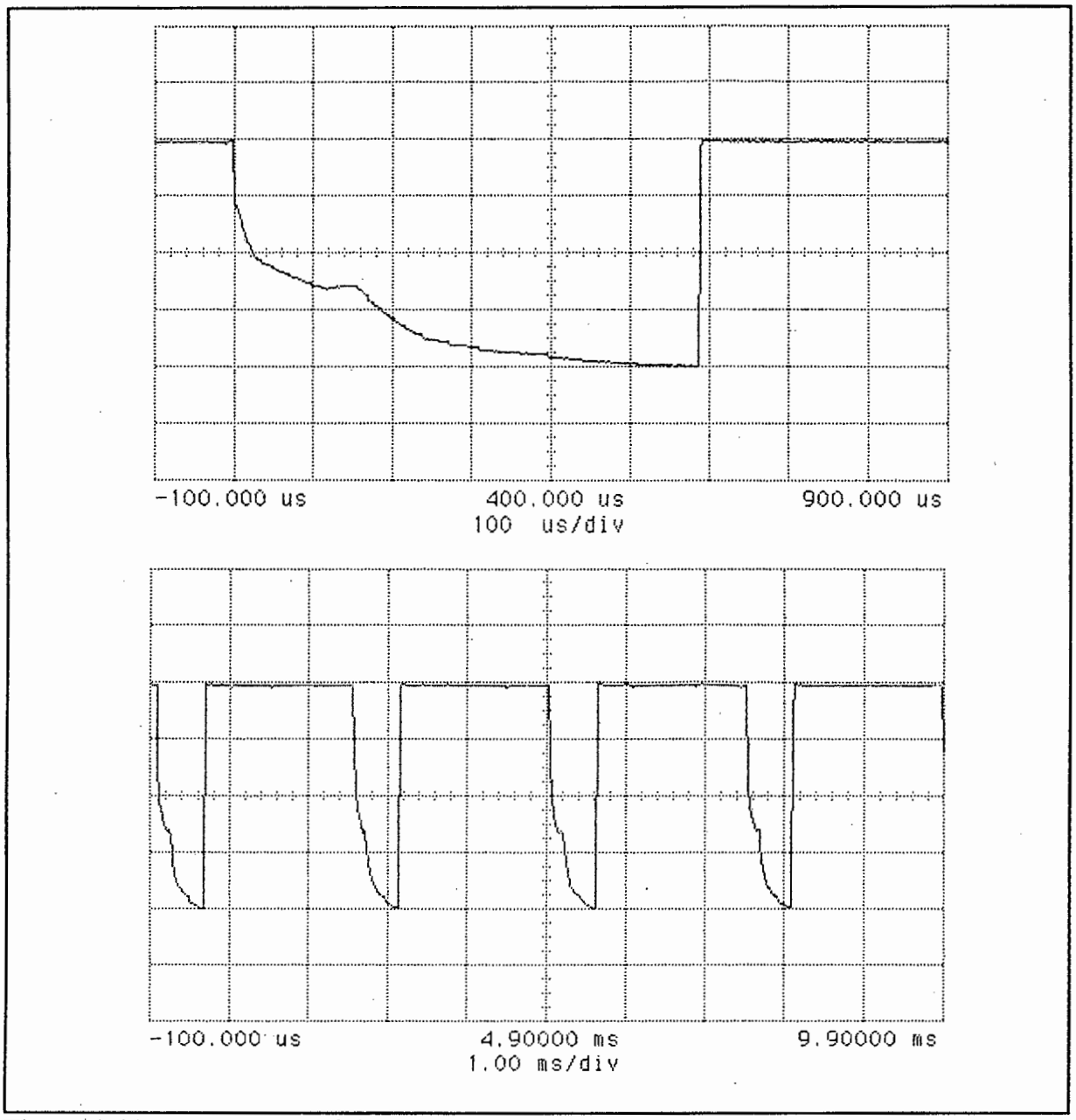

Figure 3.23 *The curve of the control voltage applied to the STC circuit. The top curve shows a close up of the section where the gain is variable. The vertical axis is set at 500mV/div with an offset of 11V.*

integrating sections, with different time constants, one after the other. The second section switches in the curve to maintain maximum attenuation. The operator can adjust the dc offset of the variable section from the front panel but not the shape of the curve. As this curve has been determined from predicted values, it has been

made possible to adjust the shape of the curve once more accurate clutter information has been obtained. The circuit diagram is shown in Figure 3.24.

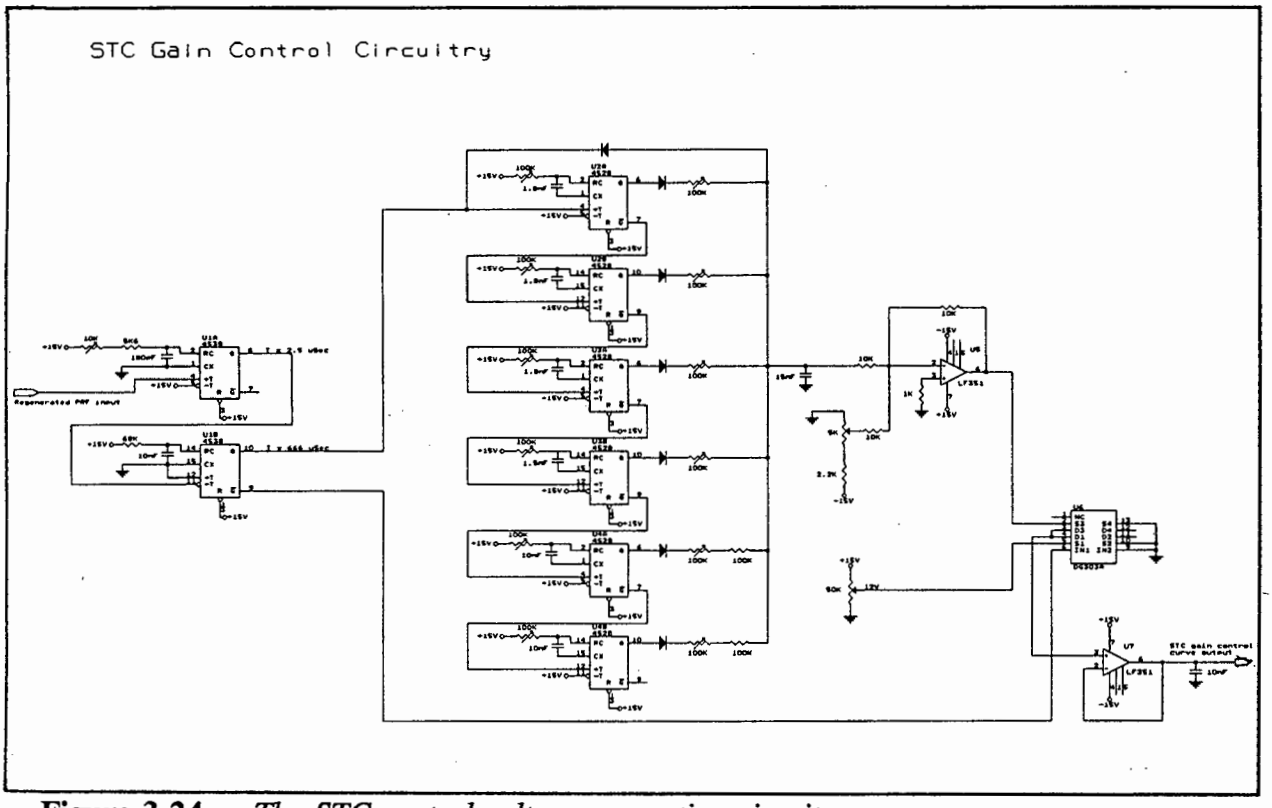

Figure 3.24 *The STC control voltage generating circuit.*

3.3.3.8 IF AMPLIFIER

This amplifier provides the main gain of the system. A 70MHz IF amplifier made by Raytheon was used as it fitted the receiver requirements and was immediately available. Unfortunately no circuit diagrams were made available for it.

The measured amplifiers parameters at 70MHz are:

1. Gain = 52dB
2. Noise figure = 10.2dB
3. 3dB Bandwidth = 20MHz to 95MHz
4. Input return loss = 12dB
5. Output return loss = 13dB
6. Maximum input power at 1dB compression point = -55dBm

Figure 3.25 shows the gain of the amplifier as a function of input power and Figure 3.26 shows the noise figure and gain as a function of frequency.

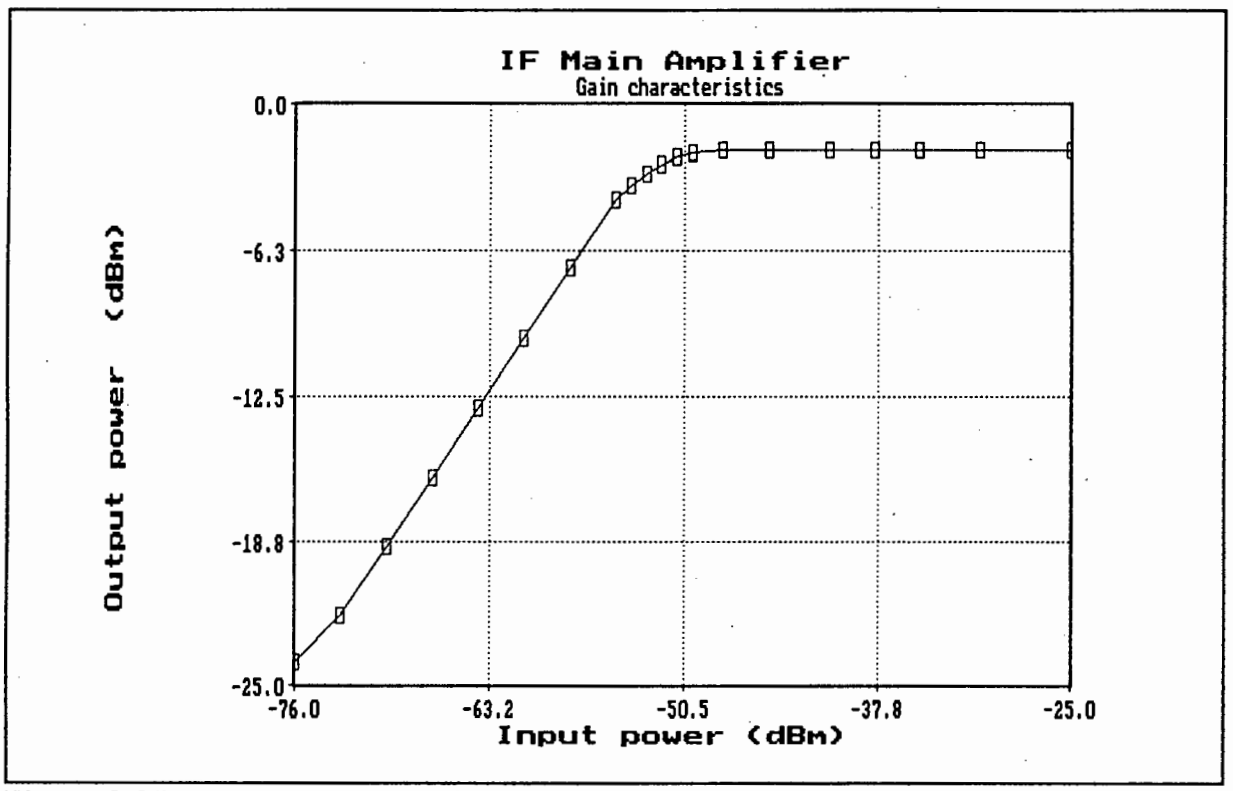

Figure 3.25 *The power gain characteristics of the main IF amplifier.*

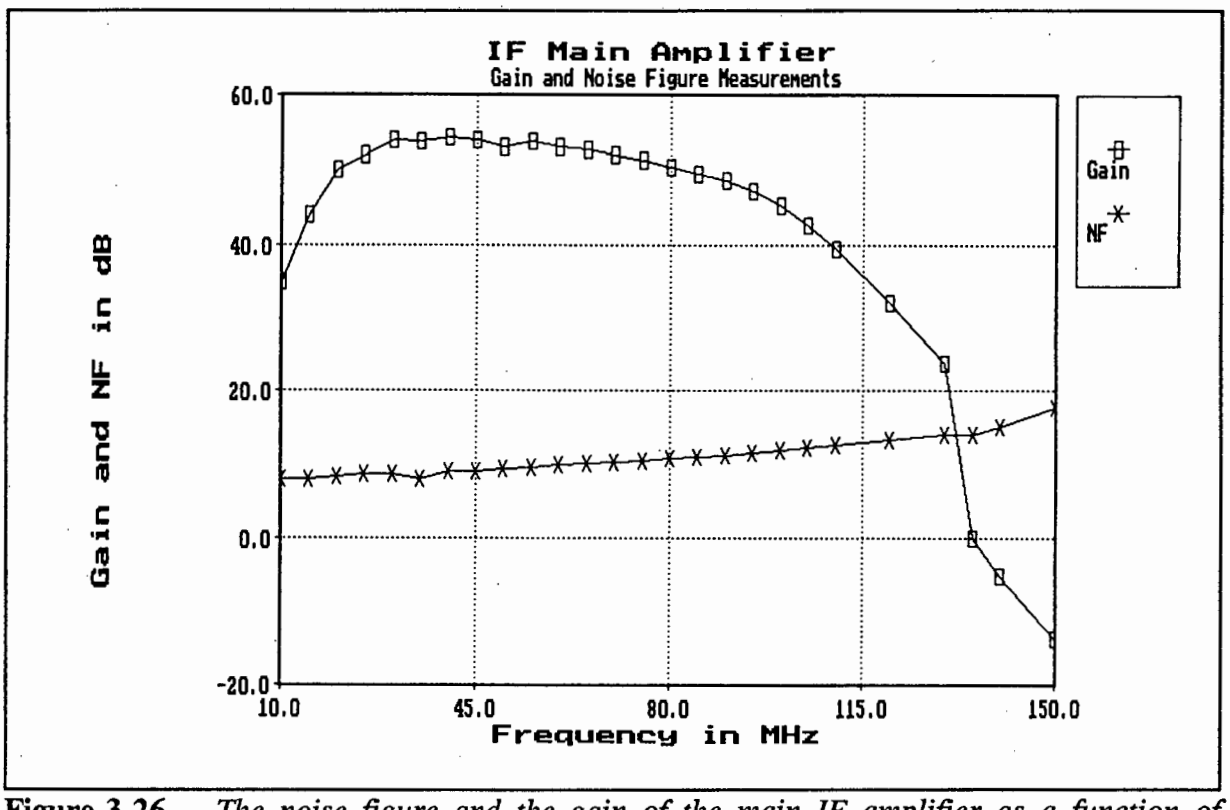

Figure 3.26 *The noise figure and the gain of the main IF amplifier as a function of frequency.*

3.3.3.9 ENVELOPE DETECTION AND INTEGRATION

Video detection of the signal after the main IF amplifier stage is necessary for display purposes. A diode detector configuration is used to achieve this. The diode used, is a Schottky barrier diode as it offers high detection efficiency. A description of various diode detector configurations can be found in reference [28]. The video signal is then amplified and level shifted to drive the PPI display.

The circuit diagram of the diode detector and the video amplifier is shown in Figure 3.27.

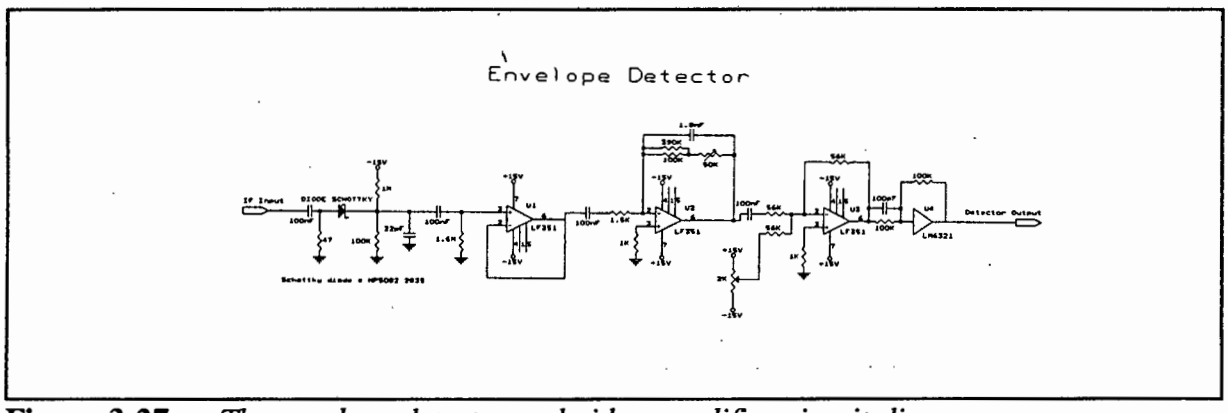

Figure 3.27 *The envelope detector and video amplifier circuit diagram.*

From Figure 3.27, a broadband biased diode detector is used. The detector can operate in either of two regions, the square law region (input power is proportional to output voltage) or the linear region (input voltage is proportional to output voltage). The progressive change over from the square law to the linear region occurs when the input signal level is approximately -20dBm [28]. As the information of the signal is not in its amplitude, the translation of the signal amplitude from IF to video is not an important parameter. The detector is therefore not restricted to operate in a specific region. The dynamic range of the detector may be defined as the difference between the maximum output level of the main IF amplifier (-4dBm) and power input corresponding to the tangential signal sensitivity (TSS). A small forward bias current, $I_o = 15\mu A$ has been applied to the diode to improve the sensitivity of the detector. The input impedance as seen by the incoming signal is the parallel combination of the 47Ω shunt resistor at the input and the video impedance (R_V) of the diode. For a Schottky barrier diode, $R_B = 28/I_o$ (in mA) hence the video impedance is 1870Ω. The relatively high diode impedance therefore has little effect on the input match of this detector. From Figure 3.28 one notes that the operation of the detector is mainly confined to the linear region, hence envelope detection.

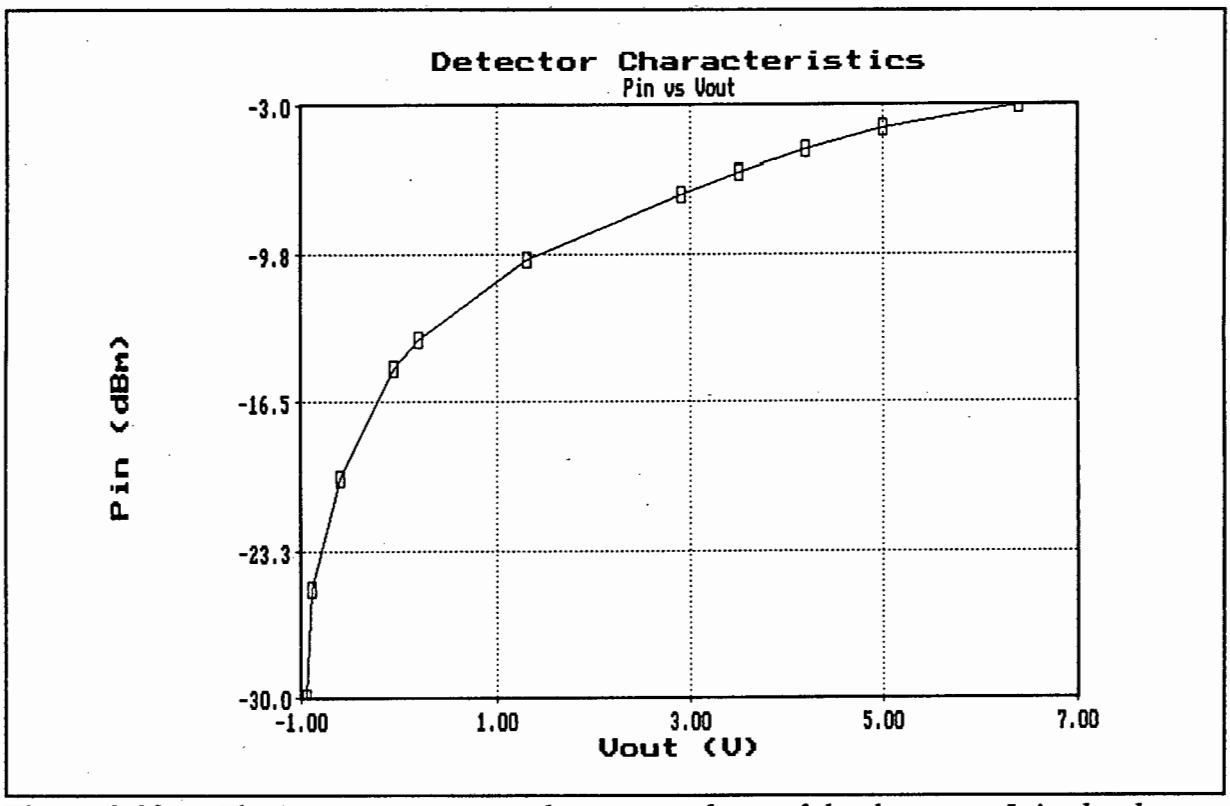

Figure 3.28 *The input power versus the output voltage of the detector. It is clearly seen that the circuit behaves as an envelope detector when the input power exceeds -30dBm.*

The filter which follows the diode removes the higher frequency components of the rectified signal, leaving the pulse envelope behind. Here matched filtering is approximated as the bandwidth of the first order filter is set at 420KHz.

For correct operation of the present display the voltage output of the detector must be in the range of -5V to +5V. At -5V the display is set at zero brightness and at +5V at maximum brightness. In order to achieve this an amplifier with a variable voltage gain (G = 53 to 86) and level shift follow the detector stage.

During the illumination period of the target several non-coherent pulses are received at the receiver and integrated. Post-detection integration is performed on a PPI display. The efficiency of post-detection integration depends on the number of pulses being integrated. The loss with respect to coherent integration is defined as [2]:

$$L_i = 10.\log(N.x_2 / x_1)$$

where: L_i = integration loss

N = number of pulses integrated

x_1 = required value S/N to produce a given probability of detection for $N = 1$

x_2 = required value of S/N to produce the same probability of detection with N pulses.

The gain of the integrator is determined by the number of pulses received during the target illumination period. The number of pulses received is:

$$N = \theta_{BW}.PRF / \delta$$

where: θ_{BW} = 3dB beamwidth of transmitter antenna

PRF = pulse repetition frequency

δ = rotation rate of transmitter antenna.

For this receiver the number of pulses received during the target illumination is 18. The integration loss determined from graph 6.5 of reference [2] is 3dB. The integration gain is then determined by:

$$G_i = 10.\log N - L_i = 9.5dB$$

Hence the integrator has a gain of 12.5dB and a 3dB loss, assuming that the PPI display has sufficient persistence to integrate all pulses.

3.3.3.10 THRESHOLD DETECTOR

The azimuth and PRF synchronization circuits require the pulses received during the dwell period in order to maintain synchronization of the receiver with the transmitter. This is achieved with a threshold or level detector.

Figure 3.29 shows the circuit of the threshold detector. The front end (diode detector and video amplifier) is identical to the envelope detector described in Section 3.3.3.9, therefore nothing more will be mentioned here.

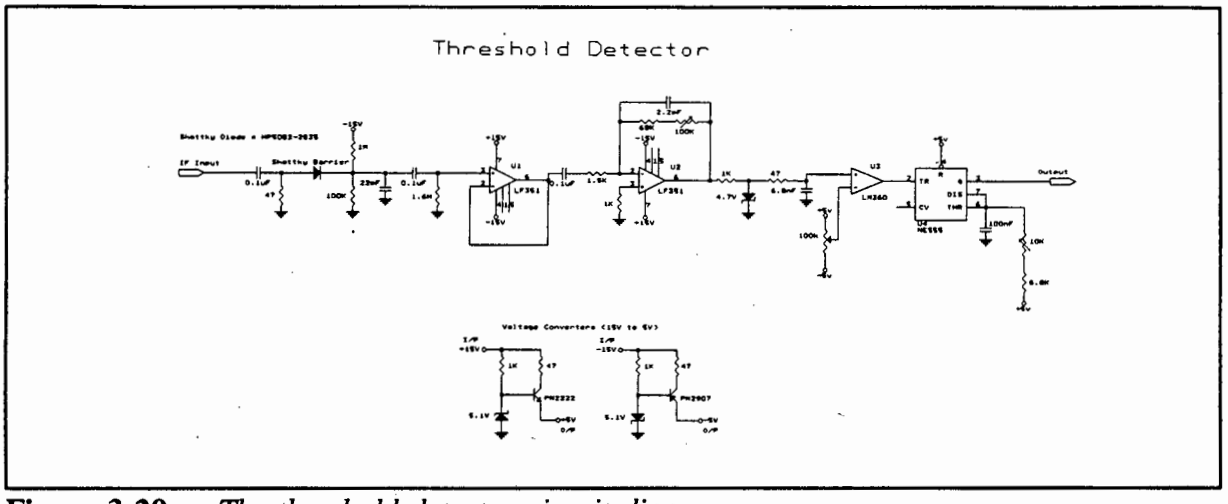

Figure 3.29 *The threshold detector circuit diagram.*

Following the video amplifier is a comparator which discriminates between the main bang pulses and the other unwanted pulses during the dwell period. As the main bang pulses are significantly larger ($\pm$40dB for the maximum variation and $\pm$10dB for the minimum variation) this is made possible. The sensitivity of the comparator can be adjusted in order to prevent the detection of false pulses. The number of pulses detected varies on a daily basis and is dependent on the weather and the transmitter being used. On average about 30 pulses are being detected. Note that the sidelobes of the transmitter antenna are also being included in the dwell period for this case. This allows more than 18 pulses to be detected which then improves the performance of the synchronization circuits. Care must be

taken not to make the comparator too sensitive as this will lead to the thresholding of false pulses and consequent loss in azimuth synchronization.

After the comparator the pulse train is given a 50% duty cycle. This improves the performance of the PRF synchronization circuitry.

3.3.4 SPECIFICATIONS OF THE RECEIVER

Until this point in the chapter the objectives and requirements of the receiver have been laid out and the components of the receiver have been described. This section will show the validity in the choice of the components and which requirements have been achieved satisfactorily.

3.3.4.1 POWER OF DETECTED DWELL PERIOD PULSES

Everytime the transmit antenna illuminates the receiver (dwell period), several pulse are detected. The maximum detected level was calculated and measured at the receiver front end. These values are shown below.

The maximum power received during the dwell period was calculated using the following radar equation:

$$P_{direct} = \frac{P_T.G_T.G_R.\lambda^2}{(4.\pi)^2.R^2}$$

where

R = *Baseline range* (15*km*)

G_T = 28*dB*

As the elevation angle of the transmit antenna is 4°, the gain of the transmit antenna, when illuminating the receiver, is 28dB and not 34dB (see Section 3.2). The calculated main bang power level is 5.5dBm.

The measured power level varied between 3dBm and 5dBm, which is in agreement with the calculated value.

3.3.4.2 MAXIMUM DETECTED POWER LEVEL OF A TARGET

The maximum echo power received from a target at the receiver is obtained when the target is in the vicinity of the transmit or receive antenna as illustrated by the ovals of Cassini in Section 2.4.5. In order to prevent the receiver from saturating, the magnitude of the echo had to be known.

Three assumptions are used in calculating this value:

1. The RCS of the target is 50m^2. This is an average value for a large aircraft taken from reference [2].

2. The target is never closer than 75m from either the transmit or receive antennas.

3. The target is on the ground hence the transmit antenna gain is 25dB as it has an elevation angle of 4°.

The bistatic radar equation shown in Section 2.4.2 is used to calculate the target echo power. All losses are assumed to be zero. The calculations are shown in Appendix 7. The calculated value is -28.9dBm.

3.3.4.3 SYSTEM NOISE FIGURE AND SENSITIVITY

This section calculates the receivers power levels, signal and noise, at different points. The noise figure of the system is also determined. Measured noise values are then compared to the calculated values.

The noise at the antenna was not measured as the equipment available was insensitive to such small power levels, however, a theoretical value is assumed. From reference [3] the effective antenna noise temperature is given by:

$$T_{ea} = 0.876.T_a + 36$$

T_a is the noise temperature of an idealized antenna facing the sky. For an antenna facing the horizon and tuned at 1.337GHz, T_a = 178K ([3], Fig 2.9). The above equation assumes that a portion of the receive antenna beam illuminates the earth which has an effective temperature of 290k and there are no antenna losses. The effective antenna noise temperature is therefore 192K. The noise power at the input to the receiver is calculated from $P_{in} = k.T_{ea}.B$ and is -120dBm.

Appendix 7 shows the calculations used to obtain the noise figure, sensitivity and target range. All the equations and theory come from references [3] and [23]. The noise after the main IF amplifier was also measured with an HP spectrum analyzer. The input to the receiver (after the antenna) was terminated in a 50Ω load during the time taken for the measurements.

One will note from the next noise measurement Figures that there is a ±21dB discrepancy between the measured and calculated results. This is due to the spectrum analyzer being incorrectly calibrated. The scaling error was determined by measuring the noise with a digital oscilloscope and converting the rms noise voltage to a power level for a 400KHz bandwidth. The spectrum analyzer and oscilloscope readings were compared and a 21dB scaling error was calculated, hence -21dB must be added to all the noise power measurements shown in the next Figures.

The receiver is designed to have a 12dB signal to noise ratio at the output. This gives the system a probability of detection equal to 80% and probability of a false alarm equal to 10^{-8} [2]. As shown in Section 3.3.3.9 the integrator has a gain of 9.5dB, therefore the signal to noise ratio at the output of the main IF amplifier must be 2.5dB. The signal to noise ratio is set at the output of the main IF amplifier because the noise contribution of the detector stage is insignificant as shown by the receiver noise figure equation in Appendix 7.

The following parameters were obtained for the receiver in various configurations:

	LNA at antenna, no STC	LNA at mixer, no STC	LNA at antenna with STC G = max	LNA at antenna with STC G = 0	LNA at antenna with STC G = min
Gain of receiver	59dB	59dB	76dB	59dB	24dB
Sensitivity	-103dBm	-102dBm	-103dBm	-101dBm	-70dBm
Signal after IF amp	-44dBm	-43dBm	-27dBm	-42dBm	-46dBm
Noise after IF amp, calculated	-46.5dBm	-45.5dBm	-29.5dBm	-44.5dBm	-48.5dBm
Noise after IF amp, measured	-44dBm	-43dBm	-28.9dBm	-43.8dBm	-54dBm
Noise Figure	14.3dB	15dBm	14.12dB	16.2dB	47dB

Table 3.1

Note that the calculated noise at the output of the IF amplifier takes into account the noise of the antenna whereas the measured values do not. This will only cause a 0.8dB variation in the two sets of values. The maximum variation between these two sets of noise values is 6dB, however, this is within the error tolerance.

Some explanations for these errors are:

1. Noise generated by the connections between components.

2. Filters do not have ideal characteristics.

3. Noise figures of some components have come from the data sheets and have not been checked due to unavailability of equipment.

4. System temperature could be greater or less than the standard room temperature of 290K.

The measured noise of the receiver when viewed on the spectrum analyzer is shown in Figures 3.30 to 3.34.

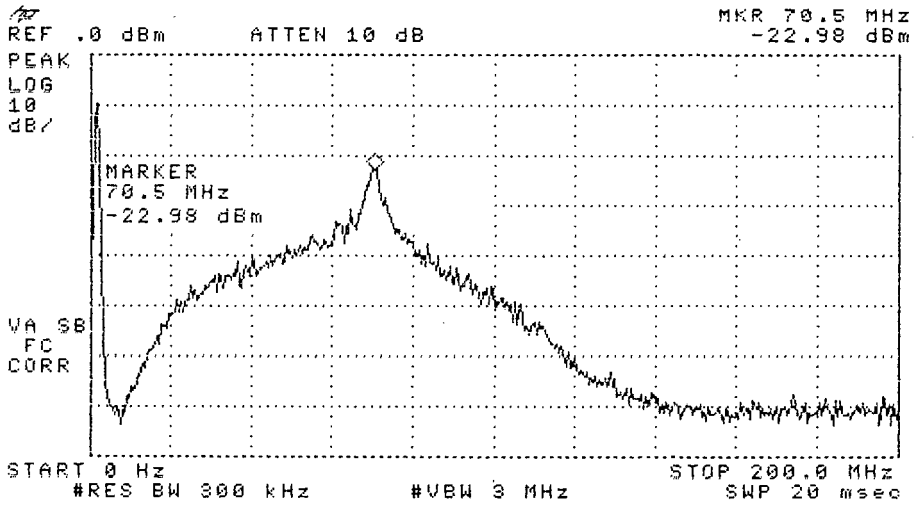

Figure 3.30 *The noise of the receiver with the LNA placed at the antenna. The receiver has no STC circuit and is terminated in 50Ω at the I/P.*

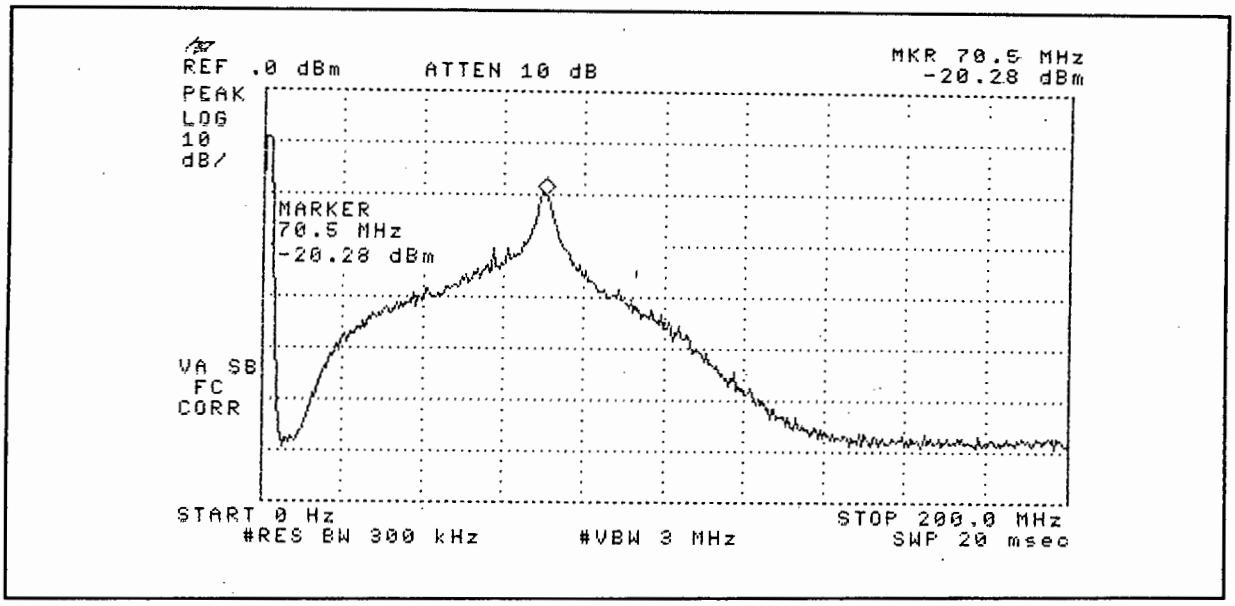

Figure 3.31 *The noise of the receiver with the LNA placed at the mixer. The receiver has no STC circuit and is terminated in 50Ω at the I/P.*

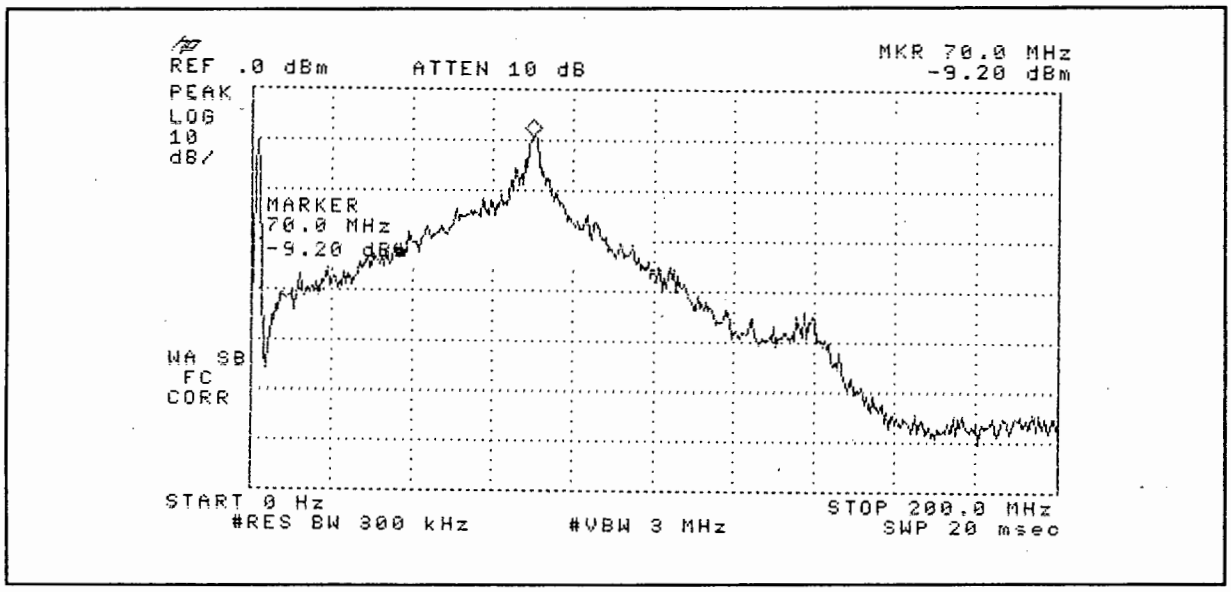

Figure 3.32 *The noise of the receiver with the STC set to give the receiver maximum gain. The input to the receiver is terminated in 50Ω.*

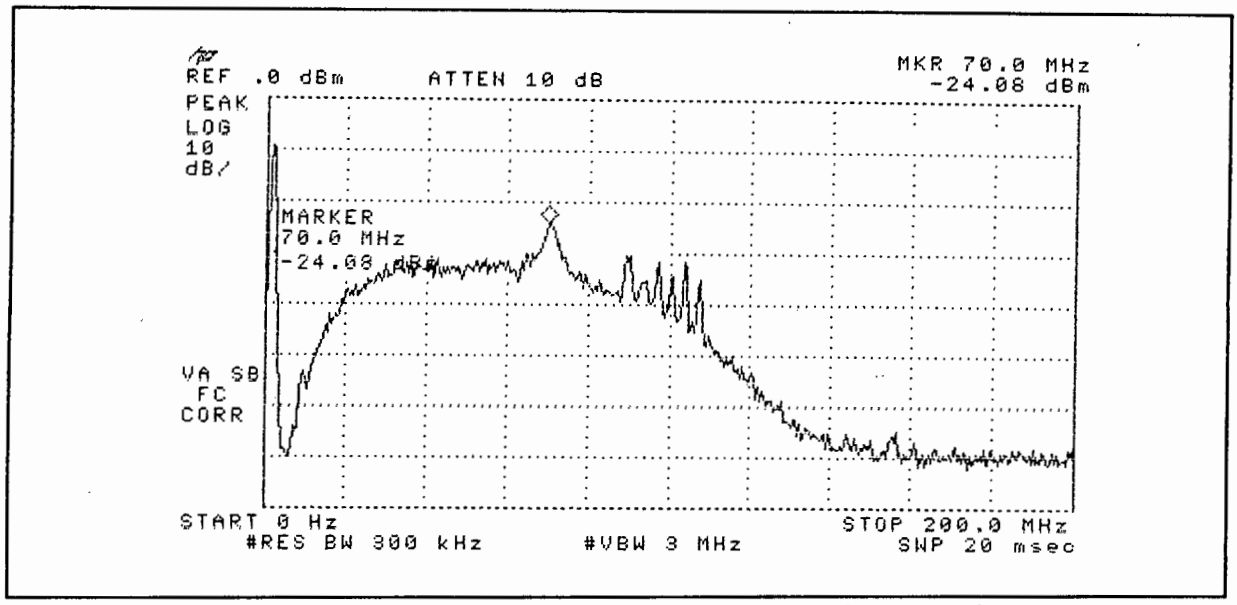

Figure 3.33 *The noise of the receiver with the STC set such that it does not cause any gain or loss in the receiver. The input of the receiver is terminated in 50Ω.*

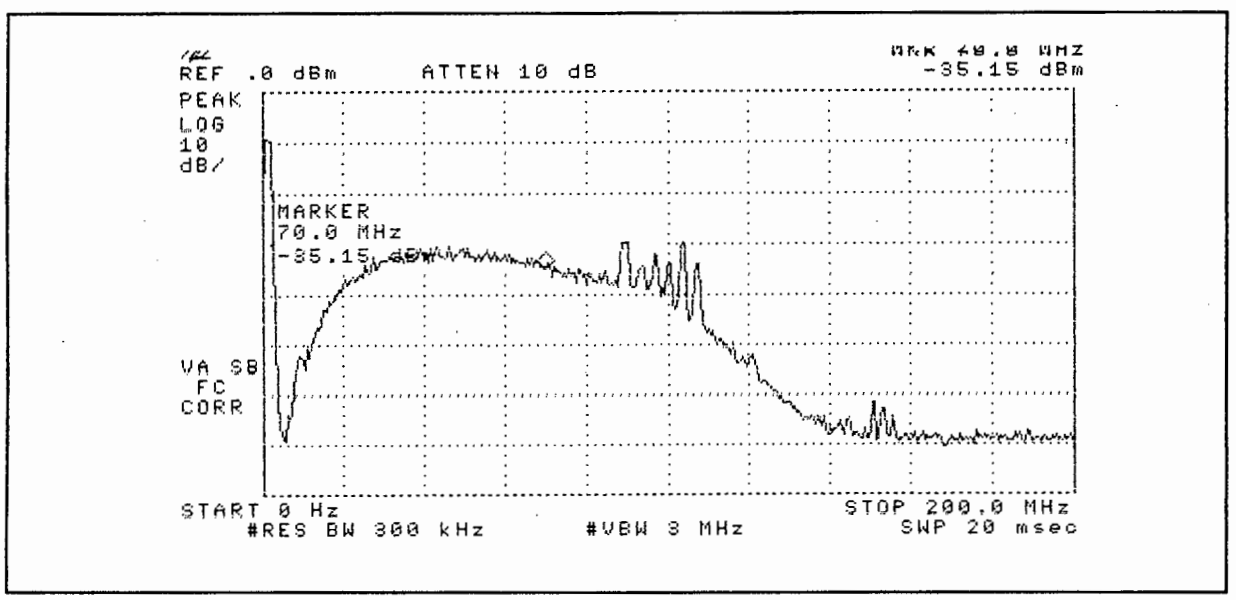

Figure 3.34 *The noise of the receiver with the STC set such that it gives the receiver maximum attenuation. The input to the receiver is terminated in 50Ω.*

From the above Figures and Table 3.1 the following can be deduced:

1. The sensitivity of the receiver is improved by 1dB if the LNA is placed before the coaxial cable at the antenna.

2. The sensitivity and noise figure of the receiver vary as the gain varies.

3. There would be a degradation in the receiver sensitivity of 11dB if the LNA is removed from the receiver.

4. The STC circuit has the largest effect on the noise figure of the receiver, especially when reducing the gain of the receiver. This is not a problem as the target range is usually small when the STC is set at maximum attenuation.

The effect that the components of the receiver have on the propagation of the signal and noise through the receiver is shown in Table 3.2. Two examples are shown. Firstly the receiver is set to have a maximum gain in order to detect the smallest target echo and secondly the receiver is set to a minimum gain so that it does not saturate when detecting the largest target echo.

	Min Signal	Noise	Max Signal	Noise
Antenna	-103dBm	-120dBm	-28.9dBm	-120dBm
LNA	-91dBm	-105dBm	-16.9dBm	-105dBm
Coaxial cable	-98.4dBm	-112.4dBm	-24.3dBm	-112.4dBm
Filter	-101.2dBm	-115.2dBm	-27.1dBm	-115.2dBm
Mixer	-110.2dBm	-116.3dBm	-35.7dBm	-116.3dBm
Filter	-112.1dBm	-117.6dBm	-37.6dBm	-117.6dBm
Preamp	-96dBm	-98.9dBm	-21.6dBm	-98.9dBm
STC	-79dBm	-81.8dBm	-56.6dBm	-111.6dBm
Main amp	-27dBm	-29.4dBm	-4.6dBm	-49dBm

Table 3.2

From Table 3.2 one will note that the receiver will not saturate for targets at close range and it meets the SNR requirements for targets at maximum receiver-target range. A problem exists, however, with the main bang pulse. This will cause all the amplifiers in the receiver to saturate. This requirement has not been met.

3.3.4.4 RADAR RANGE AND COVERAGE

The maximum range and approximate coverage of this receiver will be shown below.

From Section 3.3.4.3 the sensitivity of the receiver is -103dBm. Using the radar range equation described in Section 2.4.2 the maximum range of the receiver can be calculated. Two assumptions are made in the calculation, namely:

1. There are no propagation losses.

2. The bistatic radar equation approximates the monostatic radar equation at long target ranges (80km or more).

The calculation is shown in Appendix 7 and the calculated maximum target-receiver range is 127km for an RCS of 50m^2. The geographical coverage of this radar, taking into account the variation in the receiver gain as the target moves away from the baseline, is shown in Figure 3.0 of Section 3.1.

3.3.4.5 RESOLUTION

The theory on bistatic resolution is discussed in Section 2.4.7, however, the range and cell area resolution are calculated for this bistatic radar and illustrated in this section.

The range and cell area resolution is dependent on baseline range, pulse length, azimuth angle and range, hence there is no one figure to represent them. For the range resolution, the maximum resolution is:

Maximum Range Resolution $= c.\tau / 2 = 375$m.

The range and cell area resolution over several constant range contours was calculated by a program shown in Appendix 10. As the receiver only illuminates one direction, the resolution values have only been plotted over a receiver azimuth range from -90° to 0°. Figure 3.35 and 3.36 show the range resolution for a constant range contour of 17km and 59km respectively. From these figures one will note that the resolution degrades as the baseline is approached or when the bistatic angle increases. Note that the best resolution is achieved when the transmit antenna azimuth is -90°. A minimum constant range contour of 17km was chosen as the eccentricity of the ellipse is 0.9. At an eccentricity greater than 0.95 the equations used break down [1].

The cell area resolution degrades in a similar way to the range resolution. In this case the minimum cell area is also determined when the transmit antenna azimuth is -90°. The cell area resolution over a constant range contour of 17km and 59km is shown in Figure 3.37 and 3.38 respectively.

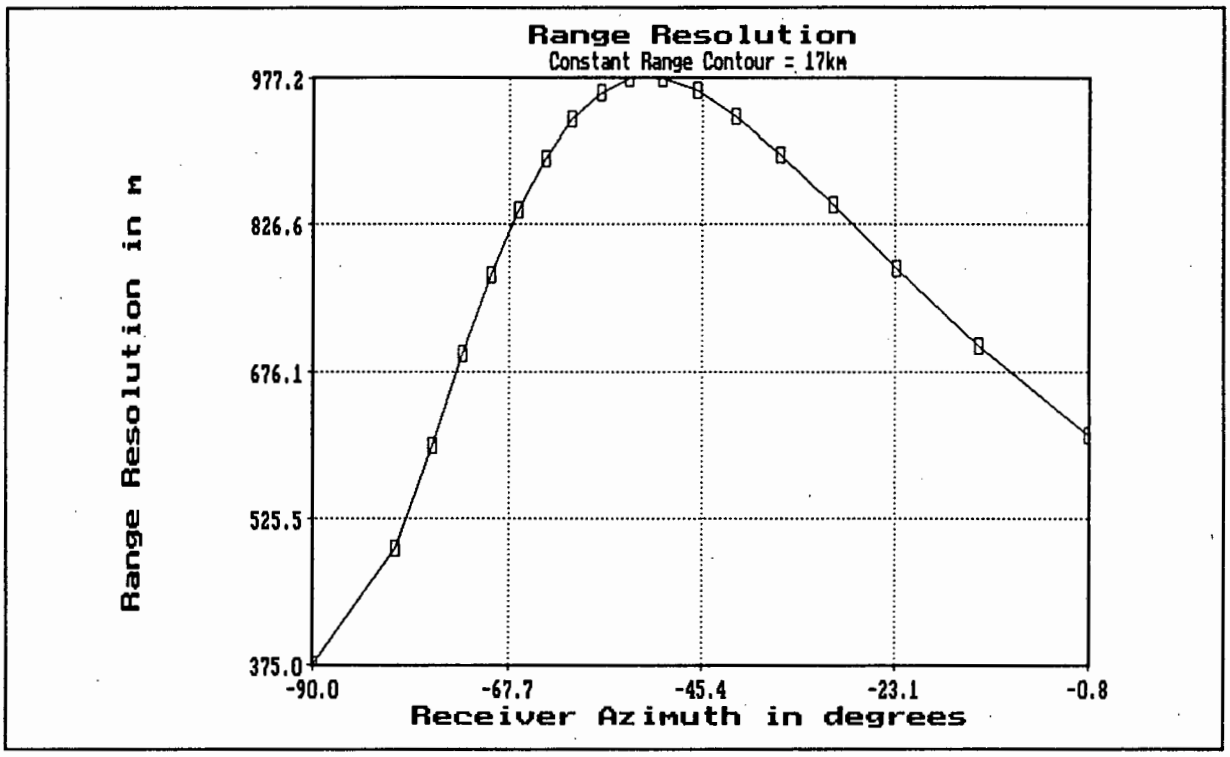

Figure 3.35 *The range resolution over a constant range contour of 17km.*

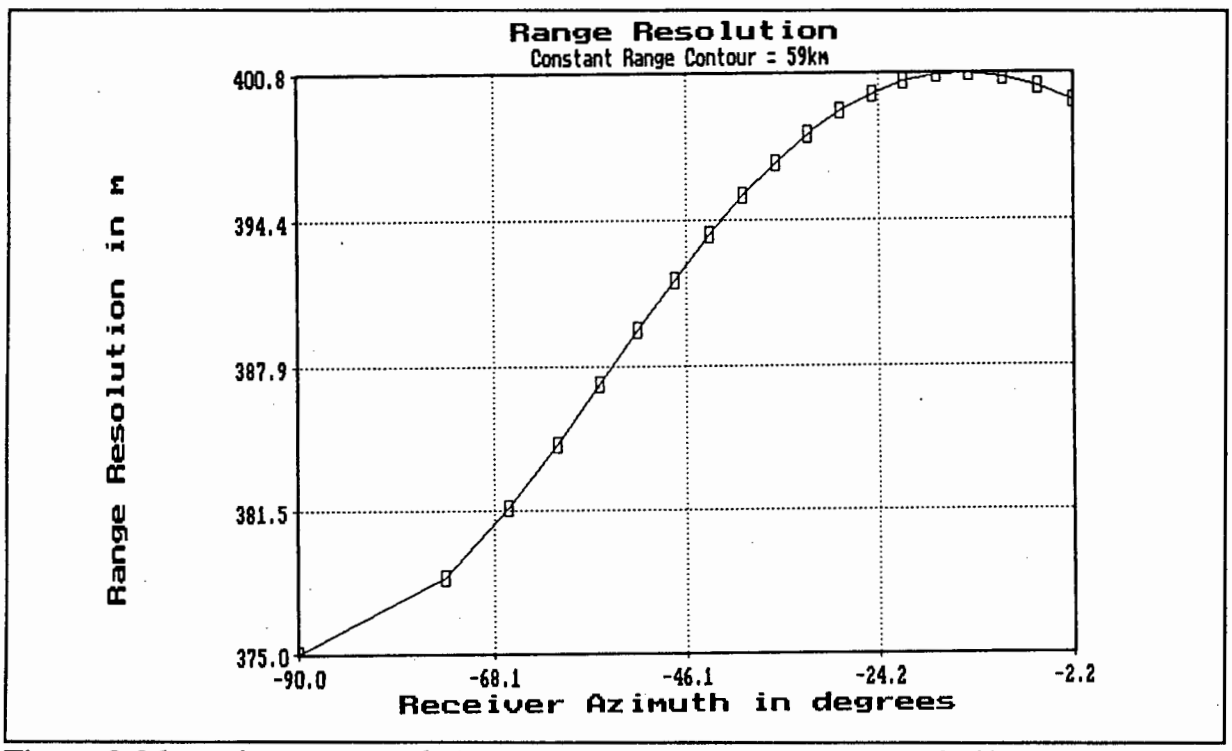

Figure 3.36 *The range resolution over a constant range contour of 59km.*

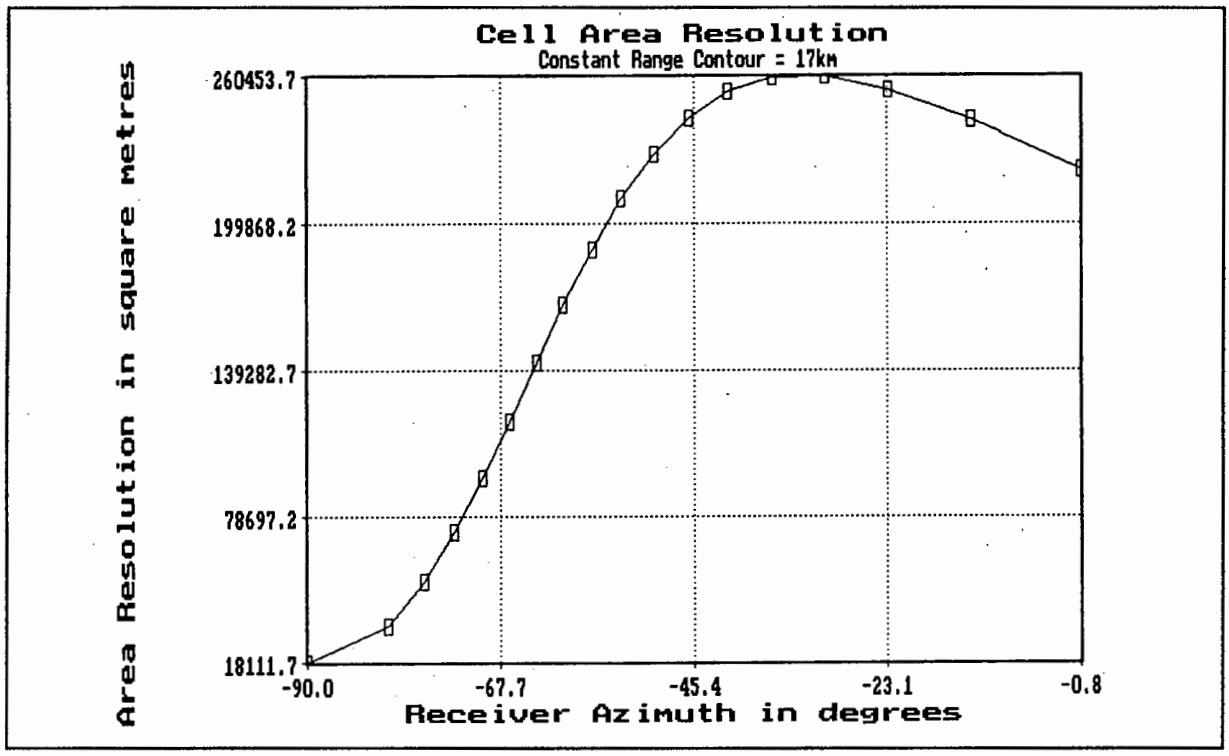

Figure 3.37 *The cell area resolution over a constant range contour of 17km.*

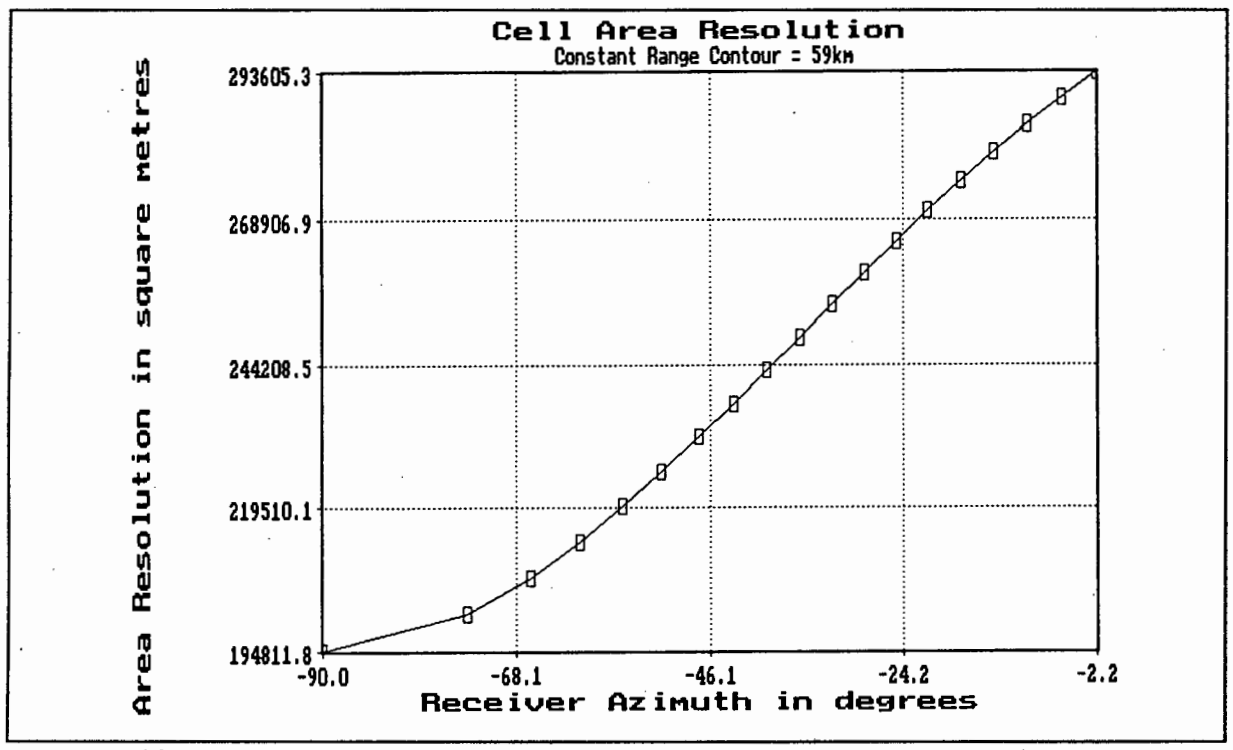

Figure 3.38 *The cell area resolution over a constant range contour of 59km.*

The range and cell area resolution on the baseline are undefined. The azimuth resolution is that of the transmitter antenna, namely 1.35°.

3.3.5 AZIMUTH SYNCHRONIZATION

The receiver needs to know, at all times, the transmitter antenna's azimuth angle in order to display accurate azimuth information of the target on a PPI display at the receiver, as was described in Section 2.4.8. Hence the receiver must be synchronized to the transmitter antenna's rotation. A digital circuit was designed to accomplish this as will be explained below.

Azimuth synchronization is performed during the dwell period. During this period about 32 direct pulses are obtained and from this the time that the main beam points at the receiver can be determined. The centre of the main beam is determined by counting the number of pulses received during the dwell period. The beam is then declared to be centred when the number of pulses counted is equal to half the number of the previous count. When the centre of the main beam is detected a counter is reset, providing a reference for the transmitter pointing angle. It then starts counting out 1024 discrete azimuth positions in the 360° rotation, giving an angular resolution of 0.35° per count. When the centre of the main beam is detected again the counter is reset and the cycle repeats itself. Before the counter is reset the final count is noted and the operator is informed whether the count rate is too fast or too slow. The rate at which the counter counts can then be adjusted by the operator to maintain synchronization. The frequency of the counter can be varied from 75Hz to 115Hz allowing tuning for a rotation period between 9sec and 13sec. A 10 bit bus, containing the azimuth information, is connected to the display processor in order to drive the PPI display. A block diagram of the azimuth synchronization circuit is shown in

Figure 3.39 which illustrates what has been described in the above paragraph. The circuit diagram is given in Appendix 8. Figure 3.40 shows the train of threshold detected pulses, determination of the centre of the main beam and then resetting of the counters.

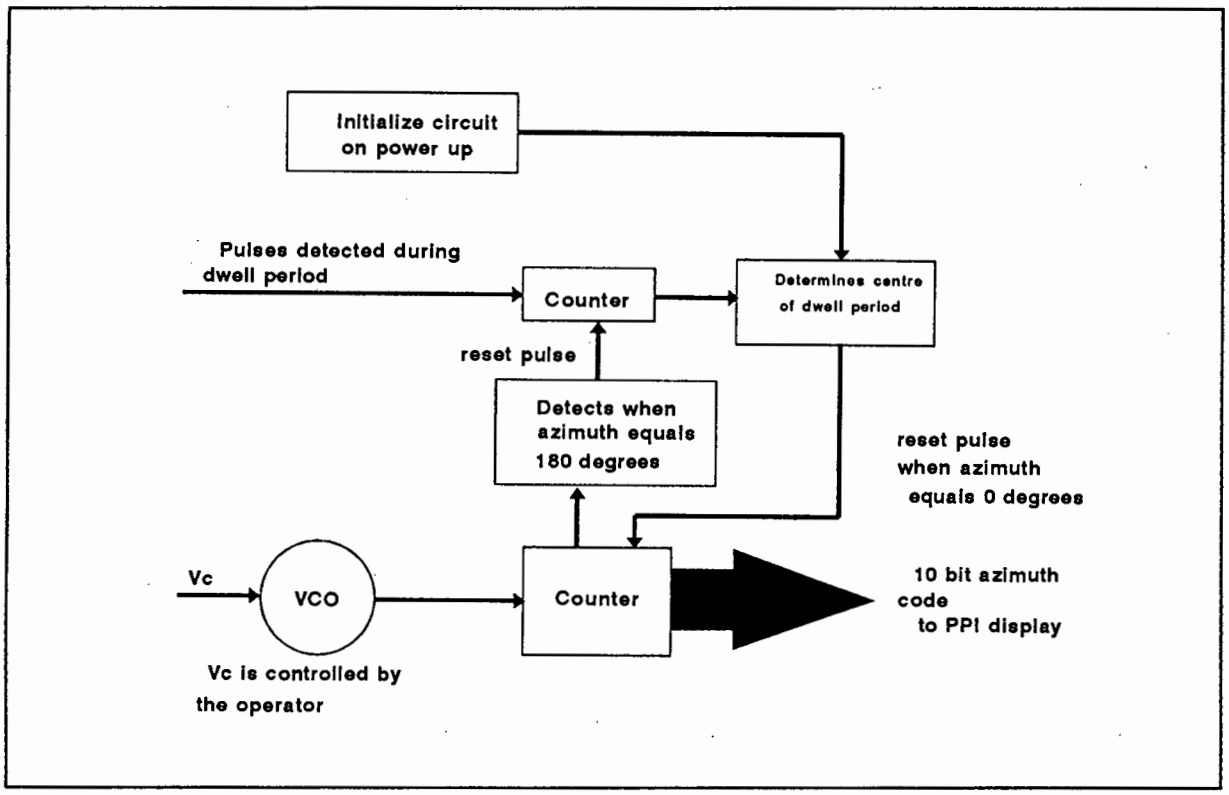

Figure 3.39 *The block diagram of the azimuth synchronization circuit.*

Two causes for an error in the synchronization can be obtained, namely:

1. The period of rotation of the transmit antenna is not consistent.

2. The within-scan rotation rate fluctuates.

The first error can be corrected for by the operator by adjusting the count rate of the counter. The second error presents a problem as the receiver has no way in determining these fluctuations without some form of communication between the

transmitter and the receiver. This therefore leads to a degradation in accuracy. As no measurements have been done to determine this error, it is assumed that for the purposes of this project that the transmit antenna scan rate is constant.

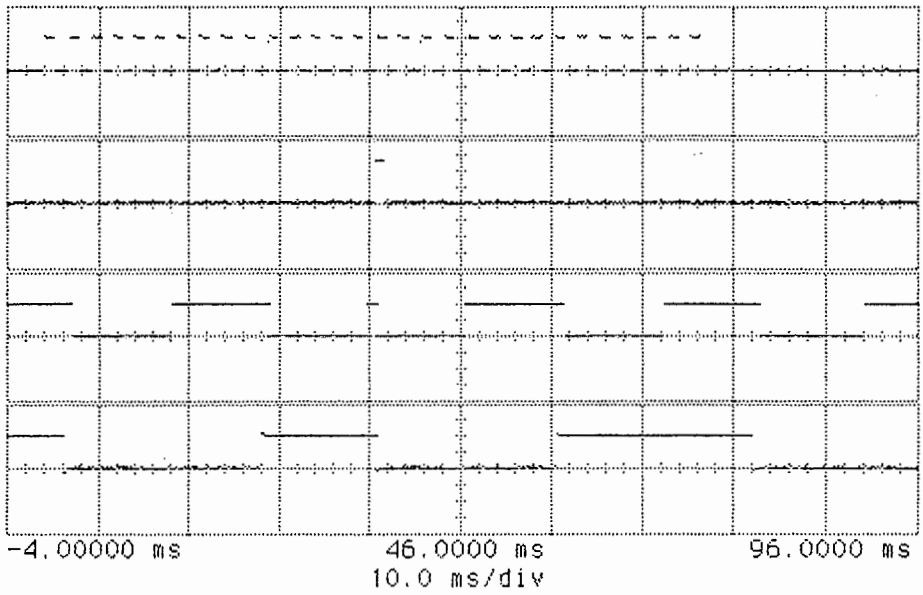

Figure 3.40 *The top two graphs show the pulses detected during the dwell period and the circuit determining the centre of the pulse train. The bottom graphs show the first two bits of the azimuth counter resetting.*

Other sources of error are the determination of the centre of the main beam signal and in alignment of the transmitter-receiver baseline and the stability of the voltage controlled oscillator which determines the azimuth count rate. The number of pulses counted during the dwell period never varied by more than 8 counts from one receiver illumination to the next. This would cause, in the worst case, the counter to be reset four pulses too soon or too late, giving a maximum error of $\pm 0.3°$. In the second case, the voltage controlled oscillator has a stability of ± 0.4Hz. This gives an error of 1.68°.

The error of the system was measured on a calm day with no wind (to avoid errors caused by in-scan variations) and shown to have an accuracy of 2.1°.

3.3.6 PULSE REPETITION FREQUENCY SYNCHRONIZATION

The receiver must regenerate the PRF of the transmitter at the receiver and maintain synchronization, in order to determine the correct target-receiver range and to trigger the STC circuit. An analog circuit consisting of a sampled phase locked loop was designed to achieve this.

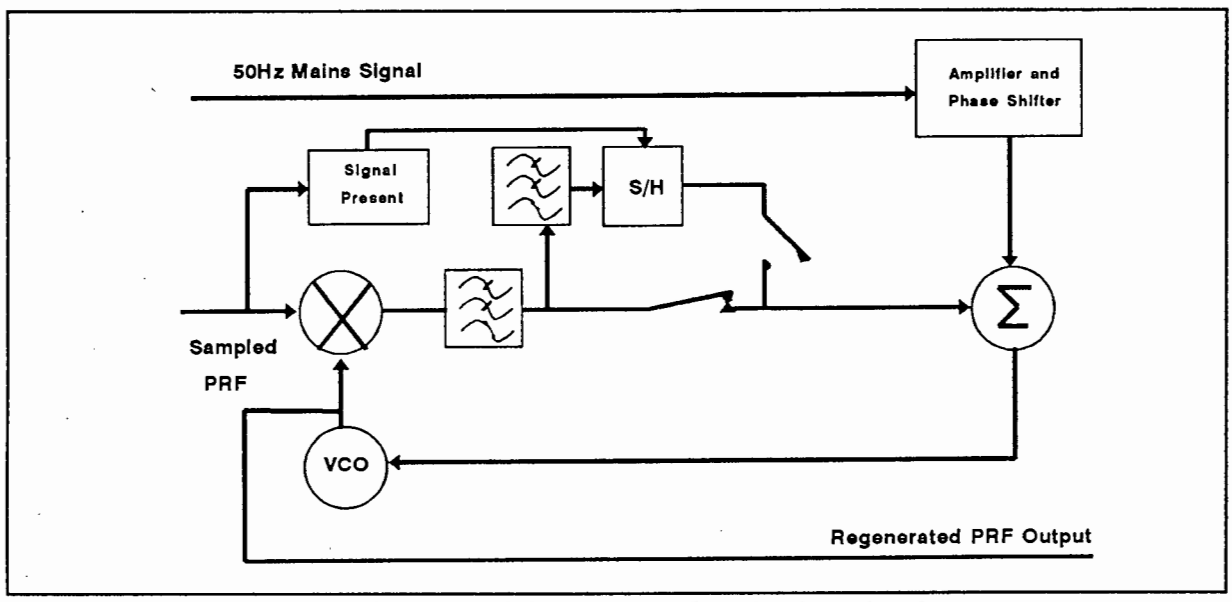

Figure 3.41 *The block diagram of the PRF synchronization circuit.*

The receiver PRF synchronization is also performed during the transmitter main beam dwell period. A block diagram of the PRF synchronization circuit is shown in Figure 3.41. Recall from Section 3.2 that the 400Hz PRF is wobulated at 50Hz. A precision voltage controlled oscillator (VCO) is tuned to its centre frequency of 400Hz. A 50Hz signal, which is tunable in phase and amplitude, is used to frequency modulate the centre frequency of the VCO thereby regenerating the PRF frequency. The 50Hz signal is obtained from the mains and is suitable as the transmitter uses the same source. Synchronization is performed during each main beam dwell period to align the transmitter and receiver PRF signals. Before this synchronization takes place the relative timing of the two PRF signals are

compared, in order that the VCO centre frequency may be altered to compensate for frequency drifts due to temperature variations in either the transmitter or receiver. This is achieved by incorporating the VCO into a phase lock loop (PLL). The error voltage out of the comparator will then adjust the VCO frequency accordingly. As the main beam dwell period only lasts for $\pm$80msec in a 12sec period, a sample and hold is required to hold the error voltage till the next dwell period. A "signal present" circuit is used to switch the sample and hold between its two modes. The circuit diagram of the PRF synchronization circuit is shown in Appendix 9.

The theory of PLL will not be dealt with here but the reader is referred to references [24] and [29]. The main criteria of the circuit is for the PLL to lock within a maximum time of 80msec. An XR-2212 PLL was chosen as it is an ideal FM detector and one has the ability to control the individual components which make up a PLL (phase comparator and VCO) independently. The specifications of this PLL are in Appendix 9. The loop damping factor is set at 0.3 making the loop underdamped thereby decreasing the lock-in time. The PLL has a gain of 432Hz/rad and a tracking bandwidth of 180Hz. The PLL has an average lock-in time of 60msec with a standard deviation of 17msec which is sufficient to achieve synchronization.

A problem which had to be overcome was the fact that the low pass filter did not sufficiently suppress the interference (2V p-p, 800Hz) on the DC error voltage. This interference caused the sample and hold to lock on at the incorrect error voltage. This was corrected by placing a low pass filter (τ = 18msec) before the sample and hold. This reduced the interference to 30mV p-p. The reduced interference will cause a maximum error of $\pm$0.7Hz and the probability of obtaining this error is 0.06. Two sample and hold circuits are used to reduce the droop rate of the held error voltage. For a hold period of 12sec an increase in frequency of 0.09Hz was observed.

The main problem in the design was to insert the 50Hz wobulation into the 400Hz signal. An initial attempt was to use two PLLs, one to lock onto the 50Hz component and the other the 400Hz component, during the main beam dwell period. The regenerated 50Hz would then be used to wobulate the 400Hz signal. This would prevent any phase error. This attempt was unsuccessful as only two cycles were present during the dwell period. The PLL required a minimum of six cycles to achieve lock. The second method, as described above, used the 50Hz from the mains. This method works but has several disadvantages, namely:

1. The circuit is not entirely independent.

2. To keep the two PRF signals in alignment, the 50Hz signal requires periodic tuning in phase and amplitude.

3. When large inductive loads are switched on and off on the electrical power network, a shift in phase is caused.

4. There is no visual indication to inform the operator that the circuit is out of synchronization.

5. It is difficult to synchronize as there are two parameters and one does not know whether the electrical network is stable at the time.

Due to the scope of this project no error measurements were taken, hence the accuracy of the system is unknown at this stage. Measurements showing the lock in time of the PLL during the dwell period are shown in Figure 3.42 and Figure 3.43. The error in the loop and the filtered error voltage used by the sample and hold are shown. Here the suppression of the interference on the error voltage to the sample and hold is clearly shown. In Figure 3.42 there is a 60° phase error in the 50Hz modulating frequency. Tuning of the PRF circuit is ideally done by reducing the AC error voltage to a DC voltage as shown in Figure 3.43.

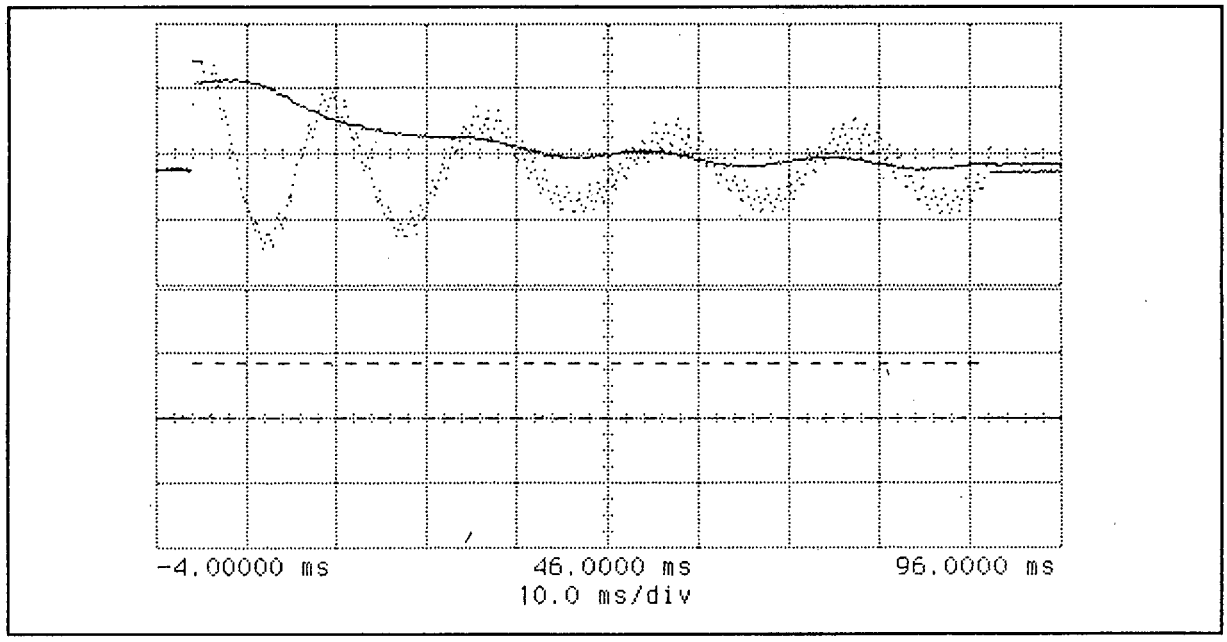

Figure 3.42 *Shows the error voltage of the PLL. The smooth curve is the filtered error voltage applied to the sample and hold. Here there is a 60° phase error in the 50Hz signal.*

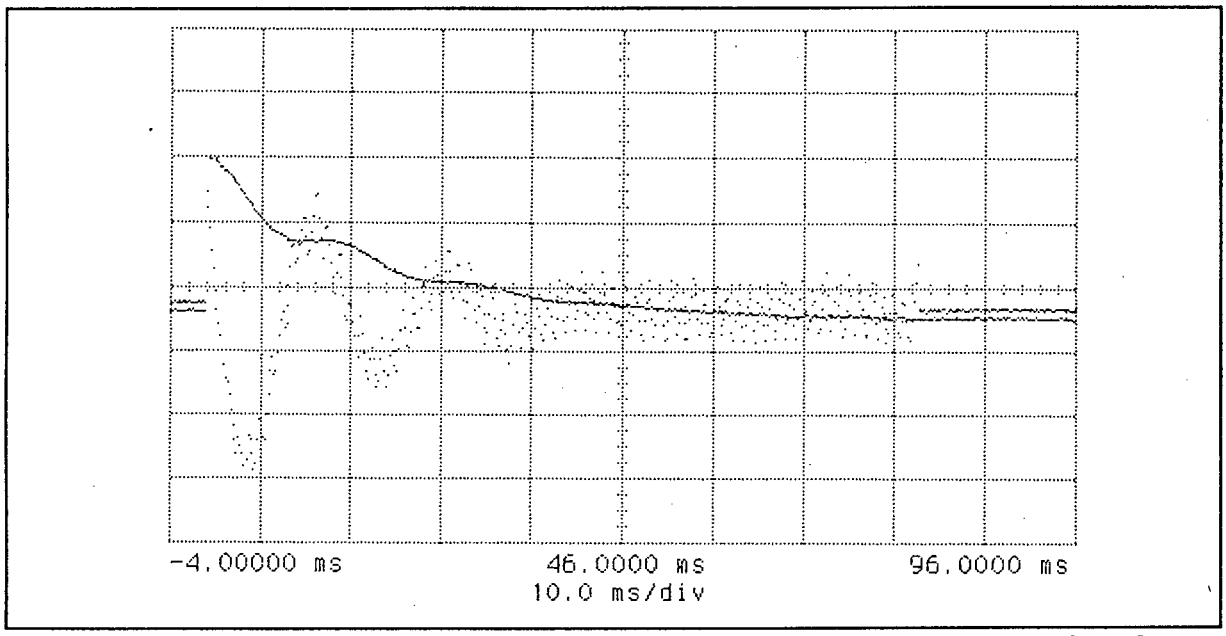

Figure 3.43 *Shows the error voltage of the PLL. The smooth curve is the filtered error voltage applied to the sample and hold. Here the circuit is tuned. The vertical scale = 2V/div with an 8V offset.*

It is felt that due to the many disadvantages, an alternative approach should be taken. This will be discussed in the Recommendations.

3.3.7 THE PLAN POSITION INDICATOR DISPLAY

In order for the operator to determine the targets position relative to himself or the receiver some form of display is required. A display system was designed and built by R. Blatch. A detailed analysis of the display system will be found in reference [30], however, a summary is provided in this Section.

A plan position indicator (PPI) is used. The display corrects for bistatic distortion which is achieved by controlling the motion of the scanning beam of the display according to the equations given in Section 2.4.8 on bistatic distortion. Basically for every discrete transmitter azimuth position the display must determine the receiver azimuth and target to receiver range for a set number of delay times. The maximum delay time is determined by the maximum range of the bistatic radar, in this case the display has been designed to monitor a maximum range of 100km. The period between two delay times is determined by the bistatic radar resolution. In order to drive the display, the polar coordinates (receiver azimuth and target to receiver range) are converted to cartesian coordinates and then applied to the x and y deflection plates of the display. The output of the detector (video output) from the receiver is connected to the z input of the display.

An EPROM based counter is used to drive the display. The EPROMs store the azimuth and range information in cartesian coordinates. A counter is used to address the memory and synchronization of the display is maintained by the PRF and transmitter azimuth information derived by the synchronization systems.

Due to availability an HP1311A is used as a PPI display. The display has three inputs, namely the x and y inputs which determine the beam position and the z input which accepts the video signal. Enhancements are made to the display with the use of an HP1350A graphics translator and an HP85 computer. These two items allow a geographical map of the coverage area and range rings to be displayed on the screen permanently. A major pitfall of the display is its low permanence phosphor. This makes it difficult for the operator to read the screen as the received echoes are short lived.

The display provides an azimuth resolution of 1.3° and a range resolution of 782m.

3.4 CLUTTER PREDICTIONS

It is important to know the clutter power returns at the receiver. This is to enable proper design of the receiver and prevent the receiver from saturating. Two projects were carried out in order to determine the expected clutter returns at the receiver at UCT. These will now be described.

The first project was carried out by Tim Courtenay [4]. As he was unable to find bistatic data on the clutter coefficients, he used monostatic data. His motivation for this is that at long target ranges compared to the baseline range (small bistatic angle), the bistatic radar starts approximating a monostatic radar. From Section 2.4.10 the bistatic-monostatic equivalence theorem states that the monostatic RCS can be used in place of the bistatic RCS under these conditions. Also for this reason only equations describing the monostatic radar were used.

The following assumptions were made in his calculations:

- low grazing angle
- radar energy scattered isotropically
- sidelobes add negligible clutter
- Cape region can be divided into discrete areas with different scattering coefficients.

The illuminated region was divided into the following areas and given three clutter coefficients [4], namely case 1, case 2, and case 3:

- urban Cape Flats, $\sigma_M^\circ = 0.04/RT^{0.5}$, $0.01/R_T^{0.5}$ and $0.05/R_T$
- Constantiaberg, $\sigma_M^\circ = 0.03$, 0.01 and 0.01
- Hottentots Holland mountains, $\sigma_M^\circ = 0.03$, 0.01 and 0.01
- Tierberg mountains, $\sigma_M^\circ = 0.03$, 0.01 and 0.01
- Sea, -45dB

The results of his project are shown in Figures 3.44, 3.45, 3.46, 3.47.

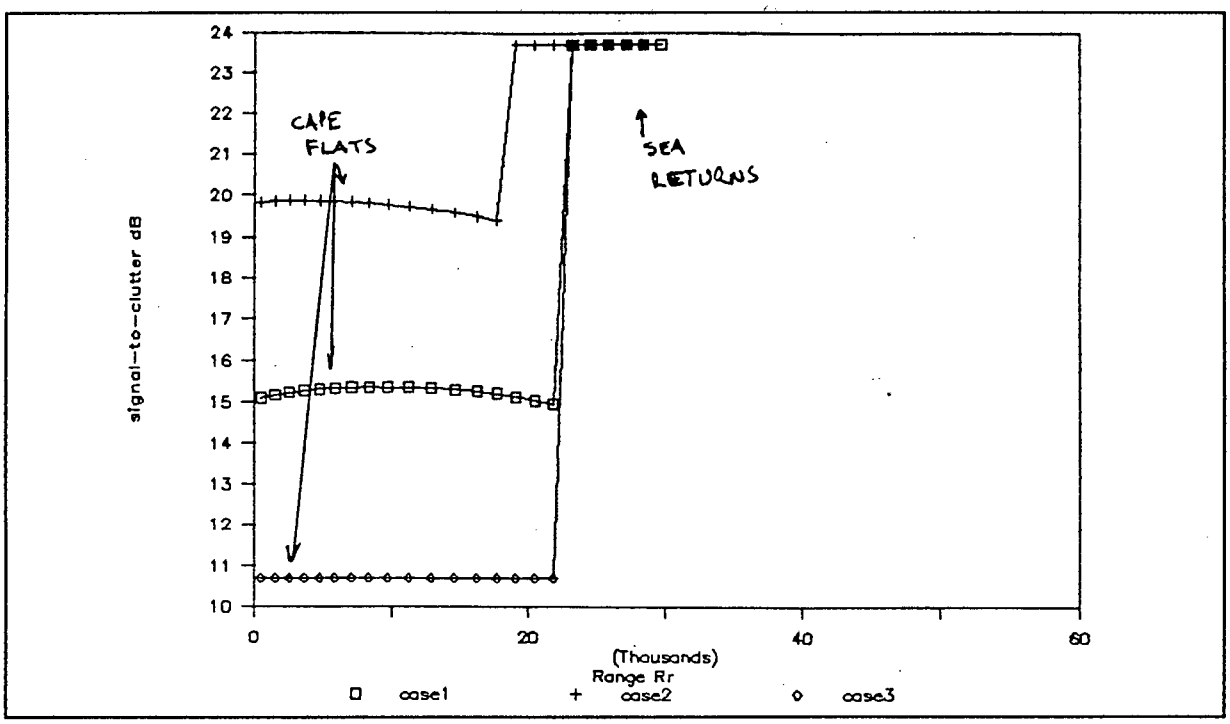

Figure 3.44 *Signal to clutter ratio for $\theta_T = 80°$.*

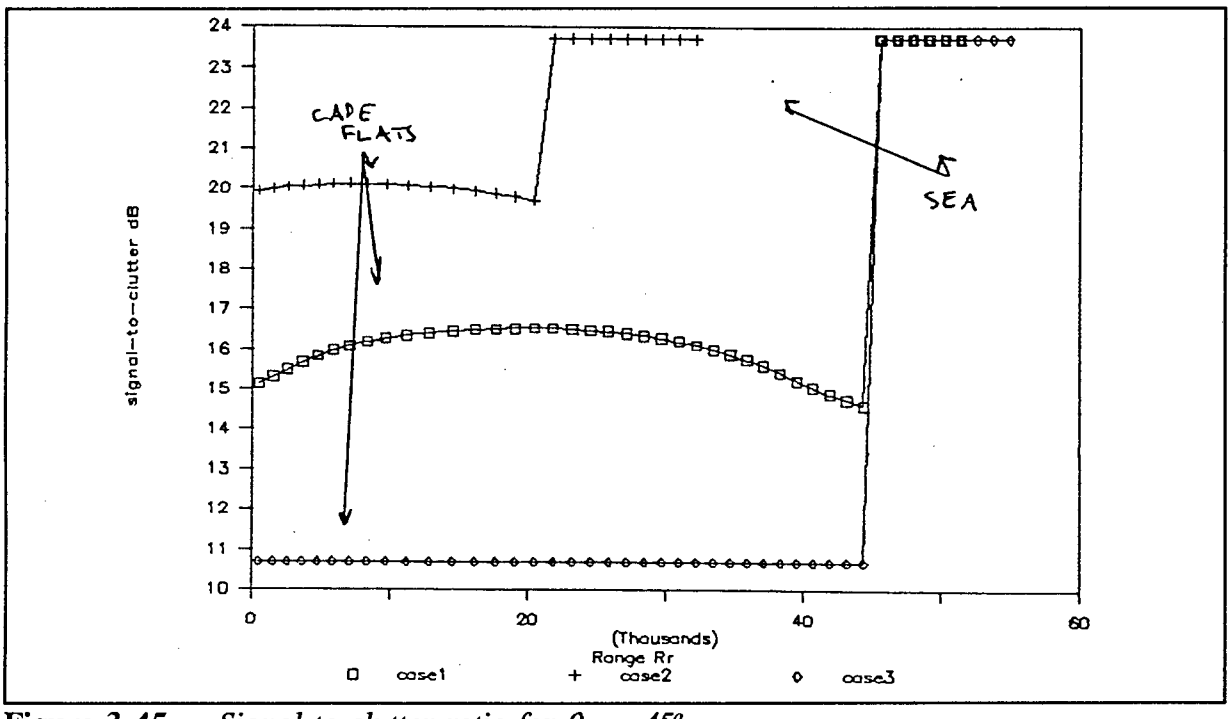

Figure 3.45 *Signal to clutter ratio for $\theta_T = 45°$.*

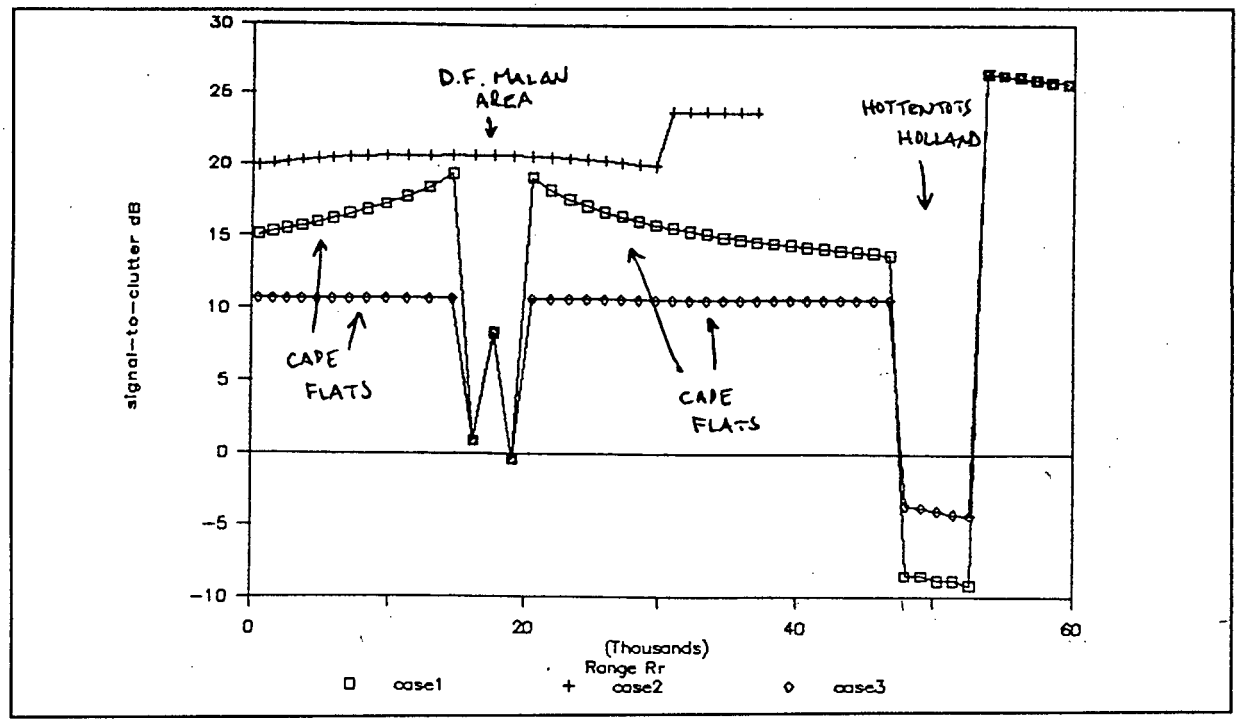

Figure 3.46 *Signal to clutter ratio for $\theta_T = 12°$.*

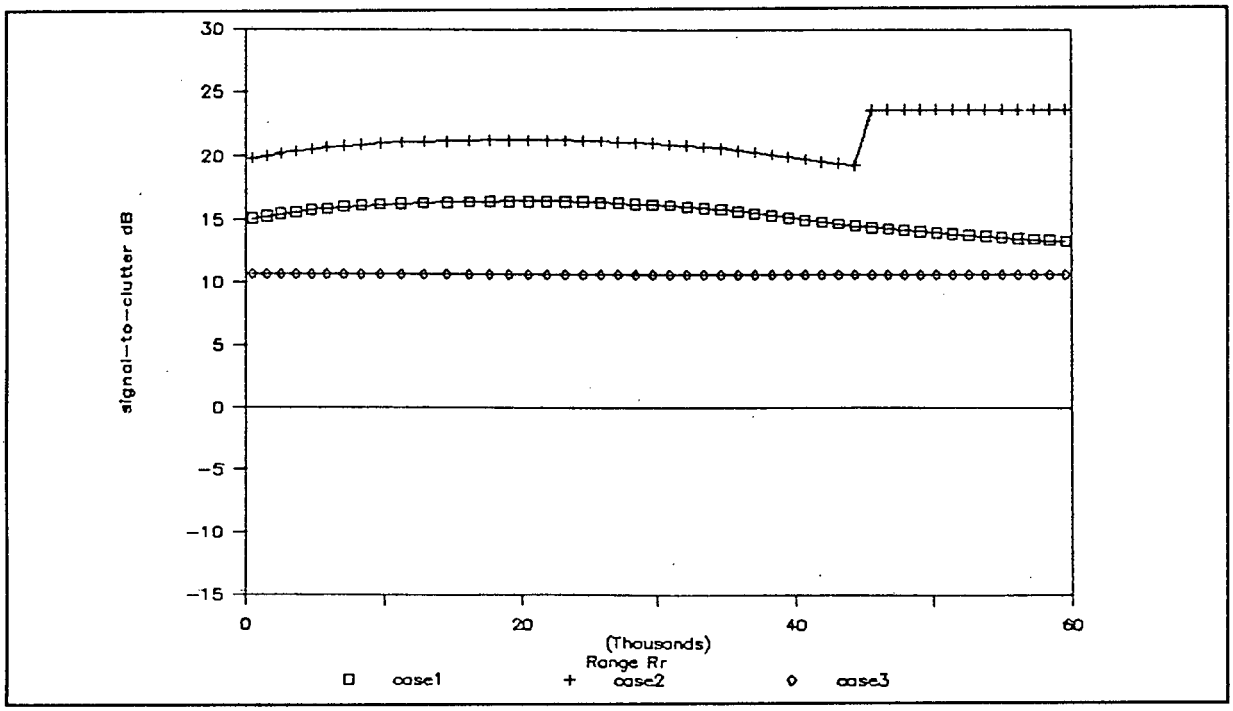

Figure 3.47 *Signal to clutter ratio for $\theta_T = 30°$.*

From these Figures, the signal to clutter ratio is high over the sea and lower over the Cape Flats region, as expected. A bad signal to clutter ratio is detected when passing the Hottentots Holland mountain range.

The second project calculates the expected clutter power returns using bistatic clutter coefficient data.

This data was obtained from Larson [1][15]. The data is out-of-plane, horizontally polarized, $\sigma_B°$ for tall weeds and scrub trees. Figure 3.48 shows Larsons L-band data.

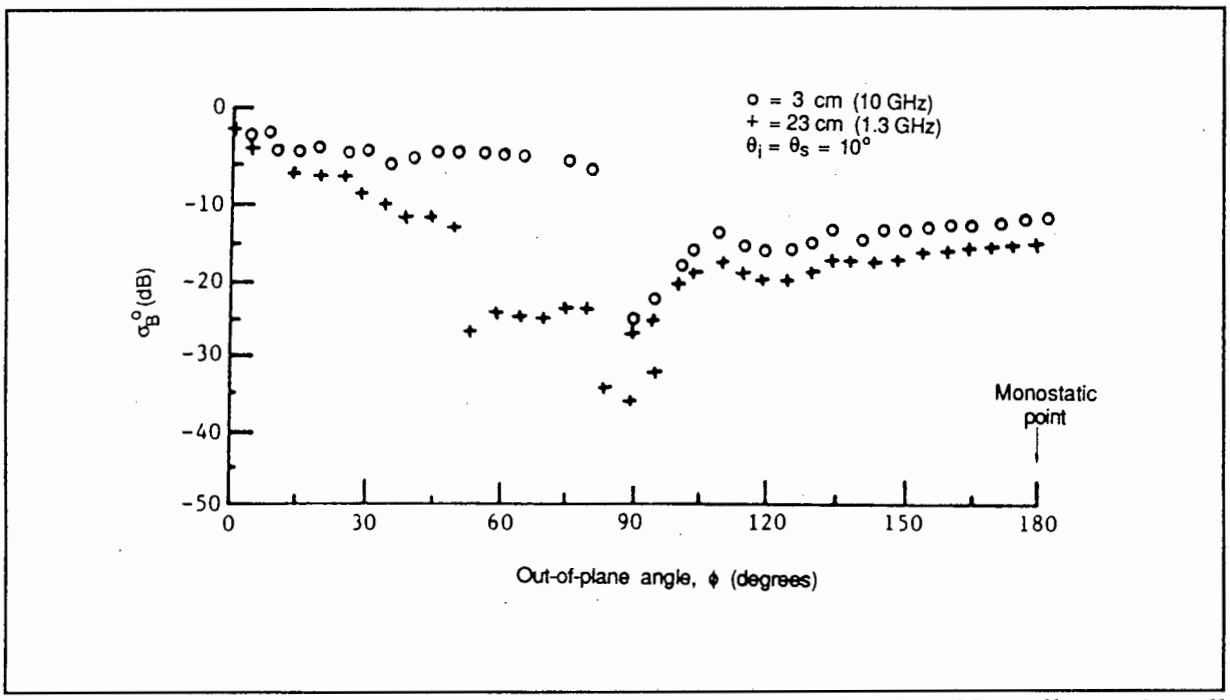

Figure 3.48 *Larson's out-of-plane, horizontally polarized, bistatic RCS coefficient for tall weeds and scrub trees.*

This data is valid for the Eastern side of D.F. Malan airport only but does not take into account the Hottentots Holland mountain range. The rest of the area is urban and no bistatic clutter coefficient data was available for this. Another difference is that the grazing angle is less than 2° at the transmitter and Larson's data is measured for a grazing angle of 10°. However, from reference [16] it was noted that the clutter coefficients for this case do not change significantly between 0 and 10 degrees.

Another approximation in the calculations, the clutter contributed by the sidelobes, has been ignored. The program which calculates the expected clutter returns is shown in Appendix 10. The signal to clutter ratio for two constant range contours of 19km and 27km are shown in Figure 3.49 and 3.50.

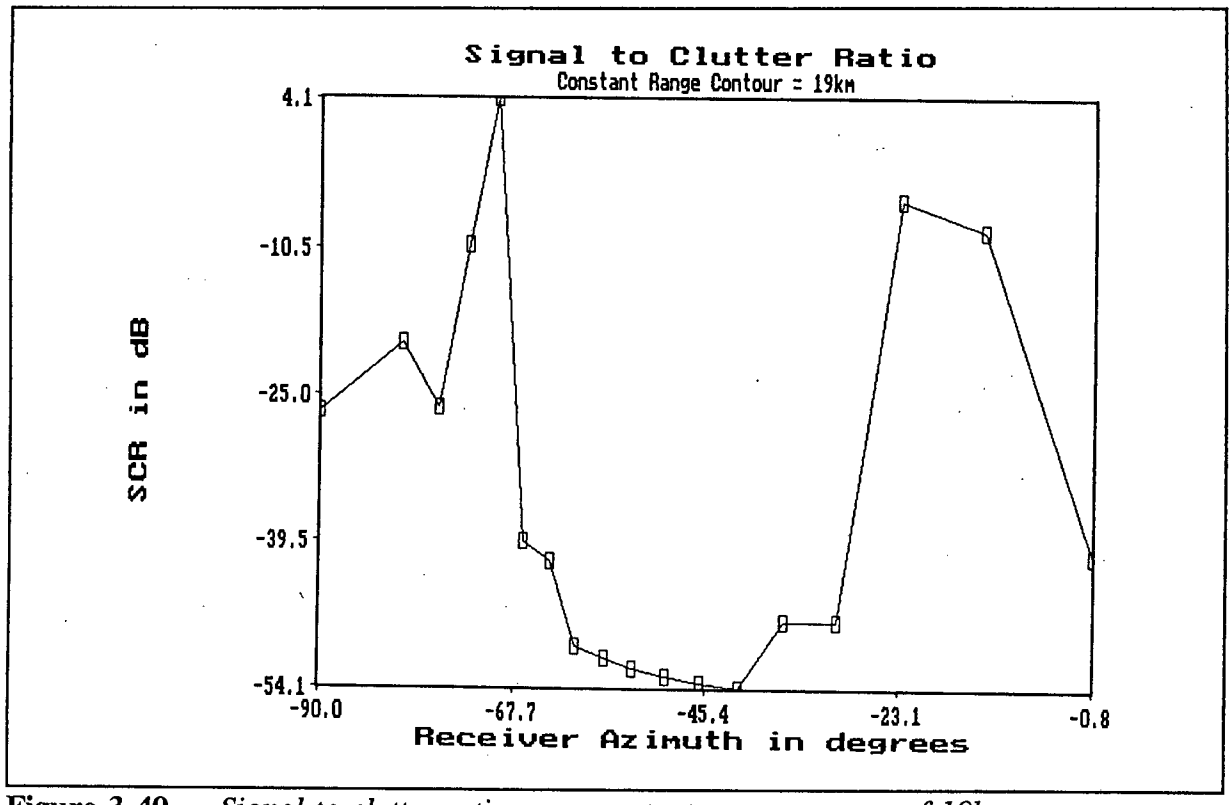

Figure 3.49 *Signal to clutter ratio on a constant range contour of 19km.*

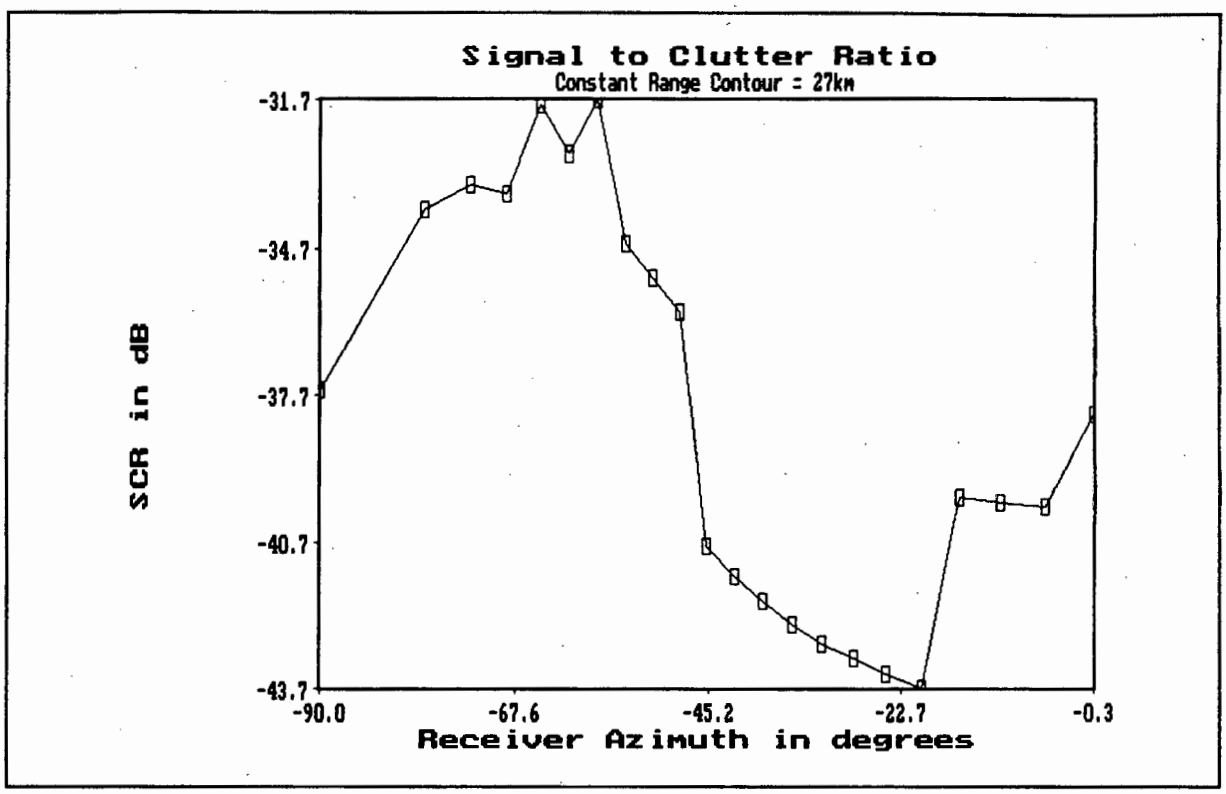

Figure 3.50 *Signal to clutter ratio on a constant range contour of 27km.*

According to these figures clutter will present a problem for a target with an RCS of $50m^2$. It appears that the SCR is large at the receiver azimuth angle of $\pm 80°$, however this is not consistent from one range contour to the next. One trend is noted: the average difference in the maximum and minimum SCR decreases as the range of the constant range contour is increased.

It is not possible to compare the two projects due to the many different assumptions made, however, it is interesting to note the vast differences. From the literature and Section 2.4.11 it is clear that bistatic radars are more susceptible to clutter than monostatic radars. This fact is definitely noticed in the above projects. For future work on this radar, it is recommended that accurate clutter measurements are taken in order to design a more appropriate STC control voltage curve or set of curves. From basic measurements on an A-scope and from the above results, the present STC circuit provides sufficient attenuation to prevent saturation, however the average sensitivity of the receiver is reduced due to the inefficiency.

3.5 CONCLUSION

Based on what has been said in this Chapter about the receiver, the following conclusions can be made:

1. The receiver sensitivity of -103dBm is sufficient to obtain a maximum dynamic range of 120km assuming no propagation losses.

2. The receiver will not be saturated by clutter or by a target with an RCS of $50m^2$ at the minimum transmitter-target or receiver-target range of 75m.

3. The power level of the pulses received during the dwell period will saturate the receiver. This requirement is not attained. This, however, is not critical as it only occurs during the dwell period when the receiver is blind.

4. The receiver regenerates the transmitter azimuth information for the purposes of this project with sufficient accuracy (2.1°).

5. The PRF synchronization circuit has several disadvantages due to the 50Hz wobulation. A problem with this circuit is that it relies on the mains to obtain the 50Hz. This is undesirable as the receiver is not totally independent. The accuracy of the regenerated PRF has not been ascertained.

6. The PPI display corrects the bistatic distortion satisfactorily. Unfortunately at the completion of the receiver and synchronization circuits the display was not operational due to an unknown electronic fault.

7. From the predicted clutter results, it appears that the detection of targets with an RCS of $50m^2$ will be severely hampered due to the large clutter echoes received.

CHAPTER 4
CONCLUSION

This report has discussed most of the aspects about bistatic radars. It was shown that the complexity of the bistatic radar is greater than the monostatic radar as remote synchronization is required and the PPI display is distorted. The performance of a bistatic radar will not exceed that of a monostatic radar, however, a bistatic radar has several advantages over the monostatic radar. Some of these advantages have been discussed. These advantages also make a bistatic radar the desired system for specific applications.

An experimental bistatic radar receiver has also been described for use in an air traffic control environment. Relatively simple and inexpensive PRF and azimuth scanning synchronization is achievable, allowing for a conventional PPI display of target information.

CHAPTER 5
RECOMMENDATIONS

To improve the performance of the bistatic radar receiver, the following recommendations are made:

1. A dedicated local oscillator can be designed to make the receiver less reliant on support equipment. This also allows the design of a sampled AFC circuit which is required to compensate for the transmitter and receiver frequency drift.

2. A limiter should be placed at the input of the low noise amplifier. This will prevent saturation of the receiver amplifiers during the main bang pulse. The limiter should be set such that the amplifiers operate just below the 1dB compression point. This will prevent the limiter from affecting the sensitivity of the level detector.

3. The azimuth resolution can be improved by replacing the VCO with a more stable oscillator such as a voltage controlled crystal oscillator or a crystal oscillator as a reference in a phased lock loop configuration. This method was used in the bistatic receiver designed at University College London. See reference [7].

4. An alternative method to regenerate the PRF should be used. One such method would require the use of a computer and an I/O card. The idea would be to sample and store the received PRF during the dwell period. The stored sample would have sufficient information to regenerate the PRF accurately. This method eliminates the need to use the unstable 50Hz from the mains.

5. Accurate clutter measurements should be taken for all azimuth positions. STC voltage control curves should then be determined for several azimuth angles. This can be done by using a look-up table. An EPROM can be used to store several curves and then the appropriate curve can be addressed for the corresponding azimuth.

6. The present display circuitry should be rebuilt onto a PC board to improve its reliability and the display must be replaced with one that has a much higher permanence phosphor.

From this report it is noted that the signal to clutter ratio could present a problem. An enhancement which can be done to improve this problem would be:

The antenna at the receiver can be replaced with a high gain directional scanning antenna. The scanning antenna can be synchronized to the existing azimuth synchronization system. In this case the antenna beam would not illuminate as much ground, hence reducing received clutter level. This system has the additional advantage that the dynamic range of the receiver would be increased.

BIBLIOGRAPHY AND REFERENCES

1. N.J. Willis, "Bistatic Radar", Artech House, 1991.
2. S.A. Hovanessian, "Radar Design and Analysis", Artech House Inc, 1984.
3. M.I. Skolnik, "Radar Handbook", McGraw-Hill Publishing Company, 2nd Edition.
4. G. Broomhall, R. Horwitz, D Gold, T Courtenay, "Bistatic Radar System Design for D. F. Malan Airport", EEE 548 Radar Project Course, University of Cape Town, 1989.
5. M. Del Mistro, M.R. Inggs, "Performance of an L-Band Bistatic Radar Receiver", AP-MTTS Conference, 1991.
6. J.I. Glaser, "Fifty Years of Bistatic and Multistatic Radar", IEE Proc., Vol. 133, No. 7, pp. 596-603, December 1986.
7. J.G. Schoenenberger, J.R. Forrest, "Principles of Independent Receivers for use with Co-operative Radar Transmitters", The Radio and Electronic Engineer, Vol. 52, No. 2, pp. 93-101, February 1982.
8. M.C. Jackson, "The Geometry of Bistatic Radar Systems", IEE Proc., Vol. 133, No. 7, pp. 604-612, December 1986.
9. E. Hanle, "Survey of Bistatic and Multistatic Radar", IEE Proc., Vol. 133, No. 7, pp. 587-595, December 1986.
10. M.I. Skolnik, "An Analysis of Bistatic Radar", IRE Trans. on Aerospace and Navigational Electronics, pp. 19-27, March 1961.
11. E.F. Ewing, "The Applicability of Bistatic Radar to Short Range Surveillance", Radar 77, pp. 53-56.
12. W.A. Pierson, C.S. Liang, R.W. Clay, "The Effect of Coupling on Monostatic-Bistatic Equivalence", Proc. of the IEE, pp. 84-86, January 1971.
13. M. Green, "Parasitic Picture", Electronics World and Wireless World, pp. 679-681, August 1991.
14. J.I. Glaser, "Bistatic RCS of Complex Objects near Forward Scatter", IEEE Trans. on Aerospace and Electronic Systems, Vol. AES-21, No. 1, pp. 70-78, January 1985.

15. R.W. Larson, A.L. Maffett, "Bistatic Clutter Measurements", IEEE Trans. on Antennas and Propagation, Vol. AP-26, No. 6, pp. 801-804, November 1978.
16. F.T. Ulaby, M.C. Dobson, "Handbook of Radar Scattering Statistics for Terrain", Artech House Inc, 1989.
17. A. Farina, E. Hanle, "Position Accuracy in Netted Monostatic and Bistatic Radar", IEEE Trans. on Aerospace and Electronic Systems, Vol. AES-19, No. 4, pp. 513-520, July 1983.
18. M. Mangel, "Three Bearing Method for Passive Triangulation in Systems with unknown Deterministic Biases", IEEE Trans. on Aerospace and Electronic Systems, Vol. AES-17, No. 6, pp. 814-819, November 1981.
19. C.C Johnson, "Triangulation Theory and Techniques", Journal of The Institute of Navigation, Vol. 17, No. 3, pp.308-324, 1970.
20. R.S. Elliott, "Antenna Theory and Design", Prentice-Hall, 1981.
21. M.I. Skolnik, "Introduction to Radar Systems", Mc Graw-Hill Book Comp., 1962.
22. "The 1990 ARRL Handbook for the Radio Amateur", published by The American Radio Relay League, edition 67, 1990.
23. K.L. Smith, "Noise-Confusion in more ways than one", Wireless World, March 1975 - May 1975.
22. RF/Microwave Amplifier Handbook, Mini-Circuits Laboratories, Volume 3, 1991.
23. G.R. Jessop, VHF UHF Manual, Radio Society of Great Britain, Fourth Edition, 1983.
24. F.G. Stremler, "Introduction to Communicatin Systems", Addison-Wesley Publishing Company, 1982.
25. H.L. Krauss, C.W. Bostian, F.H. Raab, "Solid State Radio Engineering", John Wiley and Sons.
26. H.C. Miller, "Inductance Formula for a Single-Layer Circular Coil", Proceedings of the IEEE, Vol. 75, No. 2, pp. 256-257, Febraury 1987.
27. Mixer Applications Handbook, Mini-Circuits Laboratories, 1989.
28. Alpha Microwave Semiconductors Data Book, Alpha Industries.
29. Signetics Application Notes, Signetics Corporation, pp 6-1 to 6-64, 1974.
30. R. Blatch, Radar Display System for a Monostatic and Bistatic Radar, Fourth Year Electrical Engineering Thesis, Nov. 1991.

APPENDIX 1

Table 1.1 gives some general bistatic radar applications for various transmitter and receiver configurations. The table was obtained from reference [1].

Table 1.1

Bistatic Radar Operating Regions	*Range Relationships*	*Transmitter Configuration*		
		Dedicated	*Cooperative*	*Noncooperative*
Receiver Centered	$L > 2\sqrt{\kappa}$ $R_T \gg R_R$	• Air-to-ground attack (silent penetration) • Semiactive homing missile (LOAL)[a]	• Over-the-shoulder operation • Passive situation awareness	• Passive situation awareness
Transmitter Centered	$L > 2\sqrt{\kappa}$ $R_R \gg R_T$	—	—	• Monitoring • Launch alert
Cosite	$L < 2\sqrt{\kappa}$	• Medium-range air defense • Satellite tracking • Range instrumentation • Semiactive homing missile (LOBL)[b] • Intrusion detection	—	—

Table 1.2 gives a summary of measurement programs for bistatic radar scattering coefficients. This table was obtained from reference [1].

Table 1.2

Reference (Date)	*Organization*	*Author*	*Surface Composition*	*Frequency*	*Polarization*	*Measurement Angles (degrees)* θ_i	θ_s	ϕ
42 (1965)	Ohio State University (Antenna Laboratory)	Cost, Peakes	Smooth sand Loam Soybeans	10 GHz	VV, HH, HV	5–30, 10–70	5–30, 5–90	0–145, 0, 180
			Rough sand Loam with stubble Grass			5–70	5–90	0, 180
43 (1966)	Johns Hopkins University (APL)	Pidgeon	Sea (Sea states 1, 2, 3)	C-band	VV, VH	0.2–3	10–90	180
107 (1967)			Sea (Beaufort, wind 5)	X-band	HH	1–8	12–45	180
108 (1967)			Rural land Urban land Sea (20-kt wind)			6–90*	6–180*	180, 165
109 (1968)	G.E.C. (Electronics) Ltd., England	Domville	Sea (20-kt wind)	X-band	VV, HH	≈0–90*	≈0–180*	180, 165
110 (1969)			Semidesert			≈0	?	180, 165
111 (1977) 112 (1978)	University of Michigan (ERIM)	Larson, Heimiller	Grass with cement Taxiway Weeds and scrub trees	1.3 and 9.4 GHz	HH, HV	10, 40 10, 15, 20	5, 10, 20	0–180 0–105
113 (1982) 114 (1984)	Georgia Institute of Technology (EES)	Ewell, Zehner	Sea (0.9m, 1.2–1.8 m wave heights)	9.38 GHz	VV, HH	≈0	≈0	90–160
115 (1988)	University of Michigan (Dept. of Electrical Engineering & Computer Science)	Ulaby *et al.*	Visually smooth sand			24	24	0–170
			Visually smooth sand Rough sand Gravel	35 GHz	VV, HH, VH, HV	30 30	30 10–90	0–170 0–90

APPENDIX 2

The artwork of the PC boards used in several circuits are shown in this appendix. The artwork diagrams have not been scaled.

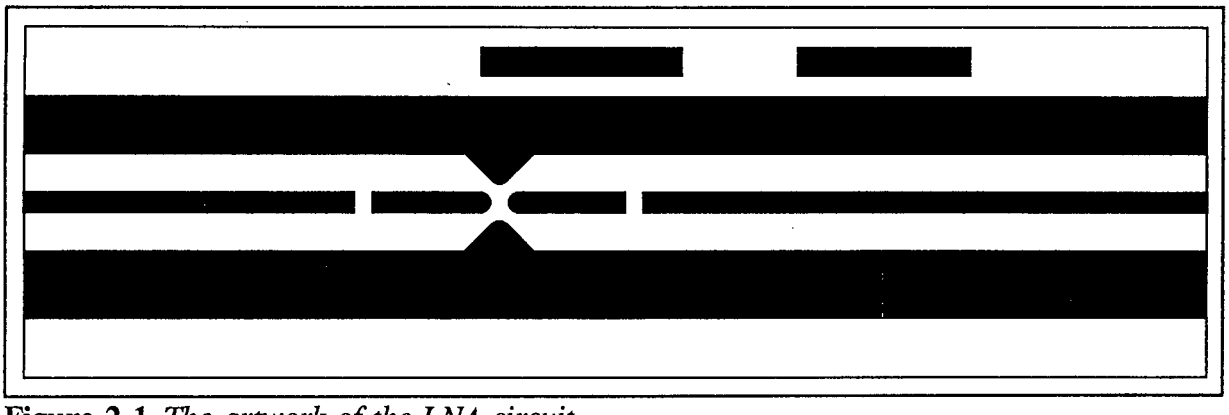

Figure 2.1 *The artwork of the LNA circuit.*

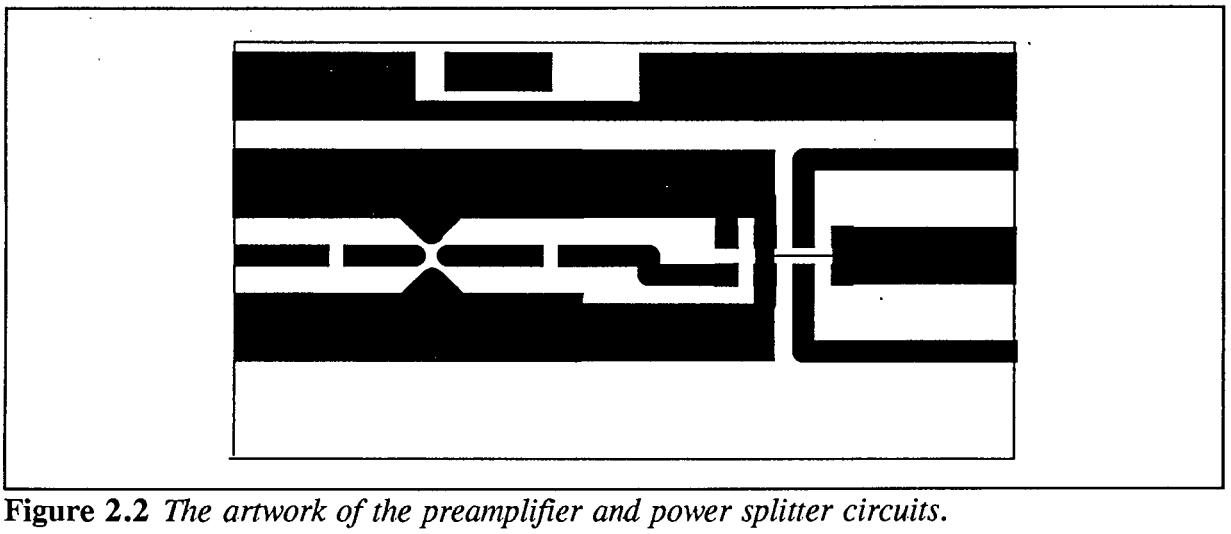

Figure 2.2 *The artwork of the preamplifier and power splitter circuits.*

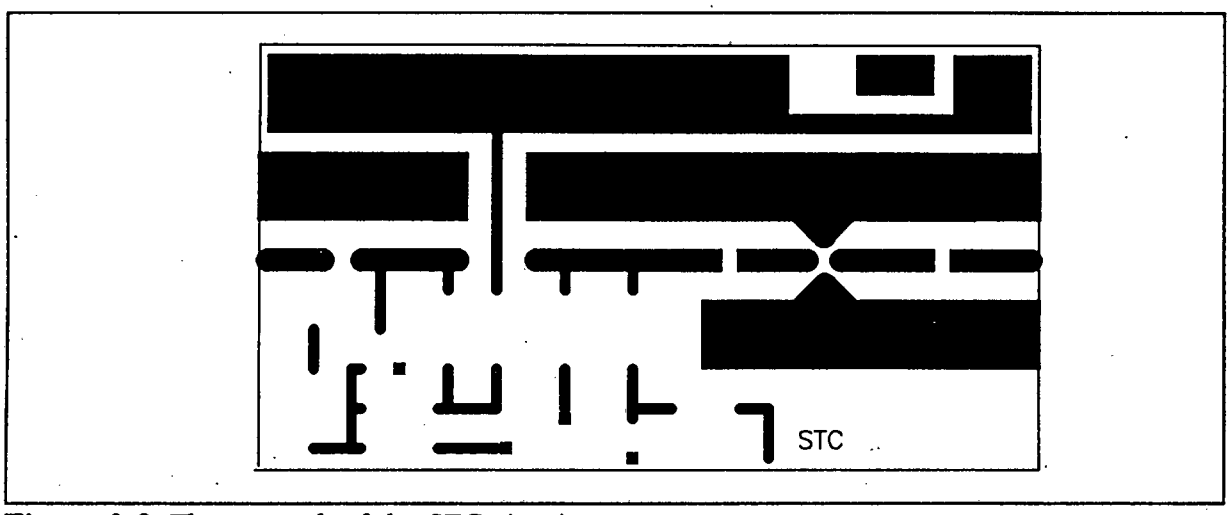

Figure 2.3 *The artwork of the STC circuit.*

APPENDIX 3

The specifications of the Mini-Circuit components used in the receiver are given below.

Power Splitter/Combiners

2 WAY–0°

DC to 4.2 GHz

case style selection

outline drawings see Table of Contents

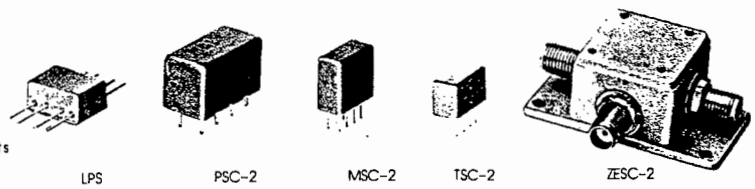

LPS PSC–2 MSC–2 TSC–2 ZESC–2

	MODEL NO.	FREQ. RANGE MHz f_L–f_U	ISOLATION dB L Typ.	L Min.	M Typ.	M Min.	U Typ.	U Min.	INSERTION LOSS, dB Above 3dB L Typ.	L Max.	M Typ.	M Max.	U Typ.	U Max.	PHASE UNBALANCE Degrees L Max.	M Max.	U Max.	AMPLITUDE UNBALANCE dB L Max.	M Max.	U Max.	PRICE $ Qty. (1–9)	DISTRIBUTOR FACTORY	LOCAL
LPS case B648	LPS-109	10-500	35	25	30	25	30	25	0.3	0.5	0.4	0.6	0.5	1.1	2.0	3.0	2.0	0.15	0.2	0.3	17.95	•	•
PSC-2 case A01	PSC-2-1	0.1-400	20	15	25	20	25	20	0.2	0.6	0.4	0.75	0.6	1.0	2.0	3.0	4.0	0.15	0.2	0.3	10.95	•	•
	PSC-2-1W	1-650	25	20	35	20	25	20	0.3	0.6	0.5	0.9	0.7	1.0	2.0	3.0	4.0	0.15	0.2	0.3	16.95	•	•
	♦ PSC-2-2	0.004-60	27	20	30	20	27	20	0.3	0.6	0.3	0.6	0.6	1.0	2.0	3.0	4.0	0.15	.25	0.3	23.95	•	•
	PSC-2-4	10-1000	30	25	25	20	25	20	0.6	1.0	0.6	1.2	0.7	1.2	2.0	8.0	20.0	0.15	0.2	0.4	23.95	•	•
	PSC-2-5	10-1400	28	18	22	17	24	17	0.3	0.6	0.6	1.0	0.9	1.6	2.0	3.0	4.0	0.15	0.2	0.4	29.95	•	•
	PSC-2-45	700-900	—	—	20	17	—	—	—	—	0.2	0.4	—	—	—	3	—	—	0.2	—	22.95	•	•
	■PSC-2375	55-85	—	—	35	25	—	—	—	—	0.3	0.5	—	—	—	1.0	—	—	0.1	—	23.95	•	•
	■PSC-2-1-75	0.25-300	20	15	30	20	20	15	0.4	0.75	0.4	0.75	0.4	1.0	2.0	3.0	5.0	0.15	0.2	0.3	13.45	•	•
	■PSC-2-4-752	10-850	31	20	32	23	23	15	0.3	0.5	0.4	0.6	0.5	1.0	2	5	10	0.1	0.2	0.5	23.95	•	•
MSC-2 case A03	MSC-2-1	0.1-450	20	15	30	20	30	20	0.3	0.5	0.4	0.75	0.6	1.0	2.0	3.0	4.0	0.15	0.2	0.3	18.95	•	•
	MSC-2-1W	2-650	22	18	30	20	22	18	0.3	0.5	0.5	0.8	0.8	1.2	1.0	2.0	4.0	0.3	0.2	0.3	20.95	•	•
	MSC-2-5	5-1500	18	16	20	16	20	14	0.6	0.8	0.6	0.8	0.6	1.1	2.0	3.0	5.0	0.2	0.3	0.4	24.95		•
	MSC-2-11	5-2000	18	16	20	16	18	11	0.6	0.8	0.6	0.8	1.2	1.8	2.0	3.0	5.0	0.2	0.3	0.5	29.95		•
SCP-2 case YY101	SCP-2-1	0.1-400	25	15	30	20	25	20	0.3	1.2	0.2	0.6	0.4	1.1	2.0	2.0	3.0	0.15	0.2	0.3	10.45		•
TSC-2 case B02	TSC-2-1	1-400	30	25	30	25	30	20	0.25	0.5	0.4	0.75	0.8	1.0	2.0	3.0	4.0	0.15	0.2	0.6	15.95	•	•

L=low range (f_L to 10 f_L) M=mid range (10f_L to f_U/2) U=upper range (f_U/2 to f_U)

♦ 1 dB compression derates approximately 13 dB from low range to mid range

PSC-2-1 Power Splitter.

broadband "drop-in"

Monolithic Amplifiers

50 ohms, up to +11 dBm out
dc to 2 GHz, surface mountable

MAR

	Model No.	Color Dot	FREQ. MHz	GAIN, dB Typical (at MHz) 100	500	1000	2000	(Note 4) MIN	MAXIMUM POWER, dBm Output (1dB) Compression	Input (no damage)	DYNAMIC RANGE Intercept pt. dBm NF dB	3rd Order Typ.	Typ.	VSWR In	Out	MAXIMUM RATING (25°C) I(mA)	P(mW)	DC POWER at Pin 3 Current (mA)	Volt. Typ.	PRICE $ Qty. (25)	DISTRIBUTOR FACTORY	LOCAL
MAR case VV105	MAR-1	Brown	DC-1000	18.5	17.5	15.5	—	13.0	0	+10	5.0	15		1.5:1	1.5:1	40	100	17	5	0.99†	●	●
	MAR-2	Red	DC-2000	13	12.8	12.5	11	8.5	+3	+15	6.5	18		1.3:1	1.6:1	60	325	25	5	1.50	●	●
	MAR-3	Orange	DC-2000	13	12.8	12.5	10.5	8.0	▲+8	+15	6.0	23		1.6:1	1.6:1	70	400	35	5	1.70	●	●
	MAR-4	Yellow	DC-1000	8.2	8.2	8.0	—	7.0	+11	+15	7.0	27		1.9:1	2.1	85	500	50	5	1.90	●	●
	MAR-6	White	DC-2000	20	19	16	11	9	0	+15	2.8	15		2:1	1.8:1	50	200	16	3.5	1.29	●	●
	MAR-7	Violet	DC-2000	13.5	13.1	12.5	10.5	8.5	+4	+15	5.0	20		2:1	1.5:1	60	275	22	4	1.90	●	●
	□ MAR-8	Blue	DC-1000	33	28	23	—	19	+10	+15	3.5	27		□	□	65	500	36	7.5	2.20	●	●

MAR-1SM thru MAR-8SM: surface mount, see case WW107 for outline drawing.

NOTES:
† quantity 100
▲ +4 dBm (1–2 GHz)
□ MAR-8 input and output impedances are not 50 ohms, see S parameter data. Conditionally stable* for source/load VSWR < 3:1.
1. Operating temperature −20°C to +85°C
   Storage temperature −55°C to +100°C
2. With no load output, derate maximum input power (no damage) by 10dB.
3. Price and specifications subject to change without notice.
4. Minimum gain at highest frequency point and over full temperature range.
5. Surface mount models are available in tape & reel.

* MAR-8, Input/Output Impedance is not 50 ohms, see data sheet.
Stable for source/load impedance VSWR less than 3:1.

Typical Biasing Configuration

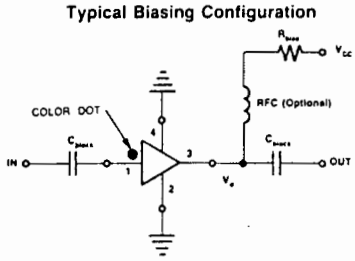

designers amplifier kit, DAK-2

5 of each model, total 35 amplifiers

only $59.95

Also, for your design convenience, Mini-Circuits offers chip coupling capacitors at 12 cents each.†

Size (mils)	Tolerance	Temperature Characteristic	Value
80 × 50	5%	NPO	10, 22, 47, 68, 100, 470, 680, 1000 pf
80 × 50	10%	X7R	2200, 4700, 6800, 10,000 pf
120 × 60	10%	X7R	.022, .047, .068, .1 μf

† Minimum Order 50 per Value

Designers kit, KCAP-1, 50 pcs. of each capacitor value, only $89.95

MAR-6 (T_A = 25°C, I_d = 16 mA)

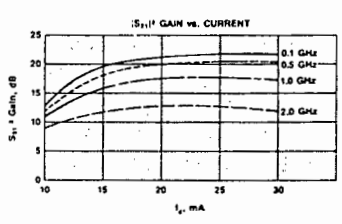

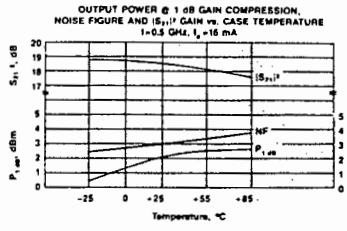

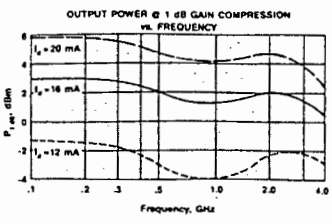

Freq. GHz	S_{11} (Input Return Loss) dB	Mag	Ang	S_{21} (Power Gain) dB	Mag	Ang	S_{12} (Isolation Out-In) dB	Mag	Ang	S_{22} (Output Return Loss) dB	Mag	Ang
0.1	27.96	.04	171	20.1	10.09	171	−22.5	.075	5	−27.96	.04	−30
0.5	26.02	.05	105	18.7	8.57	138	−21.3	.086	21	−20.00	.10	−104
1.0	17.72	.13	−118	16.4	6.57	107	−18.8	.115	28	−17.08	.14	−150
1.5	13.56	.21	140	14.1	5.06	84	−17.1	.140	28	−16.48	.15	180
2.0	10.75	.29	−163	12.0	3.98	65	−15.8	.163	26	−15.92	.16	157
2.5	9.37	.34	−176	10.3	3.26	55	−15.2	.174	28	−15.92	.16	150
3.0	7.74	.41	169	8.7	2.71	42	−14.8	.181	25	−16.48	.15	143
3.5	6.74	.46	157	7.2	2.31	30	−14.2	.194	22	−17.72	.13	144
4.0	6.20	.49	146	6.1	2.01	18	−13.8	.203	20	−20.00	.10	156

Mar-6 Monolithic Amplifier.

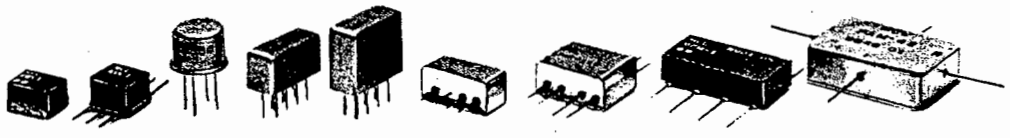

RMS *ASK ROSE TSM SAM TFM LMX SCM PAM

	MODEL NO.	FREQUENCY MHz LO/RF f_L–f_U	FREQUENCY MHz IF	CONVERSION LOSS dB Mid-Band m Typ.	CONVERSION LOSS dB Mid-Band m Max.	CONVERSION LOSS dB Total Range Typ.	CONVERSION LOSS dB Total Range Max.	LO–RF ISOLATION, dB L Typ.	LO–RF ISOLATION, dB L Min.	LO–RF ISOLATION, dB M Typ.	LO–RF ISOLATION, dB M Min.	LO–RF ISOLATION, dB U Typ.	LO–RF ISOLATION, dB U Min.	LO–IF ISOLATION, dB L Typ.	LO–IF ISOLATION, dB L Min.	LO–IF ISOLATION, dB M Typ.	LO–IF ISOLATION, dB M Min.	LO–IF ISOLATION, dB U Typ.	LO–IF ISOLATION, dB U Min.	PRICE $ Qty. (1-9)	DISTRIBUTOR FACTORY	DISTRIBUTOR LOCAL
SAM case A03	SAM-1	1-600	DC-600	5.5	7.0	6.5	8.5	55	45	45	30	35	20	50	40	40	25	30	20	16.95	•	•
	SAM-2	1-1000	DC-1000	6.0	7.5	7.0	9.5	55	45	40	25	35	20	50	40	40	25	30	25	20.45	•	•
	SAM-3	0.1-500	DC-500	5.5	7.0	6.5	8.5	60	50	50	35	35	30	50	40	45	30	30	20	19.95	•	•
	SAM-4	5-1250	0.5-1000	6.5	8.5	6.5	8.5	55	40	35	25	30	20	50	40	35	25	30	20	23.95	•	•
	SAM-5	5-1500	0.5-1000	6.5	7.5	6.5	8.5	55	40	35	25	30	20	50	40	35	25	30	20	29.95	•	•
TSM case A11	TSM-1	1-600	DC-600	6.0	7.5	6.5	8.5	60	45	45	35	35	25	55	45	40	30	35	25	19.95	•	•
	TSM-2	1-1000	DC-1000	6.0	7.5	7.0	10.0	55	45	40	20	35	18	50	40	40	20	25	18	20.95	•	•
	TSM-3	0.1-500	DC-500	5.3	7.5	6.5	8.5	60	50	50	35	35	25	55	45	45	30	35	25	21.95	•	•
	†TSM-5	5-1500	DC-1000	6.5	8.5	8.0	9.5	60	45	35	25	30	25	60	45	35	25	25	16	27.95	•	•
TFM case B02	TFM-2	1-1000	DC-1000	6.0	7.5	7.0	8.5	50	45	40	25	30	25	45	40	35	25	25	20	13.95	•	•
	†TFM-2P	1-1000	DC-1000	6.0	7.5	7.0	8.5	50	45	40	25	30	25	45	40	35	25	25	20	13.95	•	•
	TFM-3	0.04-400	DC-400	5.3	7.0	6.0	8.0	60	50	50	35	35	25	55	40	45	30	35	25	21.45	•	•
	TFM-4	5-1250	DC-1250	6.0	7.5	7.5	8.5	50	45	40	30	30	25	45	40	35	25	25	20	23.45	•	•
	TFM-5	5-1500	DC-1000	6.5	8.5	8.0	9.5	60	45	35	25	30	25	60	40	35	15	25	14	25.45	•	•
case B13	TFM-11	1-2000	5-600	7.0	8.5	7.5	9.0	50	45	35	25	25	10	45	40	27	20	25	20	47.45	•	•
	TFM-12	800-1250	50-90	—	—	6.0	7.5	35	25	35	25	35	25	30	20	30	20	30	20	47.45	•	•
	TFM-2400	750-2400	DC-400	—	—	6.7	9.0	30	20	30	20	30	20	30	10	30	10	30	10	28.95	•	•
	TFM-4300	300-4300	DC-800	—	—	8.0	10.5	30	20	—	—	30	17	15	7	—	—	10	7	38.95		
*ASK case W38	ASK-1	1-600	DC-600	5.5	7.0	6.0	8.5	50	30	35	25	30	20	45	35	30	20	25	15	6.95	•	•
	ASK-2	1-1000	DC-1000	7.0	8.0	8.0	9.8	60	40	35	18	26	16	50	30	25	17	15	10	8.25	•	•
LMX case B848	LMX-3	0.04-400	DC-400	5.3	7.0	6.0	8.0	60	50	50	35	35	25	45	40	35	25	25	20	25.95	•	•
	LMX-113	5-1000	DC-1000	6.5	7.0	7.0	8.0	50	40	40	25	35	25	45	35	35	30	30	20	16.95	•	•
	LMX-124	0.5-500	DC-500	5.5	6.5	6.0	7.0	50	40	45	25	45	22	45	40	40	30	30	20	27.95	•	•
	LMX-149	10-1500	DC-1500	6.0	7.0	6.0	10.0	55	40	45	35	30	20	50	40	40	25	20	12	29.95	•	•
	LMX-156	800-2500	DC-1500	6.5	9.0	6.5	9.0	35	25	35	25	35	25	22	17	22	17	22	17	44.95	•	•
ROSE case PP94	ROSE-1	1-600	DC-600	5.3	6.5	6.0	7.5	40	30	35	25	30	20	55	40	40	20	25	18	11.95		•
PAM case AA46	PAM-42	2.0-4.2GHz	DC-1.3GHz	—	—	7.0	8.5	—	—	25 (typ)		17 (min)		—	—	——	18 (typ)		10 (min)	——		27.95	•	•
SCM case YY101	SCM-1	1-500	DC-500	6.0	7.0	6.5	8.0	60	40	45	35	40	30	50	40	45	35	40	25	4.25		•
	SCM-2	5-1000	DC-500	6.0	7.5	7.0	9.8	50	40	40	25	35	20	55	30	40	25	30	18	5.45		•
†RMS case TT-100	RMS-1	0.5-500	DC-500	5.5	7.0	6.2	8.5	55	50	33	25	27	20	55	45	30	23	24	19	7.95	•	•
	RMS-2	5-1000	DC-1000	6.5	8.0	7.0	9.5	60	40	40	20	25	18	55	30	30	20	20	12	8.95	•	•
	◊RMS-1R	0.5-500	DC-500	5.5	7.0	6.2	8.5	55	50	33	25	27	20	55	45	30	23	24	19	14.45	•	•
	RMS-5	5-1500	DC-1000	6.5	7.5	7.5	9.5	60	40	40	20	30	18	55	30	30	18	15	8	13.95	•	•

L = low range (f_L to 10 f_L) M = mid range (10 f_L to $f_U/2$) U = upper range ($f_U/2$ to f_U)

m = mid band ($2f_L$ to $f_U/2$)

* Surface mounting available, see case KK81
Plug-in mounting available, see case X65

† Phase Detection, Polarity Positive

◊ hermetically sealed diodes

MIL-M-28837/1A, NSN GUIDE

MCL NO.	NSN	MIL-M-28837/1A*
GRA-1		07 N
GRA-1 HI-REL		07 S
GRA-3	5895-01-169-1815	
GRA-8	5895-01-217-5627	
SAM-1	5895-01-117-2926	

MCL NO.	NSN	MIL-M-28837/1A*
SAM-1TX	5840-01-196-4765	
SAM-2	5985-01-165-6621	
SAM-3	5895-01-042-9973	
SAM-5	5895-01-036-9507	
SBL-1	9058-00-256-6818	
SBL-1X	5895-01-179-8084	
SRA-1	6625-00-008-8272	03 N
SRA-1 HI-REL		03 S
SRA-1-1	5962-01-113-5431	
SRA-1-TX	5895-01-163-9247	03 S
SRA-1-1-TX	5895-01-151-6753	
SRA-11-TX	5895-01-163-9248	
SRA-1W		09 N
SRA-1W HI-REL		09 S
SRA-3	5895-01-021-5914	
SRA-4	5826-01-155-6545	
SRA-6	5895-01-124-0117	
SRA-8	5985-01-081-0977	12 N
SRA-8 HI-REL		12 S
TAK-5R		01 N
TAK-5R HI-REL		01 S
TAK-6R		02 N
TAK-6R HI-REL		02 S
TFM-2-408	5821-01-076-2497	
TFM-2	5821-01-135-1652	
TFM-3	5840-01-112-0031	
TFM-12	5821-01-179-5686	
TSM-1	5895-01-121-7958	

*units are not QPL-listed

pin connections

see case style outline drawing

SAM			TSM	TFM	ASK	LMX	PAM	RMS	SCM		ROSE
−1 −3	−4 −5	−2	all models (△)	all models ■	all models	all models	all models	all models	−1	−2	−1
8	8	8	8	4	1	8	3	1	8	8	1
1	3,4*	1	1	1	4	5	1	4	1	1	3
3,4*	1	3,4*	3,4*	2	5	4	4	5	3,4	3	2
2,5,6,7	2,5,6,7	2,5,6,7	2,5,6,7	3	2,3,6	2,3,6,7	2	2,3,6	2,5,6,7	2,5,6,7	—
2	2,5,6,7	2,5,6,7	2	3	—	2,3,6,7	2	—		4; NOT USED	4

△ TSM-5, CASE GROUND 2,7

■ TFM-2400, TFM-5, & TFM-4300 LO = 1; RF = 4

* Pins must be connected together externally.

In Stock...Immediate Delivery

LMX-149 Double Balanced Mixer.

APPENDIX 4

Given below is the listing and the results of the PSPICE program used to simulate the Chebyshev bandpass filter circuit and to predict its performance.

Pspice input file.

```
***     CASCADED HP AND LP FILTER
****      CIRCUIT DESCRIPTION
******************************************************************************

*CHEBYSHEV 5 ELEMENT
.AC LIN 500 30MEGhz 140MEGhz
VIN 1 0 AC 1volt
r1 1 2 50ohms
r2 11 0 50ohms
l1l 2 3 0.12uh
r3 3 4 0.001ohms
l3l 4 5 0.236uh
r4 5 6 0.001ohms
l5l 6 7 0.12uh
r5 7 8 0.001ohms
c2l 4 0 75.21pf
c4l 6 0 75.21pf
c1h 8 9 42.81pf
c3h 9 10 21.905pf
c5h 10 11 42.81pf
l2h 9 12 0.069uf
r6 12 0 0.001ohms
l4h 10 13 0.069uf
r7 13 0 0.001ohms
rc1 8 9 10gohms
rc2 9 10 10gohms
rc3 10 11 10gohms
.PLOT AC VDB(11)
.PROBE
.END
```

Pspice results.

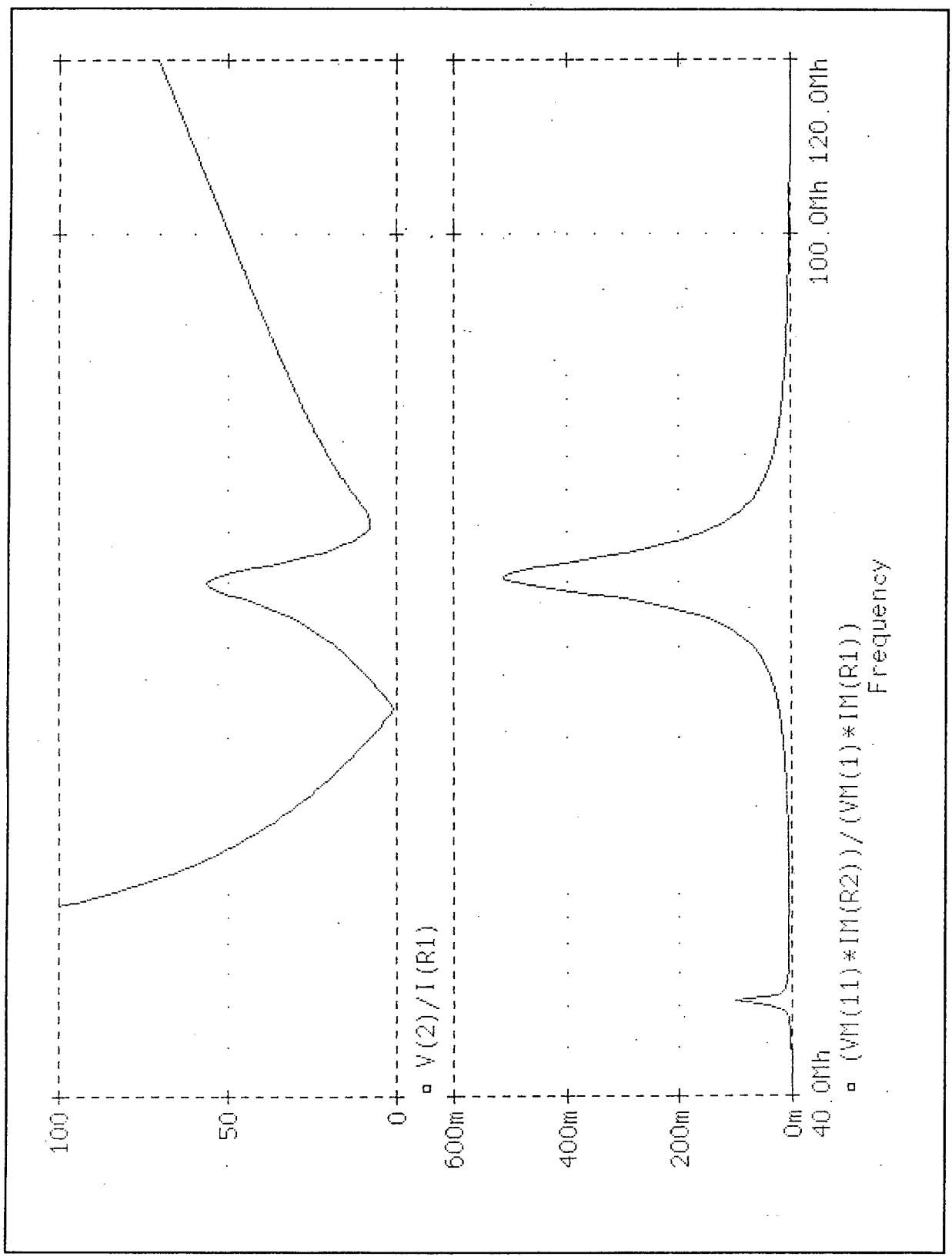

APPENDIX 5

This appendix contains a copy of the Hewlett Packard application note 936. The title of this application note is, "High Performance Pin Attenuator for Low Cost AGC Applications".

SUMMARY

PIN diodes offer an economic way of achieving excellent performance in AGC circuits. Significant improvements in crossmodulation and intermodulation distortion performance compared to transistors are obtained.

Other advantages of PIN diodes, such as good low frequency operation, constant impedance levels, and low power consumption will be discussed in this article.

INTRODUCTION

In the short time since its introduction, the PIN diode has found many areas of application. New developments in diode design have allowed the PIN diode to be useful at much lower frequencies than ever before. This article describes its use as an attenuator for automatic gain control and compares its performance to a transistorized AGC system in a television receiver.

The most important feature of the PIN diode is its inherent ability to act as a current controlled resistor at RF frequencies. Most diodes possess this capability to some degree, but the PIN diode is especially optimized in design to achieve a wide resistance range with consistently good linearity and low distortion. As typically shown in Figure 1, when the control current is varied continuously from 1 μA to 100 mA, the resistance of a PIN diode will change from over ten thousand ohms to about one ohm. This characteristic variation of resistance with current makes the PIN diode ideally suited for application in automatic gain control systems.

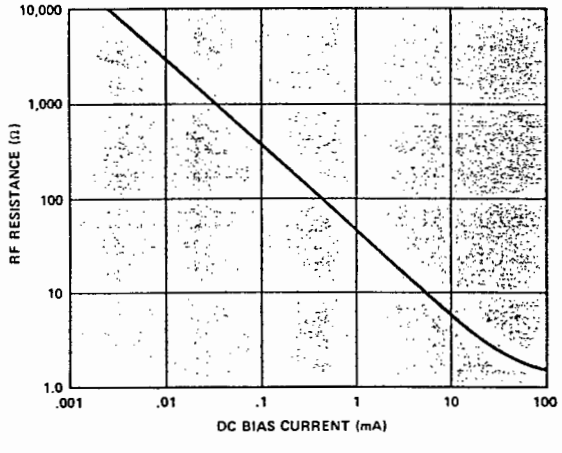

Figure 1. Typical Pin Diode Resistance Versus Control Current.

The PIN diode is similar to ordinary PN junction diodes except for an added intrinsic region (I-layer) sandwiched between the p^+ and n^+ layers. It is in this I-layer that the control of minority carriers is enhanced. The high resistance and large width of the intrinsic layer result in a high breakdown voltage and low capacitance. When forward bias is applied between p^+ and n^+ layers, the injection of minority carriers into the intrinsic region increases the conductivity of the I-layer.

Above a limiting frequency the PIN diode acts as a pure resistance. This RF resistance is controlled by varying the forward bias. Below the limiting frequency, rectification occurs as in an ordinary PN diode. In the vicinity of the limiting frequency there is some rectification with resulting distortion in RF resistance. The amount of distortion is dependent on the bias current, RF power, the frequency, and minority carrier lifetime. Distortion becomes appreciable at a frequency of operation equal to about 10 times the inverse of the minority carrier lifetime. Diodes of the HP 5082-3080 series, especially designed for low frequency operation, have a lifetime in excess of 1 microsecond, and are thus useful below 10 MHz. As an example, these low frequency PIN diodes are suitable for use in the attenuator to be described here for AGC application in television receivers.

AUTOMATIC GAIN CONTROL SYSTEMS

Many receivers today use transistors to accomplish their AGC requirements. For normal operation these transistors are biased for maximum gain. When the signal exceeds a set threshold level, automatic gain control is achieved by an increase in bias current, which results in a gain reduction. The principle of forward AGC is applied.

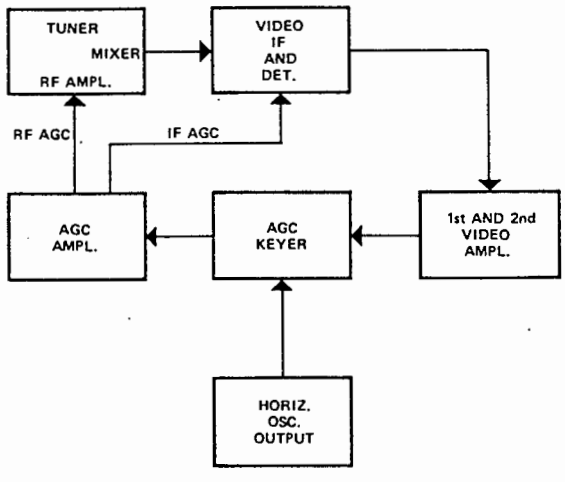

Figure 2. Block Diagram of a Typical AGC System in a TV Receiver.

A block diagram of a typical AGC system in a television receiver is shown in Figure 2. The objective is to keep the output of the video detector constant with increasing RF signal levels. The usual way of determining the signal strength of the incoming signal is to use the height of the horizontal pulses as a reference. A synchronized AGC keyer is used for this purpose. The threshold level required to trigger the keyer is preset. A winding in the flyback transformer supplies the horizontal pulses needed to bias the keyer transistor. When the keyer is off, the AGC amplifier supplies the required voltage to bias the RF and IF amplifiers for maximum gain. When the signal from the video amplifier exceeds the threshold level during the horizontal sync pulse, the keyer turns on and biases the AGC off. This results in an increased AGC voltage to the RF and IF amplifiers and thus a reduction in gain.

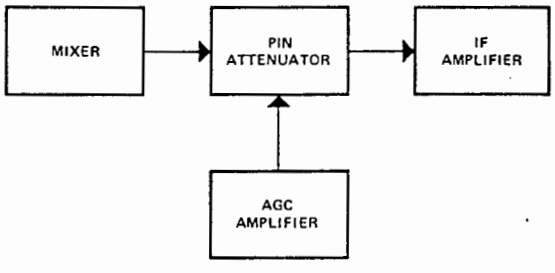

Figure 3. Use of a PIN Diode Attenuator as an Interstage for Providing AGC.

When AGC is applied to a transistor, the optimum operating point is disturbed, and the input and output impedances change drastically. This change will, of course, adversely affect the associated tuned circuit. The use of a PIN diode attenuator as an interstage, as shown in Figure 3, will provide a wide range of gain control without disturbing the optimum operating point of the associated circuit elements. This minimizes changes in impedance levels, phase shift and tuning, while achieving the required change in gain.

When the basic requirements of an attenuator for AGC application in a receiver are considered, the reasons for the superiority of PIN diodes over other PN junction diodes will become obvious. In particular, consider the use of 3 low frequency diodes in a π configuration attenuator as shown in Figure 4. The ratio of on to off resistance of PIN diodes is significantly greater than that of other diodes, so that the insertion loss is lower and the maximum attenuation is greater. In terms of AGC this means larger dynamic range. The linearity of resistance as a function of bias makes the PIN diode less susceptible to modulation distortion. In

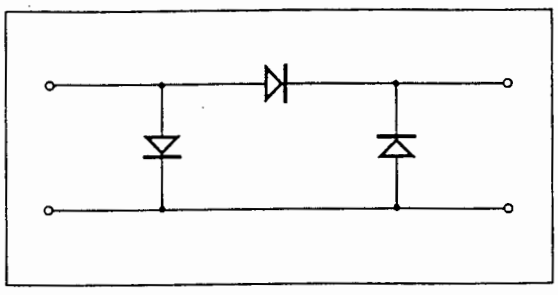

Figure 4. 3 Diode π Attenuator.

the VHF/UHF range distortion from partial rectification cannot be tolerated. The use of low frequency PIN diodes ensures that distortion be minimized at these low frequencies. HP 5082-3080 and 5082-3081 PIN diodes with lifetime, respectively, in excess of 1 and 1.5 microseconds are usable below 10 MHz.

PERFORMANCE CHARACTERISTICS

A transistorized amplifier stage and a low frequency PIN diode attenuator built for AGC performance comparison are shown, respectively, in Figures 5 and 6. In each case there is a fixed supply voltage of 12 volts and a variable voltage for AGC control.

In the transistor circuit the principle of forward AGC is applied. In addition to the fixed 12 volts an AGC voltage of −4.5 volts is required to bias the

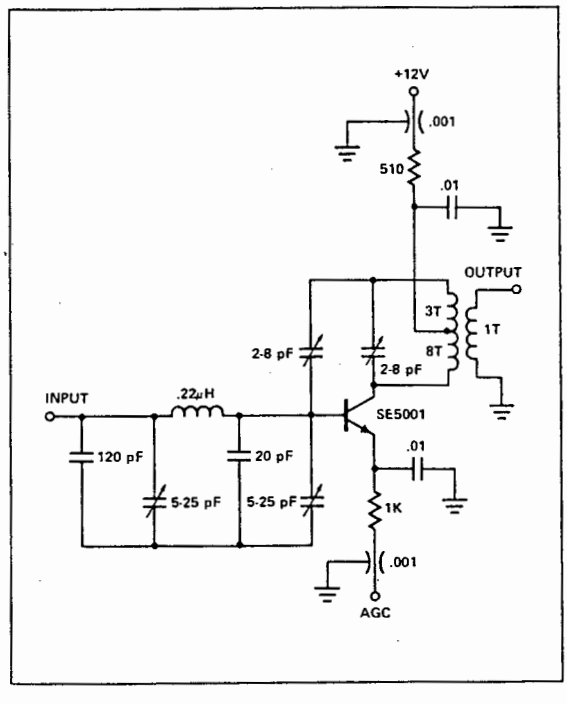

Figure 5. Transistor AGC Circuit.

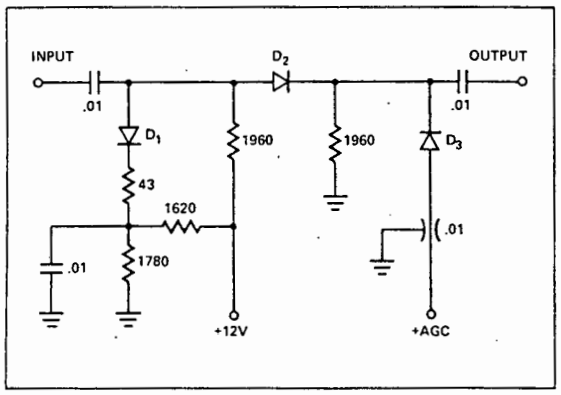

Figure 6. PIN Diode Attenuator AGC Circuit.

transistor for maximum gain. Further increase in AGC voltage results in a larger collector current and a reduction in gain. A curve of Gain Reduction versus AGC voltage at 45 MHz is shown in Figure 7. A maximum gain of approximately 40 dB is obtained at an AGC voltage of −4.5 volts. With more AGC voltage the gain decreases until a gain reduction of 40 dB is achieved at about 11.5 volts of AGC voltage.

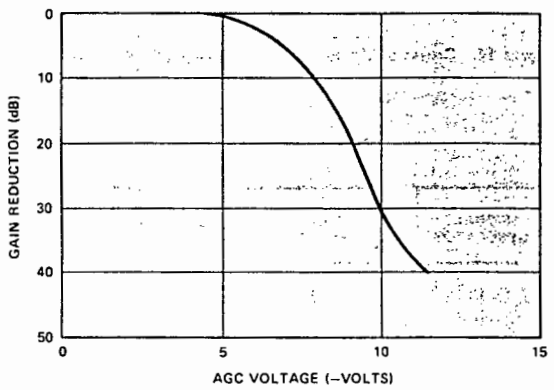

Figure 7. Gain Reduction Versus AGC Voltage Transistor AGC Circuit 45 MHz.

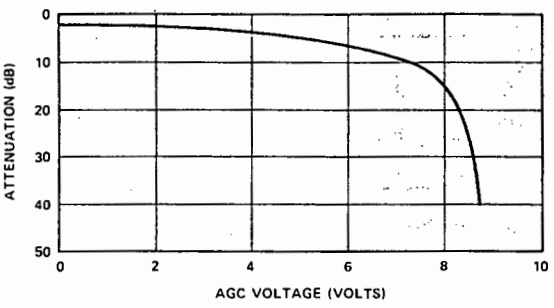

Figure 8. Attenuation Versus AGC Voltage PIN Diode Attenuator AGC Circuit 45 MHz.

Attenuation versus AGC voltage for the PIN attenuator circuit is shown in Figure 8. There is minimum attenuation when the AGC voltage is zero. The attenuation increases with AGC voltage until 40 dB of attenuation is obtained with 8.75 volts of AGC voltage. For 40 dB of attenuation the PIN attenuator requires 35 mW of power, while the transistor circuit consumes 120 mW for the same gain reduction.

Intermodulation and crossmodulation characteristics of the transistor and PIN attenuator AGC circuits are illustrated in Figures 9 through 14. A block diagram of the test equipment used for these distortion measurements is shown in Figure 15. The wave analyzer is used only for the crossmodulation tests. The tests are conducted with two equal amplitude input signals, one at 45 MHz and the other at 45.5 MHz. For the crossmodulation measurements one of the input signals is 100% modulated with a 15 KHz signal from the wave analyzer.

Examination of the distortion characteristics will reveal significant differences in performance of the two AGC circuits. Over a 30 dB dynamic range,

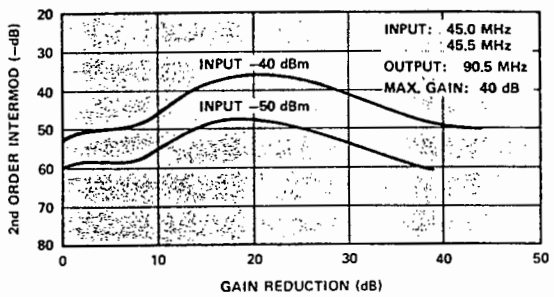

Figure 9. Second Order Intermodulation Versus Gain Reduction Transistor AGC Circuit.

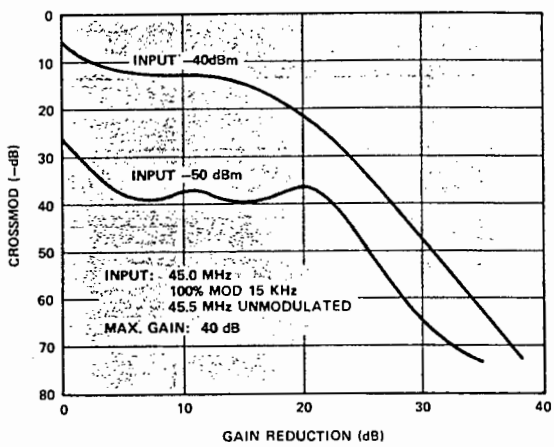

Figure 10. Crossmodulation Versus Gain Reduction Transistor AGC Circuit.

it is seen that second order intermodulation distortion at the same level of fundamental output is less in the PIN attenuator than in the transistor circuit. The difference at some points in the range is in excess of 10 dB. Longer lifetime HP 5082-3081 PIN diodes definitely show more favorable intermodulation characteristics than the HP 5082-3080 diodes. The superiority of the PIN attenuator as an AGC circuit is even more apparent with comparison of the crossmodulation characteristics. At some power levels, crossmodulation in the transistor circuit is seen to be 50 dB worse. A comparison of Figure 12 and 14 indicates better crossmodulation rejection when using HP 5082-3080 PIN diodes.

A comparison of the PIN and transistor AGC circuit performance is shown in Table 1.

TABLE 1

	PIN Diode		Transistor
	5082-3080	5082-3081	
Power Consumption, mW	35	35	120
2nd Order Intermod, dB (–20 dBm output)	–59	–64	–55
Crossmodulation (–20 dBm output)	–68	–59	–37

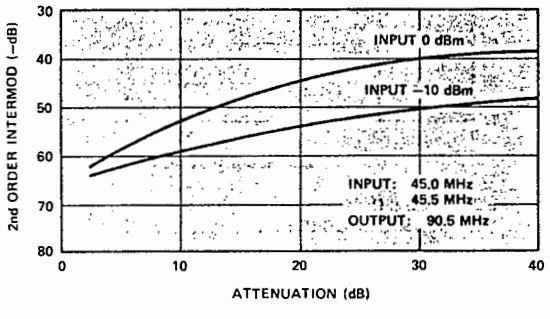

Figure 11. 2nd Order Intermodulation Versus Attenuation PIN Diode Attenuator AGC Circuit Using HP 5082-3080.

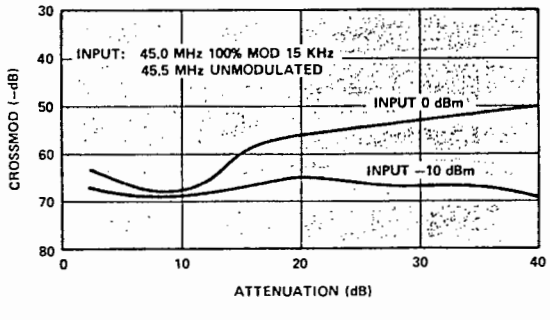

Figure 12. Crossmodulation Versus Attenuation PIN Diode Attenuator AGC Circuit Using HP 5082-3080.

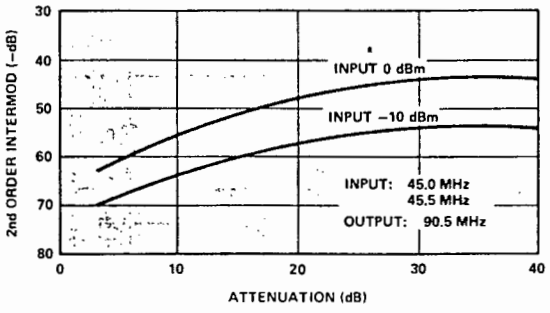

Figure 13. 2nd Order Intermodulation Versus Attenuation PIN Diode Attenuator AGC Circuit Using HP 5082-3081.

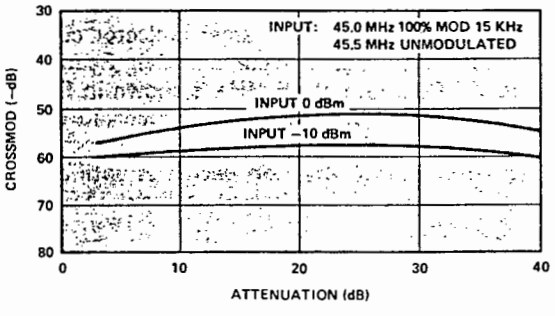

Figure 14. Crossmodulation Versus Attenuation PIN Diode Attenuator AGC Circuit Using HP 5082-3081.

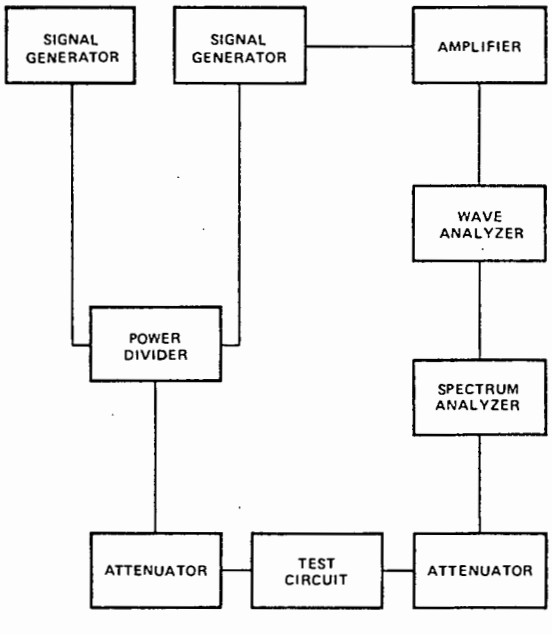

Figure 15. Block Diagram of Test Equipment used for Distortion Measurement.

CONCLUSION

Automatic gain control in a transistorized circuit requires that the optimum operating point of the AGC transistor be shifted. This produces a drastic change in the impedance level, which severely affects the adjoining tuned circuit.

The use of a PIN diode attenuator as the AGC control element will provide the required gain control without the attendant problems of large impedance shift. The result is minimum distortion in the output coupled with low power consumption. The use of long lifetime PIN diodes gives added assurance of usefulness at low frequencies for low cost applications.

APPENDIX 6

The specifications of the Pinn diode used in the STC circuit are shown below. The Pinn diode used is an HP5082-3081.

HEWLETT hp PACKARD
COMPONENTS

PIN DIODES FOR RF SWITCHING AND ATTENUATING

5082-3001/02
HPND-4165/66
5082-3039(1N5719)
5082-3042/43
5082-3077
5082-3080(1N5767)
5082-3081
5082-3168/88

Features

- LOW HARMONIC DISTORTION
- LARGE DYNAMIC RANGE
- LOW SERIES RESISTANCE
- LOW CAPACITANCE
- LOW TEMPERATURE COEFFICIENT
  - Typically Less Than 20% Resistance Change from 25°C to 100°C

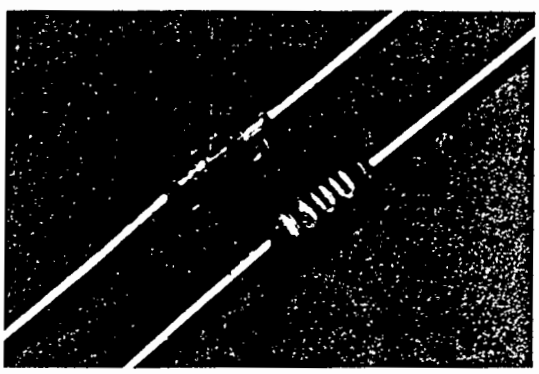

Description / Applications

These general purpose switching diodes are intended for low power switching applications such as RF duplexers, antenna switching matrices, digital phase shifters, and time multiplex filters. The 5082-3168/3188 are optimized for VHF/UHF bandswitching.

[illegible] of a P-N diode is a function of the [illegible] These current controlled resistors are specified for use in control applications such as variable RF attenuators, automatic gain control circuits, RF modulators, electrically tuned filters, analog phase shifters, and RF limiters.

	Lead Finish	Body Finish
5082-3001/02	Tin	Painted
HPND-4165/66	Tin	Painted
5082-3039 (1N5719)	Tin	Painted
5082-3042/43	Gold	Painted
5082-3077	Tin	Clear
5082-3080 (1N5767)	Tin	Clear
5082-3081	Tin	Clear
5082-3168/88	Tin	Clear

Package Dimensions

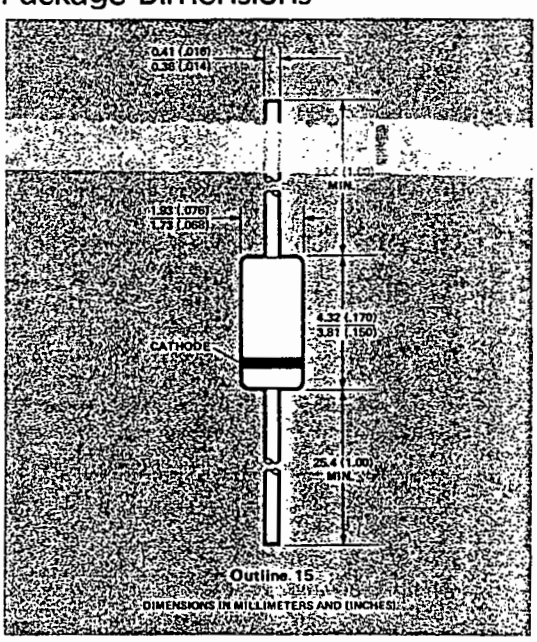

Mechanical Specifications

The HP Outline 15 package has a glass hermetic seal with dumet leads. The leads on the Outline 15 package should be restricted so that the bend starts at least 1/16 inch (1.6mm) from the glass body. With this restriction, Outline 15 package will meet MIL-STD-750, Method 2036, Conditions A (4 lbs., [1.8 kg.], tension for 30 minutes) and E. The maximum soldering temperature is 230° C for five seconds. Typical package inductance and capacitance are 2.5 nH and 0.13pF, respectively. Marking is by digital coding with a cathode band.

Maximum Ratings at T_{CASE} = 25°C

Junction Operating and Storage Temperature Range ..... -65°C to +150°C

Operation of these devices within the above temperature ratings will assure a device Mean Time Between Failure (MTBF) of approximately 1 x 10^7 hours.

Power Dissipation 250mW
(Derate linearly to zero at 150°C)

Peak Inverse Voltage (PIV) ..... V_{BR}

General Purpose Diodes
Electrical Specifications at T_A=25°C

Part Number 5082	Maximum Total Capacitance C_T (pF)	Minimum Breakdown Voltage V_{BR} (V)	Maximum Residual Series Resistance R_S (Ω)	Minimum Effective Carrier Lifetime τ (ns)	Maximum Reverse Recovery Time t_{rr} (ns)
GENERAL PURPOSE SWITCHING AND ATTENUATING					
3002	0.2	300	1.0	100	100 (typ)
3001	0.25	200	1.0	100	100 (typ)
3039	0.25	150	1.25	100	100 (typ)
IN5719	0.3**	150	1.25	100	100 (typ)
3077	0.3	200	1.5	100	100 (typ)
FAST SWITCHING					
3042	0.4*	70	1.0*	15 (typ)	5
3043	0.4*	50	1.5**	15 (typ)	10
BAND SWITCHING					
3188	1.0*	35	0.6**	40 (typ)	12 (typ)
3168	2.0*	35	0.5**	40 (typ)	12 (typ)
Test	V_R = 50V V_R = 0V V_R = 100V f = 1 MHz	$V_R = V_{BR}$ Measure $I_R \leq 10\mu A$	I_F = 100mA *I_F = 20mA **I_F = 10 f = 100 MHz	I_F = 50mA I_R = 250mA	I_F = 20mA V_R = 10V 90% Recovery

Note: Typical CW power switching capability for a shunt switch in a 50Ω system is 2.5W.

PIN Current Controlled Resistor Diodes
Electrical Specifications at T_A=25°C

Part Number	Minimum Effective Carrier Lifetime τ	Minimum Breakdown Voltage V_{BR}	Maximum Residual Series Resistance R_S	Maximum Total Capacitance C_T	High Resistance Limit, R_H		Low Resistance Limit, R_L		Maximum Difference in Resistance vs. Bias Slope, Δx
					Min.	Max.	Min.	Max.	
HPND-4165	100	100	1.5	0.3	1100	1660	16	24	.04
HPND-4166	100	100	1.5	0.3	830	1250	12	18	.04
5082-3080*	1300(typ)	100	2.5	0.4	1000			8**	
5082-3081	2000(typ)	100	3.5	0.4	1500			8**	
Units	ns	V	Ω	pF	Ω		Ω		
Test Conditions	I_F=50mA I_R=250mA	$V_R = V_{BR}$ Measure $I_R \leq 10\mu A$	I_F=100mA f=100mHz	V_R=50V f=1mHz	I_F=0.01mA f=100mHz		I_F=1.0mA **I_F=20mA f=100mHz		Batch Matched at I_F=0.01mA and 1.0mA f=100mHz

*The 1N5767 has the additional specifications: τ = 1.0 μsec minimum
I_R = 1 μA maximum at V_R = 50V
V_F = 1V maximum at I_F = 100mA.

Typical Parameters

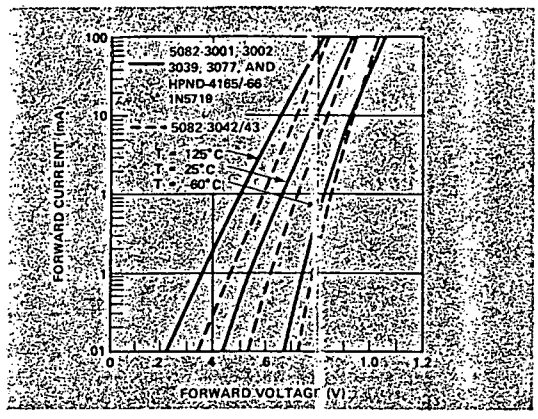

Figure 1. Typical Forward Current vs. Forward Voltage.

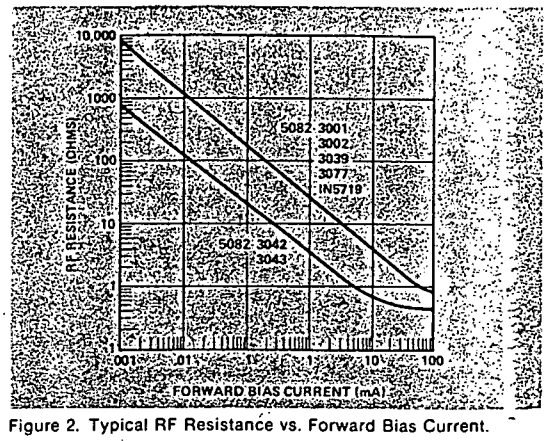

Figure 2. Typical RF Resistance vs. Forward Bias Current.

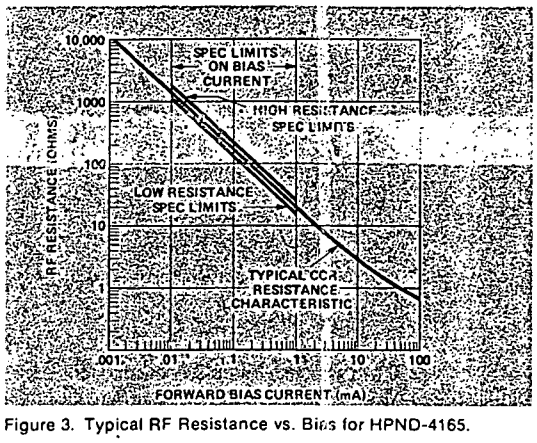

Figure 3. Typical RF Resistance vs. Bias for HPND-4165.

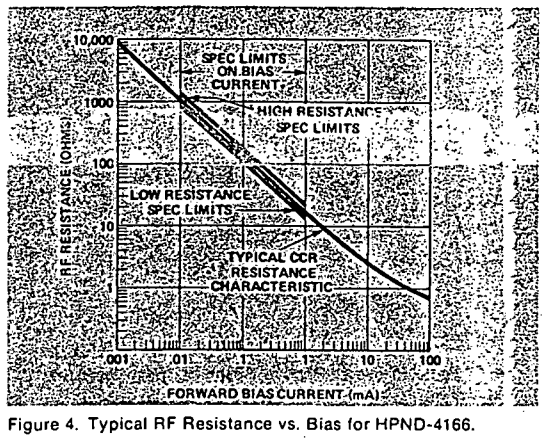

Figure 4. Typical RF Resistance vs. Bias for HPND-4166.

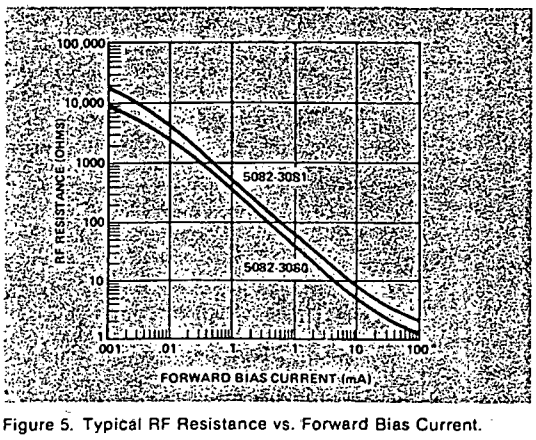

Figure 5. Typical RF Resistance vs. Forward Bias Current.

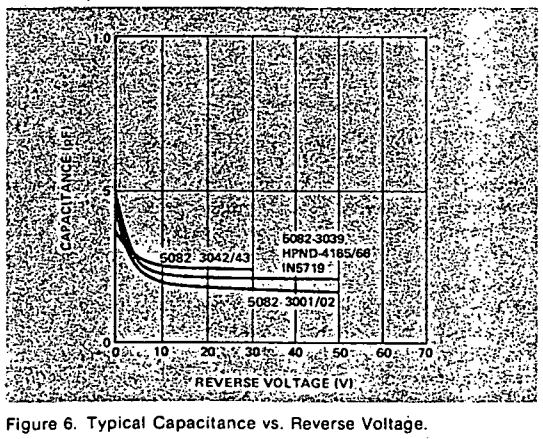

Figure 6. Typical Capacitance vs. Reverse Voltage.

Typical Parameters (Continued)

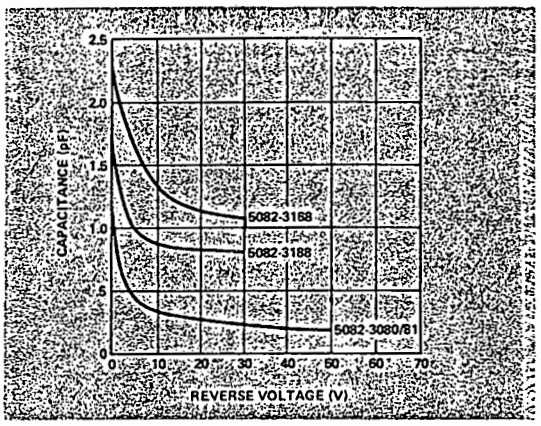

Figure 7. Typical Capacitance vs. Reverse Voltage 5082-3080, 3081, 3168, 3188.

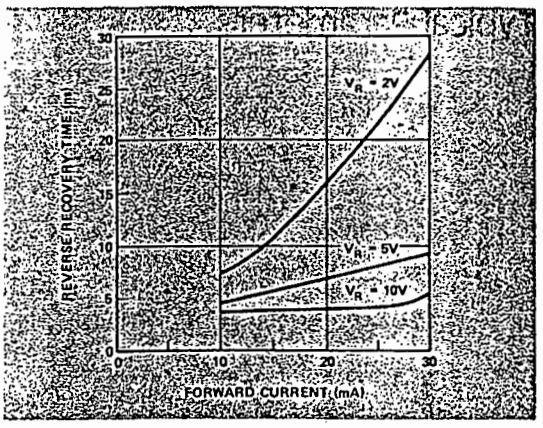

Figure 8. Typical Reverse Recovery Time vs. Forward Current for Various Reverse Driving Voltages, 5082-3042, 3043.

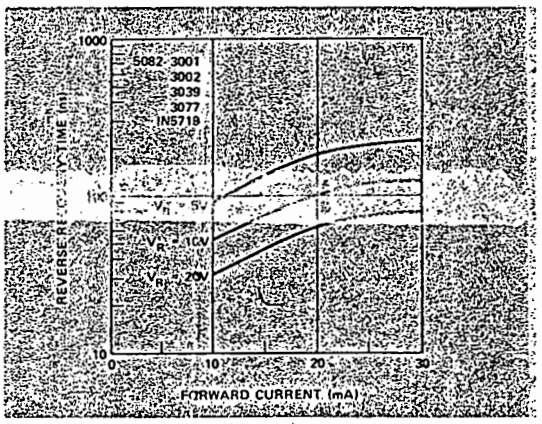

Figure 9. Typical Reverse Recovery Time vs. Forward Current for Various Reverse Driving Voltages.

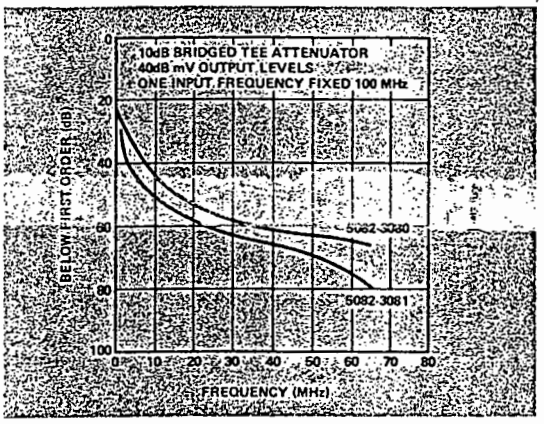

Figure 10. Typical Second Order Intermodulation Distortion.

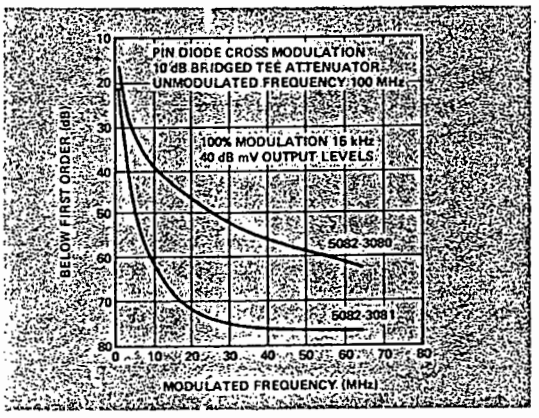

Figure 11. Typical Cross Modulation Distortion.

APPENDIX 7

The calculations to determine the noise figure, sensitivity, maximum dynamic range, power level of the pulses received during the dwell period and minimum range were done on a mathematical software package (Mathcad). The Mathcad worksheet containing these calculations is given here.

BISTATIC RECEIVER

The receiver is at UCT, and 15km from the transmitter at D.F. Malan airport. The receiver is 200m above the transmitter. The transmit antenna is elevated at 4 degrees. The peak gain of transmit antenna is 34 dB. The transmit antenna illuminates the receiver with a gain of 28 dB. 6 dB down. The height of main beam axis 100km away is 7km.

To calculate the noise figure and maximmum range of a radar receiver as well as the sensitivity.

System parameters:

$Pt := 2.5 \cdot 10^{6}$ Watts $Gt := 2511$ $Gr := 1.64$ $\sigma := 50$ m^2

$T := 273 + 23$ Kelvin

$f := 1.35 \cdot 10^{9}$ $c := 3 \cdot 10^{8}$ $\lambda := \frac{c}{f}$

$k := 1.38 \cdot 10^{-23}$ $\lambda = 0.222$

$BW := 400 \cdot 10^{3}$

SNR := 2.5 dB at the output of main IF amplifier in the receiver

Stage 1 = LNA	F1 := 3 dB	G1 := 12 dB
Stage 2 = cable	F2 := 0 dB	G2 := -7.4 dB
Stage 3 = preselector	F3 := 0 dB	G3 := -2.8 dB
Stage 4 = mixer	F4 := 11.7 dB	G4 := -9 dB
Stage 5 = matched filte	F5 := 1.3 dB	G5 := -1.96 dB
Stage 6 = preamp	F6 := 4 dB	G6 := 16 dB
Stage 7 = limiter amp	F7 := 4.6 dB	G7 := 17.27 dB
Stage 8 = IF amp	F8 := 10.2 dB	G8 := 52 dB

Convert dB's to a size

$f(x) := 10^{\frac{x}{10}}$ $g(x) := 10^{\frac{x}{10}}$

Noise figure of system is:

$$nfa := f(F1) + \frac{f(F2) - 1}{g(G1)} + \frac{f(F3) - 1}{g(G1) \cdot g(G2)} + \frac{f(F4) - 1}{g(G1) \cdot g(G2) \cdot g(G3)} + \frac{f(F5) - 1}{g(G1) \cdot g(G2) \cdot g(G3)} \cdot \lambda$$

$$nfb := \frac{f(F7) - 1}{g(G1) \cdot g(G2) \cdot g(G3) \cdot g(G4) \cdot g(G5) \cdot g(G6)} \left| \frac{}{} \right. \frac{}{g(G4)} + \frac{f(F6) - 1}{g(G1) \cdot g(G2) \cdot g(G3) \cdot g(G4) \cdot g(G5)}$$

$$nfc := \frac{f(F8) - 1}{g(G1) \cdot g(G2) \cdot g(G3) \cdot g(G4) \cdot g(G5) \cdot g(G6) \cdot g(G7)}$$

nfc = 0.037

nf := nfa + nfb + nfc

Input noise to the system is determined by the antenna. The effective noise temperature is obtained from the atmosphere. It is 150K.

Tea := 192 Kelvin
Nin := k·Tea·BW

Noise is derated due to nf therefore the effective noise at input must be:

Neff := Nin·nf NF := 10·log(nf) nf = 25.825 NF = 14.12 dB

The desired SNR is 9.5dB

$$snr := 10^{\frac{SNR}{10}}$$ converting from dB to size

Therefore the input signal must be:

$$Sin := 10\cdot\log\left[\frac{snr\cdot Neff}{0.001}\right] \qquad si := snr\cdot Neff$$

Sin = -103.127 dBm also known as the sensitivity of the receiver.

Therefore the maximum range obtainable is:

$$R := \left[\frac{Pt\cdot Gt\cdot Gr\cdot\lambda^{2}\cdot\sigma}{(4\cdot\pi)^{3}\cdot si}\right]^{\frac{1}{4}}$$

$$\frac{R}{1000} = 127.37 \quad km$$

Gtot := G1 + G2 + G3 + G4 + G5 + G6 + G7 + G8 Gtot = 76.11 dB

Determine maximum input power without saturating the receiver. In this case the target is at the airport and is at all times not within 75m of the transmit antenna. The gain of the transmit antenna is 9dB down from the peak gain at this level, hence Gta = 316.

Rtmin := 75 Gta := 316
Rrmin := 14925

$$prmax := \left[\frac{Pt\cdot Gta\cdot Gr\cdot\lambda^{2}\cdot\sigma}{3\quad 2\quad 2}\right.$$

$$\left[(4\cdot\pi)\cdot Rtmin\cdot Rrmin\right]$$

$$Prmax := 10\cdot\log\left[\frac{prmax}{0.001}\right] \qquad Prmax = -28.906 \quad dBm$$

Determine the power of the main bang pulse. The gain of the transmitter antenna is 6dB down from the peak gain when it illuminates the receiver antenna.

$$Gte := 10^{\frac{10\cdot\log(Gt)-6}{10}}$$

$$prmb := \left[\frac{Pt\cdot Gte\cdot Gr\cdot\lambda^{2}}{16\cdot\pi^{2}\cdot 15000^{2}}\right]$$

$$Prmb := 10\cdot\log\left[\frac{prmb}{0.001}\right] \qquad Prmb = 5.556 \quad dBm$$

APPENDIX 8

The azimuth synchronization circuit diagram and the artwork for the PC board is given in this appendix.

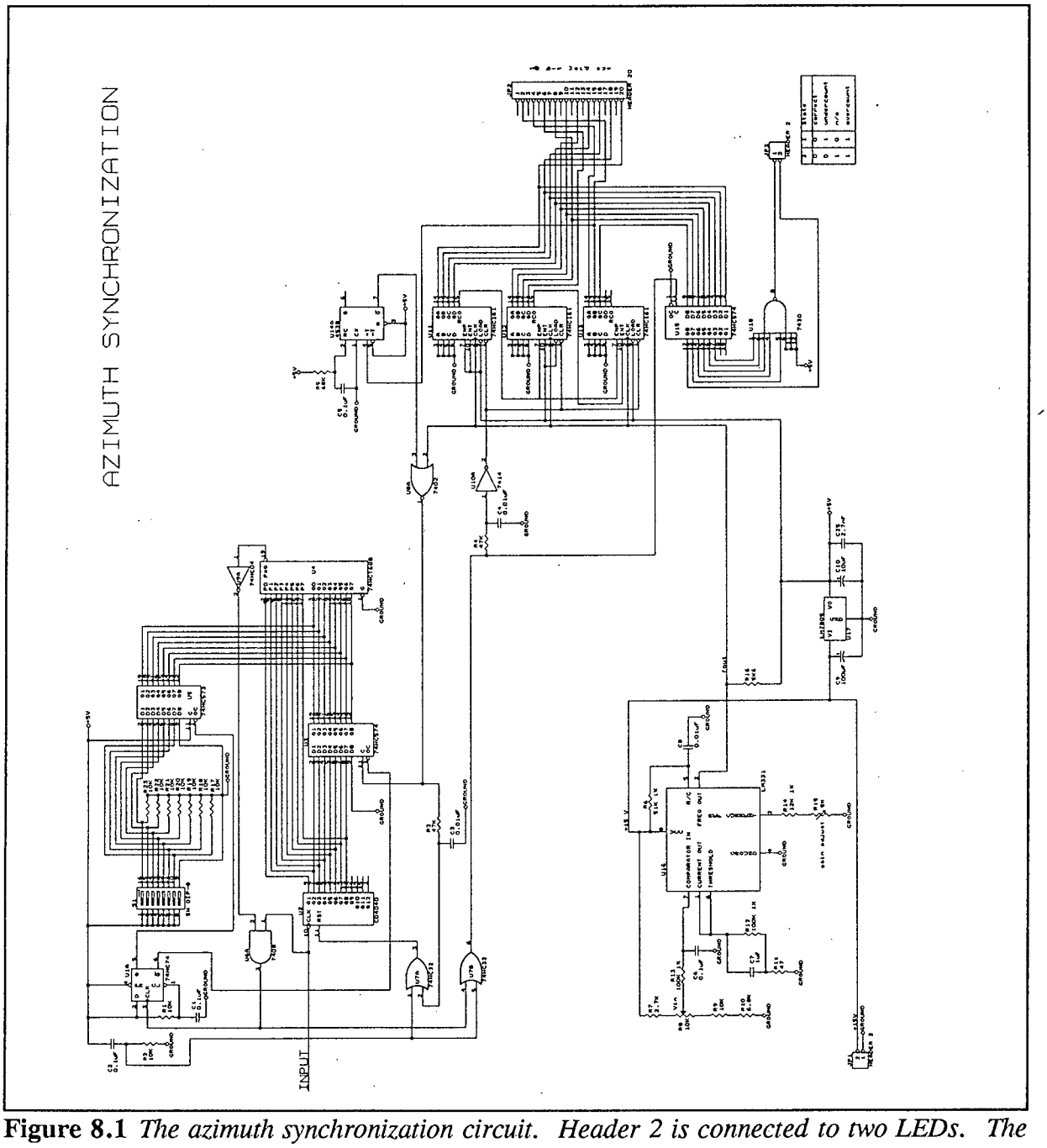

Figure 8.1 *The azimuth synchronization circuit. Header 2 is connected to two LEDs. The LEDs show the operator whether the circuit is synchronized or not.*

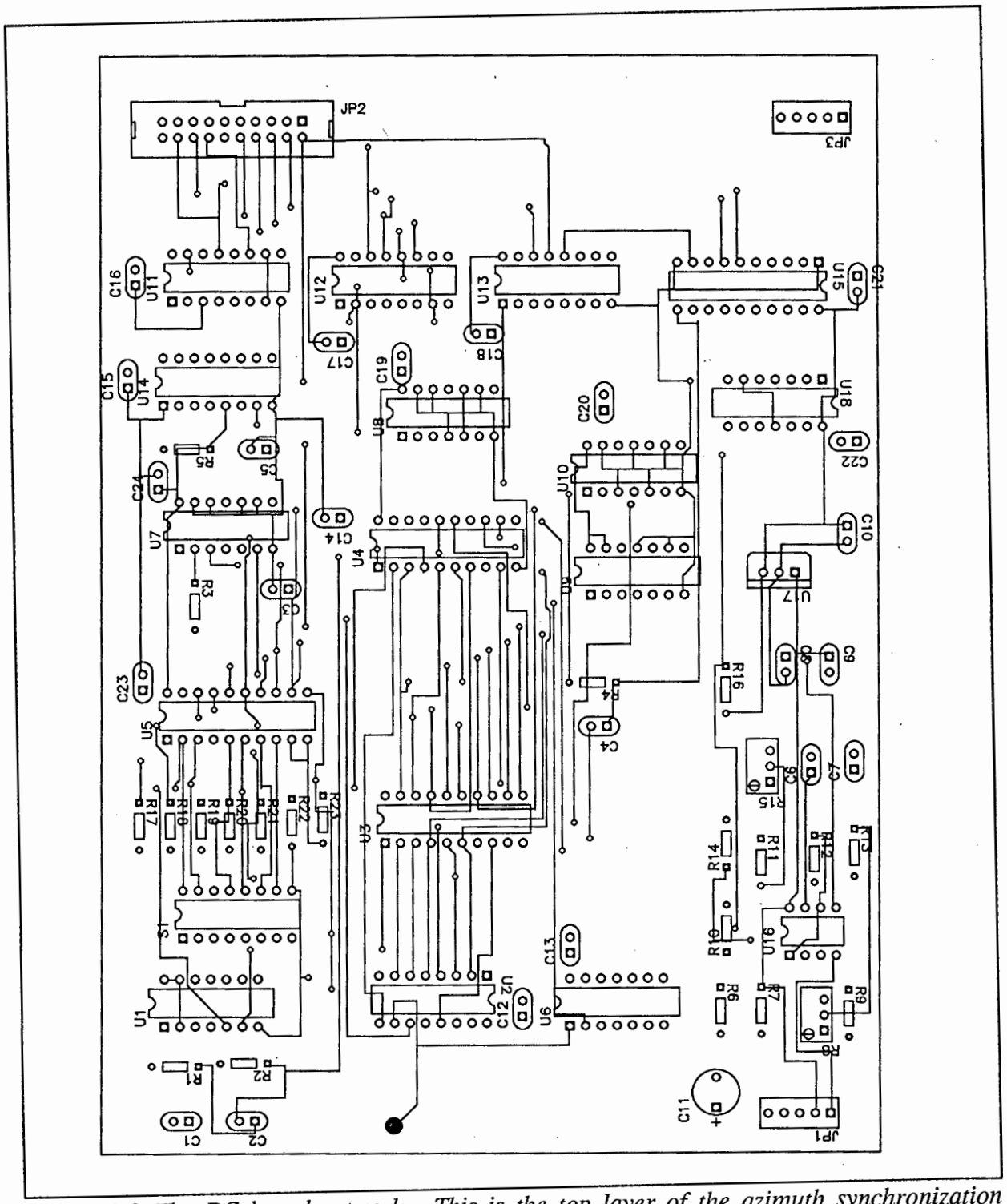

Figure 8.2 *The PC board artwork. This is the top layer of the azimuth synchronization board.*

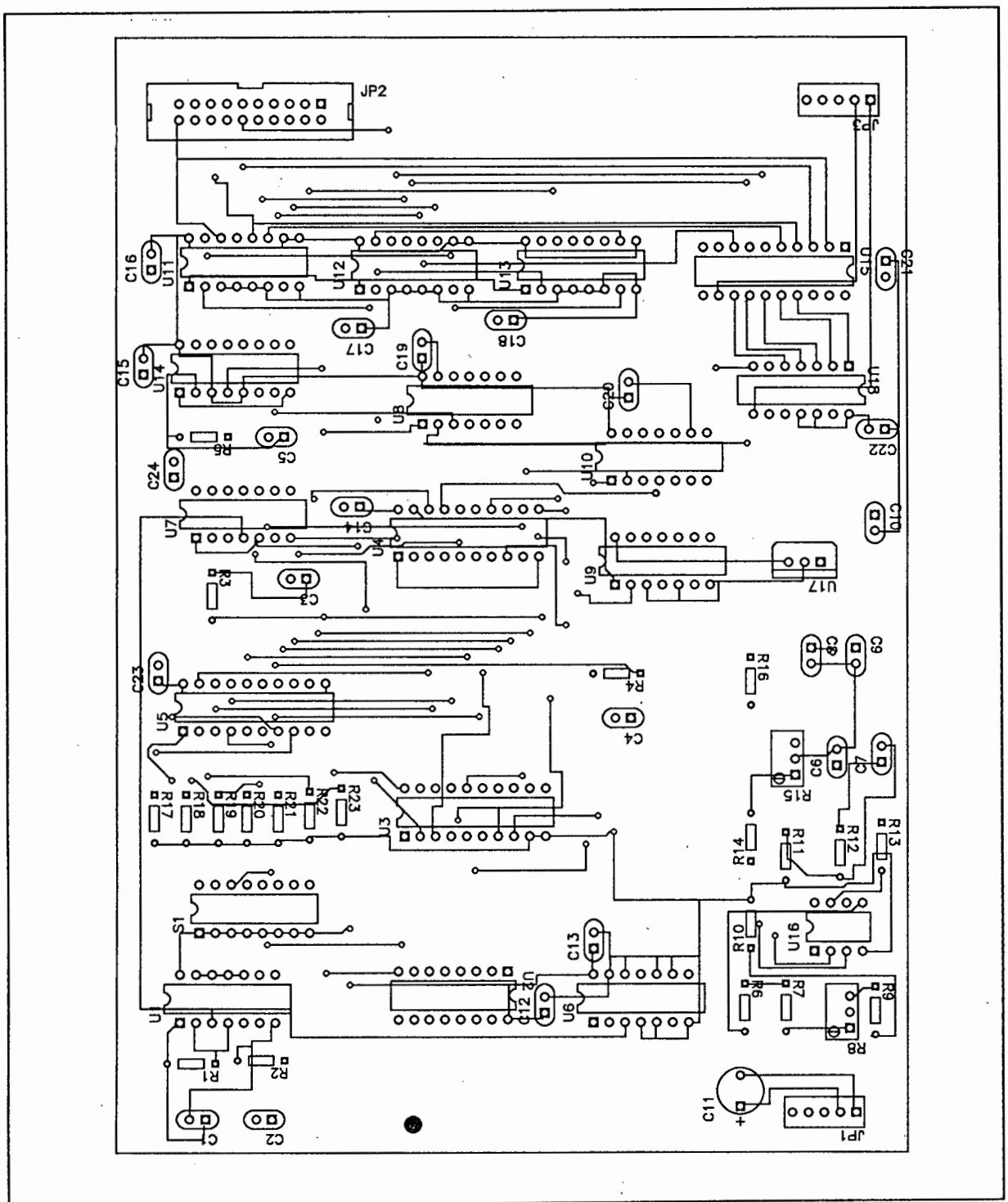

Figure 8.3 *The PC board artwork. This is the bottom layer of the azimuth synchronization board.*

APPENDIX 9

This appendix contains the circuit diagram of the PRF synchronization circuit and specifications of the XR-2212 PLL used in the circuit.

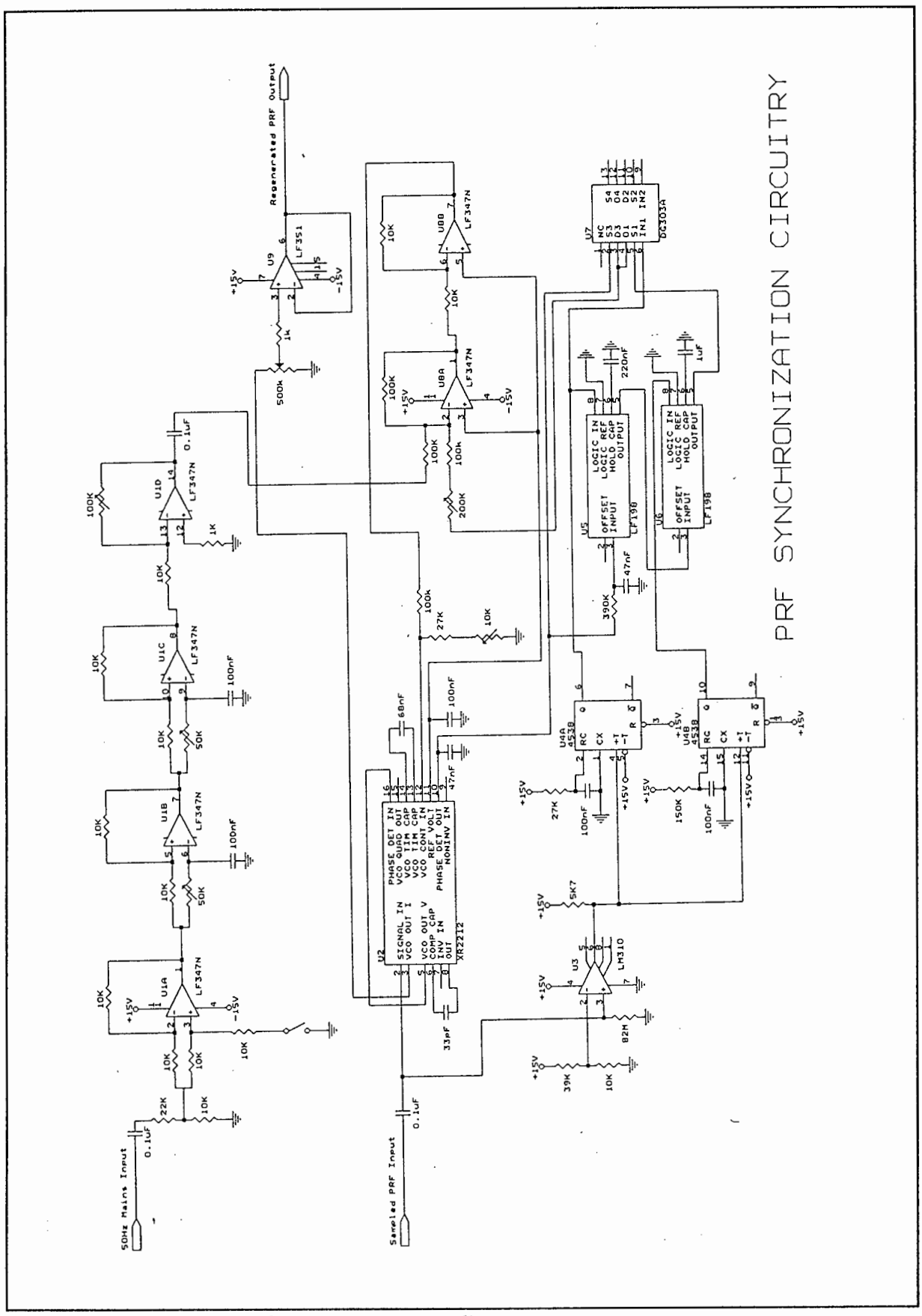

Figure 9.1 *The PRF synchronization circuit diagram.*

Precision Phase-Locked Loop

GENERAL DESCRIPTION

The XR-2212 is an ultra-stable monolithic phase-locked loop (PLL) system especially designed for data communications and control system applications. Its on board reference and uncommitted operational amplifier, together with a typical temperature stability of better than 20 ppm/°C, make it ideally suited for frequency synthesis, FM detection, and tracking filter applications. The wide input dynamic range, large operating voltage range, large frequency range, and ECL, DTL, and TTL compatibility contribute to the usefulness and wide applicability of this device.

FEATURES

Quadrature VCO Outputs	
Wide Frequency Range	0.01 Hz to 300 kHz
Wide Supply Voltage Range	4.5V to 20V
DTL/TTL/ECL Logic Compatibility	
Wide Dynamic Range	2 mV to 3 Vrms
Adjustable Tracking Range (±1% to ±80%)	
Excellent Temp. Stability	20 ppm/°C, Typ.

APPLICATIONS

Frequency Synthesis
Data Synchronization
FM Detection
Tracking Filters
FSK Demodulation

ABSOLUTE MAXIMUM RATINGS

Power Supply	18V
Input Signal Level	3 Vrms
Power Dissipation	
Ceramic Package:	750 mW
Derate Above T_A = +25°C	6 mW/°C
Plastic Package:	625 mW
Derate Above T_A = +25°C	5 mW/°C

FUNCTIONAL BLOCK DIAGRAM

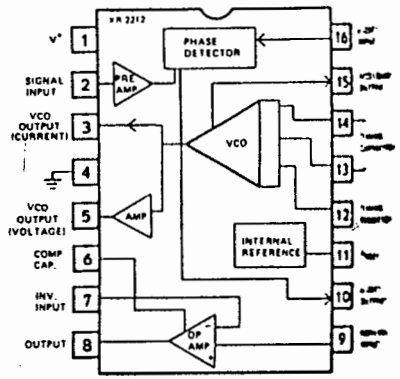

ORDERING INFORMATION

Part Number	Package	Operating Temperature
XR-2212M	Ceramic	−55°C to +125°C
XR2212CN	Ceramic	0°C to +70°C
XR-2212CP	Plastic	0°C to +70°C
XR-2212N	Ceramic	−40°C to +85°C
XR-2212P	Plastic	−40°C to +85°C

SYSTEM DESCRIPTION

The XR-2212 is a complete PLL system with buffered inputs and outputs, an internal reference and an uncommitted op amp. Two VCO outputs are provided, one sources current, the other sources voltage. This enables operation as a frequency synthesizer using an external programmable divider. The op amp section can be used as an audio preamplifier for FM detection or as a high speed sense amplifier (comparator) for FSK demodulation. The center frequency, bandwidth and tracking range of the PLL are controlled independently by external components. The PLL outputs are directly compatible with MOS, DTL, ECL and TTL logic families as well as microprocessor peripheral systems.

The precision PLL system operates over a supply voltage range of 4.5 V to 20 V, a frequency range of 0.01 Hz to 300 kHz, and accepts input signals of the order of 2 mV to 3 Vrms. Temperature stability of the VCO is typically better than 20 ppm/°C.

XR-2212

ELECTRICAL CHARACTERISTICS

Test Conditions: V^+ = +12V, T_A = +25°C, R_0 = 30 kΩ, C_0 = 0.033 µF, unless otherwise specified. See Figure 2 for component designation.

PARAMETERS	XR-2212/2212M			XR-2212C			UNITS	CONDITIONS
	MIN	TYP	MAX	MIN	TYP	MAX		
GENERAL								
Supply Voltage	4.5		15	4.5		15	V	
Supply Current		6	10		6	12	mA	$R_0 \geq$ 10 KΩ. See Fig. 4
OSCILLATOR SECTION								
Frequency Accuracy		±1	±3		±1		%	Deviation from $f_0 = 1/R_0C_0$
Frequency Stability								$R_1 = \infty$
Temperature		±20	±50		±20		ppm/°C	See Fig. 8.
Power Supply		0.05	0.5		0.05		%/V	V^+ = 12 ±1 V. See Fig. 7.
		.2			.2		%/V	V^+ = 5 ±0.5 V. See Fig. 7.
Upper Frequency Limit	100	300			300		kHz	R_0 = 8.2 KΩ, C_0 = 400 pF
Lowest Practical Operating Frequency			0.01		0.01		Hz	R_0 = 2 MΩ, C_0 = 50 µF See Fig. 5.
Timing Resistor, R_0								
Operating Range	5		2000	5		2000	KΩ	
Recommended Range	15		100	15		100	KΩ	See Fig. 7 and 8.
OSCILLATOR OUTPUTS								
Voltage Output								Measured at Pin 5.
Positive Swing, V_{OH}		11			11		V	
Negative Swing, V_{OL}	.8	.4			.5		V	
Current Sink Capability		1			1		mA	
Current Output								Measured at Pin 3.
Peak Current Swing	100	150			150		µA	
Output Impedance		1			1		MΩ	
Quadrature Output								Measured at Pin 15.
Output Swing		0.6			0.6		V	
DC Level		0.3			0.3		V	Referenced to Pin 11.
Output Impedance		3			3		KΩ	
LOOP PHASE DETECTOR SECTION								Measured at Pin 10.
Peak Output Current	±150	±200	±300	±100	±200	±300	µA	
Output Offset Current		±1			±2		µA	
Output Impedance		1			1		MΩ	
Maximum Swing	±4	±5		±4	±5		V	Referenced to Pin 11.
INPUT PREAMP SECTION								Measured at Pin 2.
Input Impedance		20			20		KΩ	
Input Signal to Cause Limiting		2	10		2		mVrms	
OP AMP SECTION								
Voltage Gain	55	70		55	70		dB	R_L = 5.1 KΩ, $R_F = \infty$
Input Bias Current		0.1	1		0.1	1	µA	
Offset Voltage		±5	±20		±5	±20	mV	
Slew Rate		2			2		V/µsec	
INTERNAL REFERENCE								Measured at Pin 11.
Voltage Level	4.9	5.3	5.7	4.75	5.3	5.85	V	
Output Impedance		100			100		Ω	AC Small Signal
Maximum Source Current		80			80		µA	

The XR-2212 data sheet.

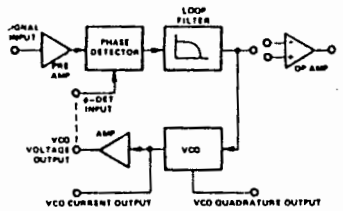

Figure 1. Functional Block Diagram of XR-2212 Precision PLL System

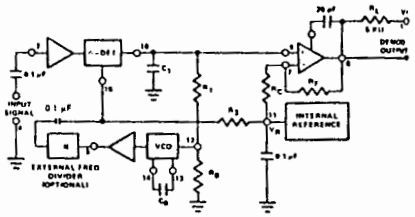

Figure 2. Generalized Circuit Connection for FM Detection, Signal Tracking or Frequency Synthesis

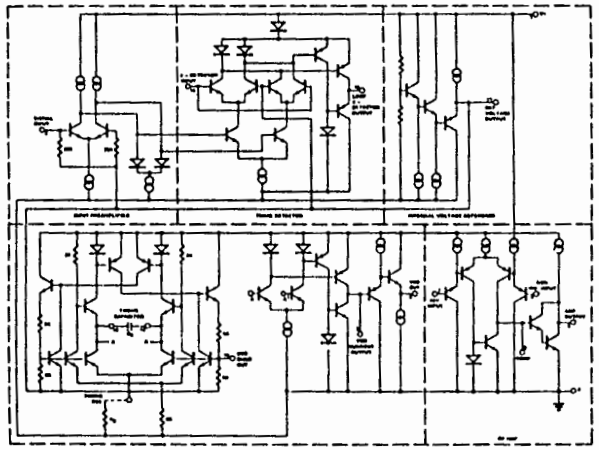

Figure 3. Simplified Circuit Schematic of XR-2212

CAL CHARACTERISTICS

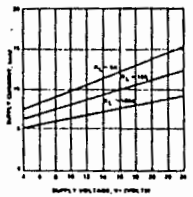

re 4. Typical Supply Current vs V+ (Logic Outputs Open Circuited)

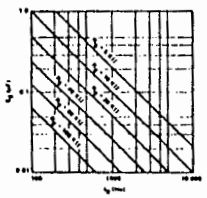

Figure 5. VCO Frequency vs Timing Resistor

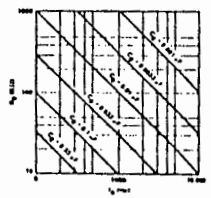

Figure 6. VCO Frequency vs Timing Capacitor

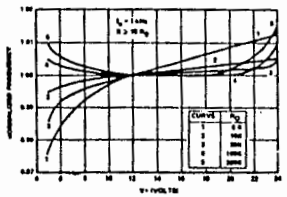

Figure 7. Typical f_0 vs Power Supply Characteristics

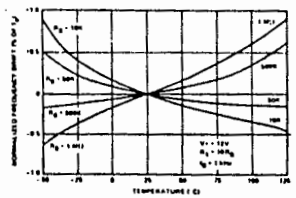

Figure 8. Typical Center Frequency Drift vs Temperature

DESCRIPTION OF CIRCUIT CONTROLS

Signal Input (Pin 2): Signal is ac coupled to this terminal. The internal impedance at Pin 2 is 20 KΩ. Recommended input signal level is in the range of 10 mV to 5V peak-to-peak.

VCO Current Output (Pin 3): This is a high impedance (MΩ) current output terminal which can provide ±100 μA sink capability with a voltage swing equal to V+. This output can directly interface with CMOS or NMOS logic families.

VCO Voltage Output (Pin 5): This terminal provides a low-impedance (≈ 50Ω) buffered output for the VCO. It can directly interface with low-power Schottky TTL. For interfacing with standard TTL circuits, a 750Ω pull-down resistor from pin 5 to ground is required. For operation of the PLL without an external divider, pin 5 can be dc coupled to pin 16.

Op Amp Compensation (Pin 6): The op amp section is frequency compensated by connecting an external capacitor from pin 6 to the amplifier output (pin 8). For unity-gain compensation a 20 pF capacitor is recommended.

Op Amp Inputs (Pins 7 and 9): These are the inverting and the non-inverting inputs for the op amp section. The common-mode range of the op amp inputs is from + 1V to (V+ − 1.5) volts.

Op Amp Output (Pin 8): The op amp output is an open-collector type gain stage and requires a pull-up resistor, R_L, to V+ for proper operation. For most applications, the recommended value of R_L is in 5 kΩ to 10 kΩ range.

Phase Detector Output (Pin 10): This terminal provides a high-impedance output for the loop phase-detector. The PLL loop filter is formed by R_1 and C_1 connected to Pin 10 (see Figure 2). With no input signal, or with no phase-error within the PLL, the dc level at Pin 10 is very nearly equal to V_R. The peak voltage swing available at the phase detector output is equal to $\pm V_R$.

Reference Voltage, V_R (Pin 11): This pin is internally biased at the reference voltage level, V_R: $V_R = V+/2$—550 mV. The dc voltage level at this pin forms an internal reference for the voltage levels at pins 10, 12 and 16. Pin 1 *must* be bypassed to ground with a 0.1 μF capacitor, for proper operation of the circuit.

VCO Control Input (Pin 12): VCO free-running frequency is determined by external timing resistor, R_0, connected from this terminal to ground. For optimum temperature stability, R_0 must be in the range of 10 KΩ to 100 KΩ (see Figure 8).

VCO Frequency Adjustment: VCO can be fine-tuned by connecting a potentiometer, R_X, in series with R_0 at Pin 12 (see Figure 10).

This terminal is a low-impedance point, and is internally biased at a dc level equal to V_R. The maximum timing current drawn from Pin 12 must be limited to ≤ 3 mA for proper operation of the circuit.

VCO Timing Capacitor (Pins 13 and 14): VCO frequency is inversely proportional to the external timing capacitor, C_0, connected across these terminals (see Figure 5). C_0 must be nonpolar, and in the range of 200 pF to 10 μF.

VCO Quadrature Output (Pin 15): The low-level (≈0.6 Vpp) output at this pin is at quadrature phase (i.e. 90° phase-offset) with the other VCO outputs at pins 3 and 5. The dc level at pin 15 is approximately 300 mV above V_R. The quadrature output can be used with an external multiplier as a "lock detect" circuit. In order not to degrade oscillator performance, the output at pin 15 must be buffered with an external high-impedance low-capacitance amplifier. When not in use, pin 15 should be left open-circuited.

Phase Detector Input (Pin 16): Voltage output of the VCO (pin 5) or the output of an external frequency divider is connected to this pin. The dc level of the sensing threshold for the phase detector is referenced to V_R. If the signal is capacitively coupled to pin 16, then this pin must be biased from pin 11, through an external resistor, R_B (R_B ≈ 10 KΩ). The peak voltage swing applied to pin 16 *must not* exceed (V+ − 1.5) volts.

PHASE-LOCKED LOOP PARAMETERS:

Transfer Characteristics:

Figure 9 shows the basic frequency to voltage characteristics of XR-2212. With no input signal present, filtered phase detector output voltage is approximately equal to the internal reference voltage, V_R, at pin 11. The PLL can track an input signal over its tracking bandwidth, shown in the figure. The frequencies f_{TL} and f_{TH} represent the lower and the upper edge of the tracking range, f_0 represents the VCO center frequency.

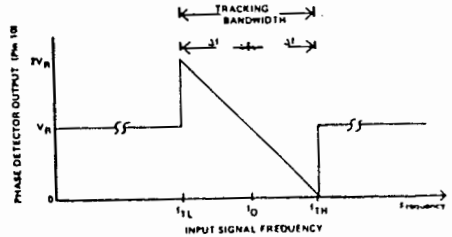

Figure 9. Phase Detector Output Voltage (Pin 10) as a Function of Input Signal Frequency. Note: Output Voltage is Referenced to Internal Reference Voltage V_R at Pin 11

Design Equations:

(See Figure 2 and Figure 9 for definition of components.)

1. VCO Center Frequency, f_0: $f_0 = 1/R_0C_0$ Hz

...al Reference Voltage, V_R (measured at Pin 11)

$V_R = V+/2 - 650$ mV

Loop Low-Pass Filter Time Constant, τ: $\tau = R_1C_1$

Loop Damping, ζ: $\zeta = 1/4\sqrt{\frac{NC_0}{C_1}}$

where N is the external frequency divider modular (See 2). If no divider is used, N = 1.

. Loop Tracking Bandwidth, $\pm\Delta f/f_0$: $\Delta f/f_0 = R_0/R_1$

. Phase Detector Conversion Gain, K_ϕ: (K_ϕ is the differential dc voltage across Pins 10 and 11, per unit of phase error at phase-detector input) $K_\phi = -2V_R/\pi$ volts/radian

. VCO Conversion Gain, K_0: (K_0 is the amount of change in VCO frequency, per unit of dc voltage change at Pin 10. It is the reciprocal of the slope of conversion characteristics shown in Figure 9). $K_0 = -1/V_RC_0R_1$ Hz/volt

). Total Loop Gain, K_T:

$K_T = 2\pi K_\phi K_0 = 4/C_0R_1$ rad/sec/volt

). Peak Phase-Detector Current, I_A; available at pin 10.

$I_A = V_R$ (volts)/25 mA

APPLICATION INFORMATION

FM DEMODULATION:

XR-2212 can be used as a linear FM demodulator for both narrow-band and wide-band FM signals. The generalized circuit connection for this application is shown in Figure 10, where the VCO output (pin 5) is directly connected to the phase detector input (pin 16). The demodulated signal is obtained at phase detector output (pin 10). In the circuit connection of Figure 10, the op amp section of XR-2212 is used as a buffer amplifier to provide both additional voltage amplification as well as current drive capability. Thus, the demodulated output signal available at the op amp output (pin 8) is fully buffered from the rest of the circuit.

In the circuit of Figure 10, R_0C_0 set the VCO center frequency, R_1 sets the tracking bandwidth, C_1 sets the low-pass filter time constant. Op amp feedback resistors R_F and R_C set the voltage gain of the amplifier section.

Design Instructions:

The circuit of Figure 10 can be tailored to any FM demodulation application by a choice of the external components R_0, R_1, R_C, R_F, C_0 and C_1. For a given FM center frequency and frequency deviation, the choice of these components can be calculated as follows, using the design equations and definitions given on page 1-34, 1-35 and 1-36.

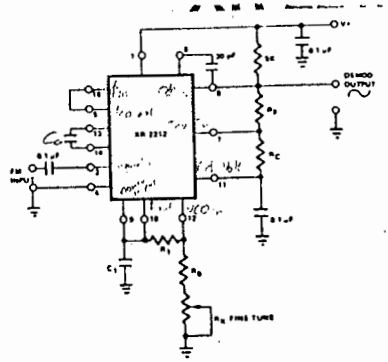

Figure 10. Circuit Connection for FM Demodulation

a) Choose VCO center frequency f_0 to be the same as FM carrier frequency.

b) Choose value of timing resistor R_0, to be in the range of 10 KΩ to 100 KΩ. This choice is arbitrary. The recommended value is $R_0 \cong 20$ KΩ. The final value of R_0 is normally fine-tuned with the series potentiometer, R_X.

c) Calculate value of C_0 from design equation (1) or from Figure 6:

$$C_0 = 1/R_0f_0$$

d) Choose R_1 to determine the tracking bandwidth, Δf (see design equation 5). The tracking bandwidth, Δf, should be set significantly wider than the maximum input FM signal deviation, Δf_{SM}. Assuming the tracking bandwidth to be "N" times larger than Δf_{SM}, one can re-unite design equation 5 as:

$$\frac{\Delta f}{f_0} = \frac{R_0}{R_1} = N\frac{\Delta f_{SM}}{f_0}$$

Table I lists recommended values of N, for various values of the maximum deviation of the input FM signal.

% Deviation of FM Signal ($\Delta f_{SM}/f_0$)	Recommended value of Bandwidth Ratio, N ($N = \Delta f/\Delta f_{SM}$)
1% or less	10
1 to 3%	5
1 to 5%	4
5 to 10%	3
10 to 30%	2
30 to 50%	1.5

TABLE I

Recommended values of bandwidth ratio, N, for various values of FM signal frequency deviation. (Note: N is the ratio of tracking bandwidth Δf to max. signal frequency deviation, Δf_{SM}).

e) Calculate C_1 to set loop damping (see design equation 4). Normally, $\zeta = 1/2$ is recommended. Then, $C_1 = C_0/4$ for $\zeta = 1/2$.

Calculate R_C and R_F to set peak output signal amplitude. Output signal amplitude, V_{out}, is given as:

$$V_{out} = \left(\frac{\Delta f_{SM}}{f_0}\right)\left(V_R\right)\left(\frac{R_1}{R_0}\right)\left[\frac{R_C + R_F}{R_C}\right]$$

In most applications, $R_F = 100$ KΩ is recommended; then R_C, can be calculated from the above equation to give desired output swing. The output amplifier can also be used as a unity-gain voltage follower, by open circuiting R_C (i.e., $R_C = \infty$).

Note: All calculated component values except R_0 can be rounded-off to the nearest standard value, and R_0 can be varied to fine-tune center frequency, through a series potentiometer, R_X. (See Figure 10.)

Design Example:

Demodulator for FM signal with 67 kHz carrier frequency with ±5 kHz frequency deviation. Supply voltage is +12V and required peak output swing is ±4 volts.

Step a) f_0 is chosen as 67 kHz.

Step b) Choose $R_0 = 20$ KΩ (18 KΩ fixed resistor in series with 5 KΩ potentiometer).

Step c) Calculate C_0: from design Eq. (1).

$C_0 = 746$ pF

Step d) Calculate R_1. For given FM deviation, $\Delta f_{SM}/f_0 = 0.0746$, and N = 3 from Table I.

Then:

$R_0/R_1 = (3)(0.0746) = 0.224$

or:

$R_1 = 89.3$ KΩ.

Step e) Calculate $C_1 = (C_0/4) = 186$ pF.

Step f) Calculate R_C and R_F to get ±4 volts peak output swing: Let $R_F = 100$ KΩ. Then,

$R_C = 80.6$ KΩ.

Note: All values except R_0 can be rounded-off to nearest standard value.

FREQUENCY SYNTHESIS

Figure 11 shows the generalized circuit connection for frequency synthesis. In this application an external frequency divider is connected between the VCO output (pin 5) and the phase-detector input (pin 16). When the circuit is in lock, the two signals going into the phase-detector are at the same frequency, or $f_S = f_1/N$ where N is the modulus of the external frequency divider. Conversely, the VCO output frequency, f_1 is equal to Nf_S.

In the circuit configuration of Figure 11, the external timing components, R_0 and C_0, set the VCO free-running frequency; R_1 sets the tracking bandwidth and C1 sets the loop damping, i.e., the low-pass filter time constant (see design equations).

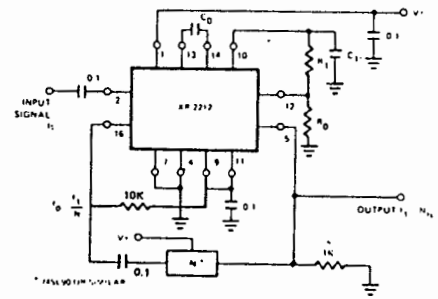

Figure 11. Circuit Connection for Frequency Synthesizer

The total tracking range of the PLL (see Figure 9), should be chosen to accommodate the lowest and the highest frequency, f_{max} and f_{min}, to be synthesized. A recommended choice for most applications is to choose a tracking half-bandwidth Δf, such that:

$$\Delta f = f_{max} - f_{min}$$

If a fixed output frequency is desired, i.e. N and f_S are fixed, then a ±10% tracking bandwidth is recommended. Excessively large tracking bandwidth may cause the PLL to lock on the harmonics of the input signals; and the small tracking range increases the "lock-up" or acquisition time.

If a variable input frequency and a variable counter modulus N is used, then the maximum and the minimum values of output frequency will be:

$f_{max} = N_{max}(f_S)_{max}$ and $f_{min} = N_{min}(f_S)_{min}$

Design Instructions:

For a given performance requirement, the circuit of Figure 11 can be optimized as follows:

a) Choose center frequency, f_0, to be equal to the output frequency to be synthesized. If a range of output frequencies is desired, set f_0 to be at mid-point of the desired range.

b) Choose timing resistor R_0 to be in the range of 15 KΩ to 100 KΩ. This choice is arbitrary. R_0 can be fine tuned with a series potentiometer, R_X.

c) Choose timing capacitor, C_0 from Figure 6 or Equation 1.

APPENDIX 10

The listing of a C program is given in this section. The program calculates the expected signal to clutter ratio at the receiver, the cell area and range resolution. The data is then written to a file called "Clutter.dat".

```
/*          CLUTTER PREDICTIONS FOR A BISTATIC RADAR                    */
/* This program calculates the expected clutter power received.  The    */
/* bistatic radar is situated at the University of Cape Town and        */
/* D.F. Malan airport.  The radar clutter cross sectional data used is  */
/* Larsons L Band data.  This data assumes that the surroundings are tall */
/* weeds and scrub trees.  This however is only true for the western side */
/* of the airport.                                                      */

#include <stdio.h>
#include <conio.h>
#include <stdlib.h>
#include <math.h>

#define c  3e8                  /* speed of light */
#define Pt 2.5e6                /* transmitter power */
#define Gt 331                  /* transmitter antenna gain */
#define Gro 1.64                /* receiver antenna gain */
#define LAMDA 0.222             /* wavelength */
#define BEAMWID 0.02356         /* transmitter antenna beamwidth */
#define PULSEWID 2.5e-6         /* pulse width */
#define base 7500               /* half baselength */
#define PI 3.14159

FILE *fptr;                     /* to create an output data file */

/* Out of plane, horizontally polarized radar clutter cross sectional
      coefficients for tall weeds and scrub trees.  Larsons L Band data.  */

float coeficient[37] = {0.63,0.4,0.25,0.25,0.25,0.16,0.1,0.06,0.06,0.05,0.002,
  0.04,0.035,0.035,0.044,0.044,0.0004,0.0003,0.0007,0.0032,0.011,0.016,0.025,
  0.016,0.011,0.011,0.016,0.02,0.02,0.02,0.02,0.028,0.028,0.035,0.035,0.04,
  0.04};

float plane_angd[37] = {0,5,15,20,25,30,35,40,45,50,55,60,65,70,75,80,85,90,
  94,96,100,105,110,115,120,125,130,135,140,145,150,155,160,165,170,175,180};

/* main program */
main()
  {
       int i, m, p, q;
       float a, b;
       float area, coef, clutter_area, Gr, Prc, SCR, Rres;
       float x, y, xkm, ykm, Rt, Rtkm, Rr, Rrkm, Rtotal, Pr, Prdb, lookang;
       float theta1, theta2, alpha, bistat, bistatang, plane_ang[37];

       fptr = fopen("a:\clutter.dat","wt");   /* open data file to write  */
                                              /* data information         */
       for (m=0 ; m<=36 ; m++ )
           plane_ang[m] = (plane_angd[m] / 180) * PI;
       m = 0;
       a = 7550;
       for ( p=0 ; p<=20 ; p++ )
           {
            /* Determine equation for first range ellipse */
            m = m + 1;
            b = sqrt(pow(a,2) - pow(base,2));
            fprintf(fptr,"\nRange Ring  %d\n",m);
            fprintf(fptr,"Bistat_Angle Rx_Lookang Rt Rtot Pr Cross_Area Area \n");
```

```
x = (-a);
do
 {
     y = pow(b,2) - ((pow(x,2) * pow(b,2)) / pow(a,2));
     if (y <= 0)
          y = 0;
     else
          y = sqrt(y);

     /* Determine out of plane angle. */
     if (x >= -7500)
          theta1 = atan( y / (x + base));
     else
          theta1 = PI - atan(y / fabs(x + base));

     if (x <= 7500)
          theta2 = atan( y / fabs(x - base));
     else
          theta2 = PI - atan( y / (x - base));

     /* Determine receiver look angle. */
     if (x == base)
          lookang = 0;
     else
          lookang = ((theta2/PI)*180) - 90;

     /* Determine bistatic data. */
     alpha = theta1 + theta2;
     bistatang = (PI - alpha);
     bistat = ((PI - alpha) / PI) * 180;
     i = 0;

     /* Extrapolate cross sectional coefficient from Larsons data */
     while (!((alpha >= plane_ang[i]) && (alpha <= plane_ang[i+1])))
          i = i + 1;
     coef = (coeficient[i] + coeficient[i+1]) / 2;

     if (theta1 == 0)
          theta1 =  theta1 + 0.0008;
     if (theta2 == 0)
          theta2 = theta2 + 0.0008;

     /* Determine transmitter to clutter and receiver to clutter */
     /* range.                                                   */
     if ((y > -0.01) && (y < 0.01) && (x < (-base)))
          Rt = fabs(x + base);
     else if ((y > -0.01) && (y < 0.01) && (x > (-base)))
          Rt = (2 * base) + (x - base);
     else if (x <= (-base))
          Rt = y / sin(PI - theta1);
     else
          Rt = y / sin(theta1);

     if ((y > -0.01) && (y < 0.01) && (x < base))
          Rr = (2 * base) + fabs(x + base);
     else if ((y > -0.01) && (y < 0.01) && (x > base))
          Rr = x - base;
     else if (x >= base)
          Rr = y / sin(PI - theta2);
     else
          Rr = y / sin(theta2);

     /* Determine area covered by the crossing of the Tx and Rx */
     /* beams.  Then calculate the clutter cross sectional area */

     area = (Rt*BEAMWID*c*PULSEWID) / (2*pow(cos(bistatang/2),2));
     clutter_area = area * coef;

    /* Gr is the gain of the receiver as a function of theta2 */

     if (theta2 >= 1.562)
          Gr = 0.000000001;
     else
          Gr = Gro*(cos((PI/2)*sin(theta2)) / cos(theta2));
```

```
                /* power received due to target echo */
                Pr = (Pt*2511.8*Gr*pow(LAMDA,2)*50) /
                          (pow((4*PI),3)*pow(Rt,2)*pow(Rr,2));

                /* power received due to clutter */
                Prc = (Pt*Gt*Gr*pow(LAMDA,2)*clutter_area) /
                           (pow((4*PI),3)*pow(Rt,2)*pow(Rr,2));

                /* determine signal to clutter ratio */
                SCR = Pr / Prc;

                if (SCR == 0)
                     SCR = -200;
                else
                     SCR = 10*log(SCR);

                /* Determine range resolution */
                Rres = (c*0.0000025) / (2*pow(cos(bistatang/2),2));

                Rtkm = Rt / 1000;
                Rrkm = Rr / 1000;
                xkm = x / 1000;
                ykm = y / 1000;
                Rtotal = Rtkm + Rrkm;
                fprintf(fptr,"%5.1f %5.1f %5.2f %5.1f %5.1f %5.2f",
                      bistat, lookang, Rrkm, Rtotal, SCR, clutter_area);
                fprintf(fptr,"  %6.2f", area);
                fprintf(fptr," %6.2f \n", Rres);

                /* Increment to next x axis position */
                if ((a >= 20000) && (a <= 30000))
                     x = x + 2000;
                else if (a > 30000)
                     x = x + 4000;
                else
                     x = x + 1000;
           }
           while((x <= a) && (theta2 <= (PI/2)));
           /* Increment to next range ring */
           a = a + 2000;
        }
     fclose(fptr);
}
```

APPENDIX 11

This appendix shows the precision power supply and its PC board used to power the receiver. The power supply generates a constant $\pm 15V$ at the output.

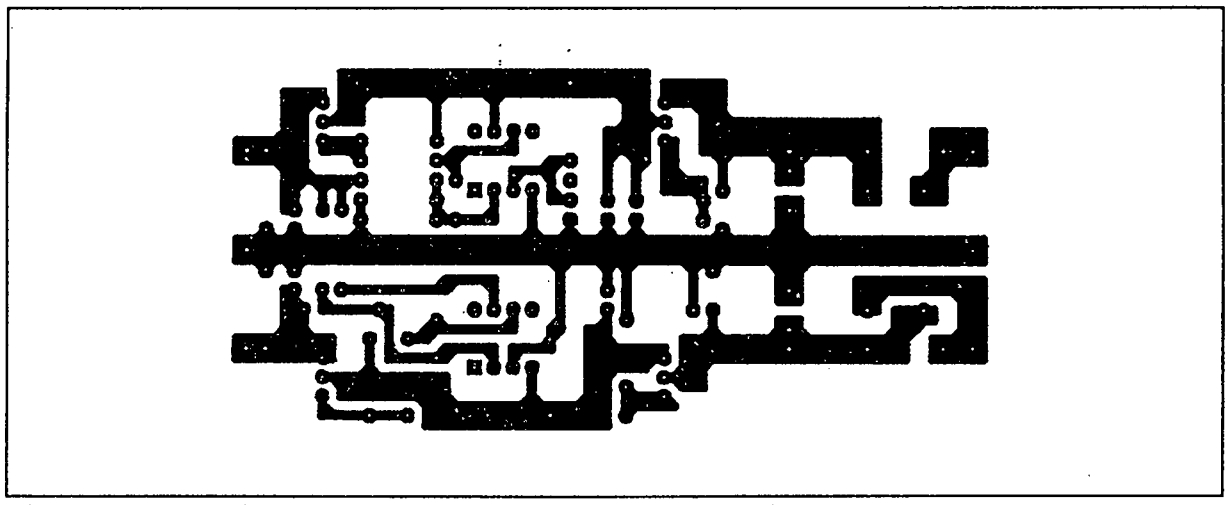

Figure 11.1 *The PC board artwork of the power supply.*

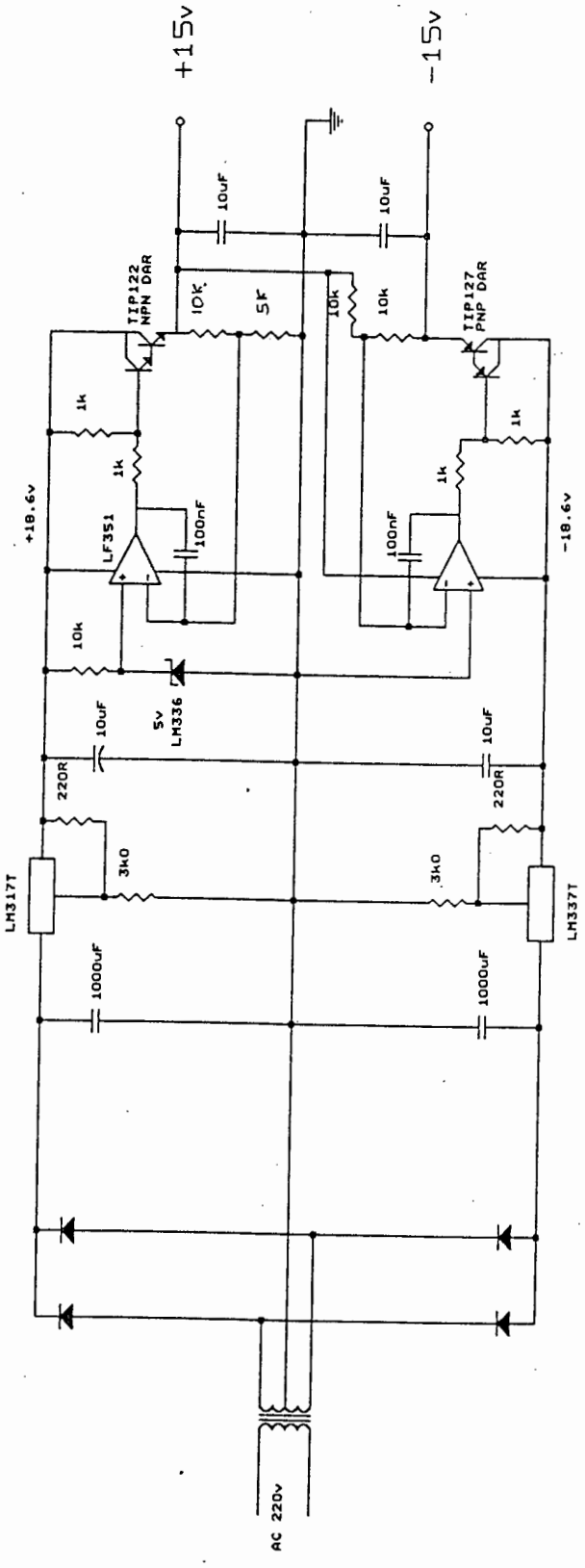

Figure 11.2 *The precision ±15V Power supply circuit diagram.*